The Dissertation Committee for Joaquín M. Campos
certifies that this is the approved version of the following dissertation:

Hydro-Pneumatic Pulse Forming Networks

Committee:

Raul G. Longoria, Supervisor

Joseph J. Beaman

Eric Fahrenthold

John A. Mallick

Hydro-Pneumatic Pulse Forming Networks

by

Joaquín M. Campos

DISSERTATION

Presented to the Faculty of the Graduate School of

The University of Texas at Austin

in Partial Fulfillment

of the Requirements

for the Degree of

DOCTOR OF PHILOSOPHY

THE UNIVERSITY OF TEXAS AT AUSTIN

August 2017

To my beloved parents Juan and Esther. For their unwavering support, prayers, and encouragement all these years.

Acknowledgments

Firstly, I would like to express my deep appreciation and gratitude to my supervisor, Dr. Raul Longoria, for his wise mentorship, insightful tutelage, and unrelenting effort to make me keep my eye on the goal with his persistent 'patadas', for moral as well as financial support when times were hard, and ultimately in his patience, never loosing faith in me over this long and tiring effort. Much of the fluidity of this dissertation is owed to his detail oriented editorial effort. For all these things I am truly and deeply grateful to him.

I would also like to thank my committee members, Drs. Joseph Beaman, Eric Fahrenthold, and especially Dr. John Mallick, for their input and helpful guidance, albeit not used quite as much as I should have, they were available and often gave words of much needed encouragement.

I am indebted to the efforts of Drs. Harry Fair, Ian McNab, and Mark Crawford, for securing initial funding for this effort, and for their thoughtful guidance and encouragement in motivating me to begin this journey.

I am grateful to my dear friend and mentor Dr. Steven Kornguth whose deeply encouraging talks helped get me though the hardest parts of this journey and whose wise counsel has and will continue to serve me well for the rest of my life.

I am greatly indebted to one of my best friends Akash Sharma, for gen-

erosity with his time, his patience, and his immeasurable help in creating the ingenious measurement system that allowed me to finish this research effort. His creativity and knowledge in the use and creation of National Instrument software tools is unmatched.

I am deeply appreciative for the moral and spiritual support I received from my family, especially my parents Dr. Juan and Esther Campos. To my father who has always been my biggest inspiration and will continue to be until the day I leave this earth. To my mother for her tender heart which has been and is a source of great encouragement and spiritual strength. To my siblings Javier, Rebecca, and Monica, for their constant prayers and words of encouragement.

I would be remiss if I did not mention my beloved Erica. To whom I am greatly indebted for her loving prayers, daily encouragement, and 'carinhos' the helped make the last stretch of this journey bearable. It is truly a blessing to have the love that she gives me from day to day.

There are many whom The Lord has put in my path during this journey each with their own contribution both great and small to whom I am truly indebted, including many that may not be mentioned here but whose contribution either moral or spiritual made it possible for me to complete this degree.

Finally and most importantly, I thank my GOD for the people He has put in my life and for shaping the circumstances that have brought me to

this point. Whether in 'good times' or 'bad times', His loving kindness and provision has never failed me, for the mercies that I have received are only possible because of the grace I found through my salvation in Yeshua (Jesus) the Messiah. May HIS glorious name be praised for ever and ever, YHWH our loving and merciful creator.

Hydro-Pneumatic Pulse Forming Networks

Joaquín M. Campos, Ph.D.
The University of Texas at Austin, 2017

Supervisor: Raul G. Longoria

A novel method that combines energy storage and power conditioning for renewable energy systems is presented. This method utilizes hydro-pneumatic energy storage elements, also known as hydraulic accumulators, as mechanical capacitors arranged in such a fashion as to create a hydro-pneumatic pulse forming network (HPPFN) in a manner similar to sequentially fired pulsed formed networks (SFPFNs) used for electromagnetic railgun launch. This pulse forming network has the ability to create a power output of nearly constant amplitude for short durations, which is particularly well-suited for supplying power to constant amplitude, duty-cycle-type loads.

The foundational principles are established herein for how HPPFN systems can be modeled and synthesized, so that systems can be designed and scaled for practical applications. This foundation was established incrementally in three parts. First, a working experimental test-bed system was constructed to prove the feasibility of operating a sequentially-fired pulse forming network using hydro-pneumatic energy storage elements in a manner analogous to electromagnetic sequentially-fired PFNs. Next, a modeling framework was

developed for hydro-pneumatic pulse forming network synthesis. Finally, the model-based synthesis approach was experimentally validated using the test-bed to demonstrate that sizing and practical construction of HPPFN systems can be accomplished. Suggestions for future work to extend these methods and the applications of HPPFNs are provided.

Table of Contents

List of Tables

List of Figures

Chapter 1

Introduction

Pulse forming networks (PFNs) were first developed in the early 1940's by Guillemin et. al [10] as a means of providing extremely short duration (microseconds) constant amplitude pulses of very high power for microwave applications typically associated with radar. Although radar applications have continued to be the primary use for PFNs a more recent application has been in the area of electromagnetic railgun systems, where they are employed as a technique for providing an efficient motive force during ballistic launch [16, 18]. Even though the general concept of firing multiple capacitors or inductors to form a square-shaped power output is at the core of both applications, the means by which the PFN is synthesized in the two cases are significantly different due to the non-linear nature of the railgun load [7]. It is this synthesis technique for a non-linear system that has application to the novel system to be studied herein. Indeed, it was the intimate knowledge and experience the author had with the operation and design of modern railguns that led in part to the inspiration to extrapolate across energy domains, and extend the concept to a larger family of practical applications.

The core motivation that led to this effort can be attributed to the

author's experience while conducting combat and humanitarian aid and assistance operations in Afghanistan with the U.S. Army in 2006. A need was observed for remote cold storage of agricultural products to aid local farmers in preserving produce for longer periods of time, increasing crop value, and increasing produce-to-market availability. A concept was conceived for a mobile cool storage platform capable of remote operation with little or no maintenance. This platform needed to be powered almost exclusively by sustainable sources, such as solar panels and micro scale wind turbines, and had to be maintainable using locally-sourced labor and materials. The concept initially entailed the use of chemical energy storage (deep cycle lead acid batteries) as the primary means of energy storage, and power electronic based charge controllers to charge the batteries. It was noted by local aid agencies that other solar systems that had been installed for previous projects in the area had been unsuccessful primarily due to the lack of maintenance on the battery systems. This presented a need for a more robust energy storage system. It wasn't until the author returned to active academic research in 2007, and after discussions with Dr. Raul Longoria (Univ. of Texas Dept. of Mechanical Engineering) and Dr. Mark Crawford (Institute for Advanced Technology, Univ. of Texas), that an alternative solution was conceived that would have potential to be a more robust energy storage solution.

Recognizing that loads for refrigeration have constant amplitude duty cycles, it was hypothesized that a power output similar to that used to power the railgun could be used, if it could be made to match the required time

scale and power amplitudes for the intended remote applications, where time scales are typically on the order of minutes. After studying a number of simple and robust forms of energy storage, it was determined that compressed air energy storage devices, such as hydro-pneumatic accumulators, would be viable storage analogs to the electrical capacitors used in railgun systems. This led to an effort to test this hypothesis through modeling studies combined with a table-top demonstration of a sequentially-fired, pulsed forming network using hydro-pneumatic accumulators.

A hydro-pneumatic pulse forming network (HPPFN) utilizes the energy storage and release capabilities of Compressed Air Energy Storage (CAES) to create a pulse forming network (PFN). This design, as illustrated in Figure1.1, is meant to convert the non-deterministic or stochastic inputs usually associated with renewable power sources into relatively constant amplitude pulsed output power. This power conditioning would be ideal for constant amplitude cyclic loads, such as refrigeration and communications equipment. The envisioned system would cycle in a manner that it be charged by the stochastic inputs and then would discharge into the constant amplitude duty cycle load as needed. It is theoretically possible so long as discharge is not impeded that the system could be charging at the same time that it is discharging.

The CAES has a well-established track-record, and thus can provide the robust, long-term energy storage solution, combined with simplicity of operation and maintenance needed for standalone, remote, and off-grid applications. Due to the nature of the physical construction of these types of systems, they

are also inherently environmentally benign. These attributes make the proposed design a particularly attractive alternative to the conventional chemical battery - controller systems commonly used in sustainable energy systems at the present.

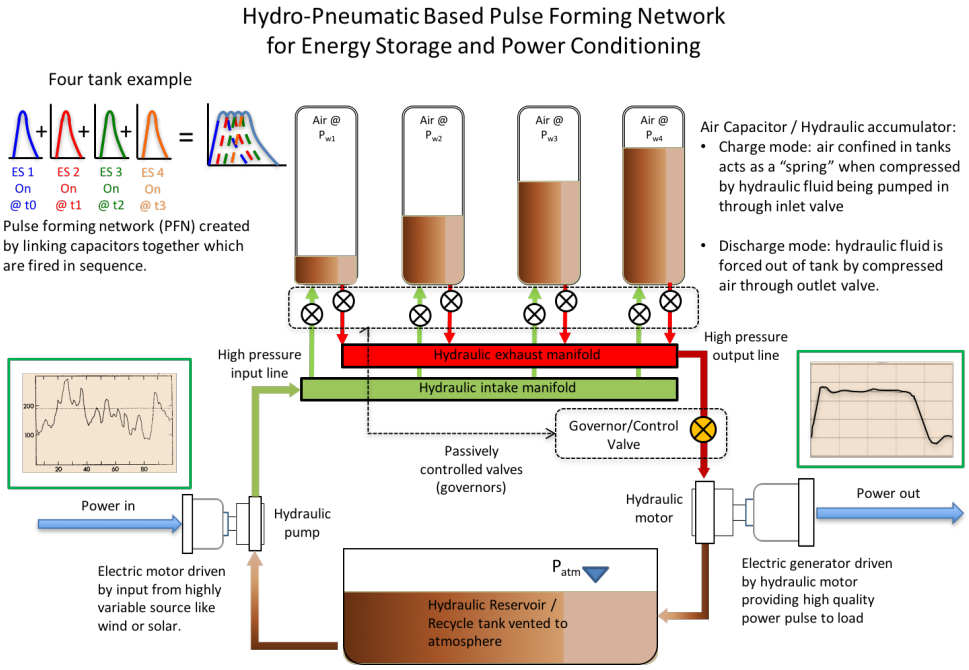

Figure 1.1: HPPFN system overview

Figure 1.2 shows a simple comparison between a typical renewable energy system with conventional batteries and a system that implements the HPPFN. There are two central challenges to the integration of renewable energy capture devices with a micropower system: 1) the power quality of the output, and 2) dealing with the stochastic nature of the power input. The proposed HPPFN design attempts to address both by combining energy storage

and power conditioning in a system that is less complex and more physically and operationally robust than conventional power electronic controlled chemical energy storage systems. This research effort investigates the second of the two issues in order to demonstrate the power pulse forming viability of the proposed technique.

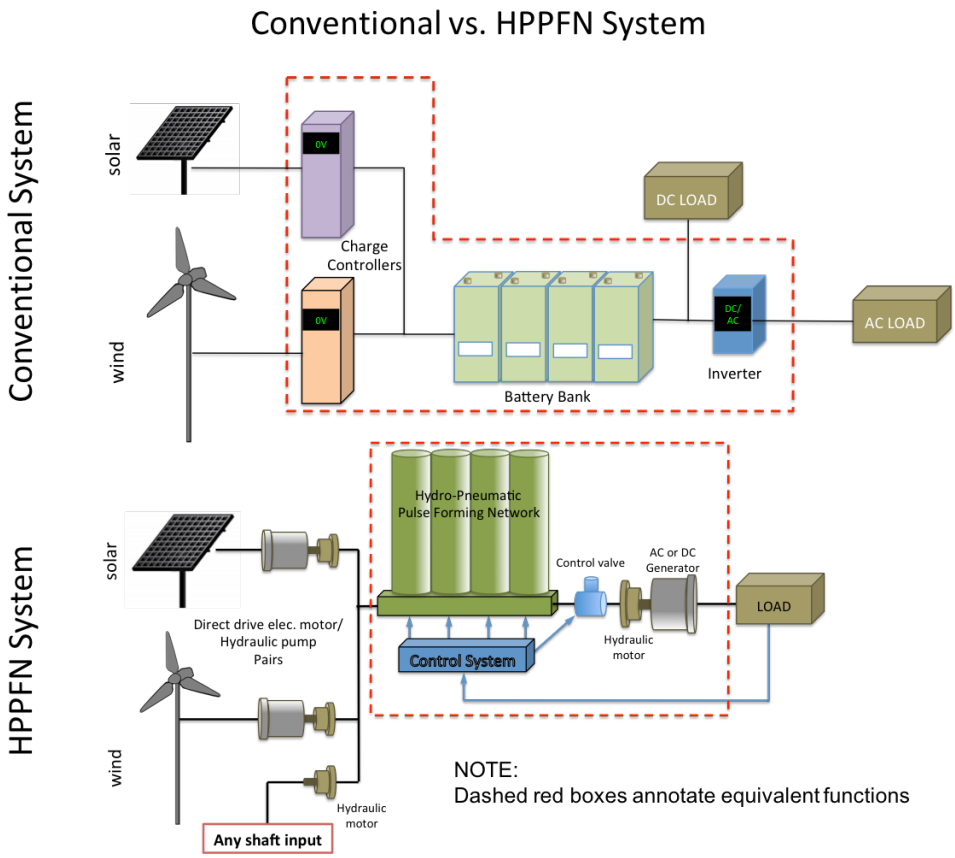

Figure 1.2: System comparison

Theoretically, this pulse forming network has the potential to deliver power in the form required. Refinement and evaluation of the design requires

models that can properly capture the non-linear behavior inherent to this system. These models support a *pulse synthesis technique* that specifies how to form power pulses of a desired magnitude and duration. In the HPPFN, a key requirement of this synthesis method is the specification of discharge timing of the hydro-pneumatic accumulators that form the pulsed power output.

1.1 Research Objectives

The focus of this research has been to determine the feasibility of synthesizing and operating a *sequentially-fired* PFN using hydro-pneumatic energy storage elements, in a manner analogous to an electromagnetic sequentially-fired PFN. Due to the difference in the system dynamics between electromagnetic and hydro-mechanically realized PFN, particularly the highly nonlinear behavior of the latter, it is not a straightforward extrapolation to implement established PFN synthesis techniques as presented by Glasoe et al. [8]. In short, prior to this research effort no methods existed that addressed the design and synthesis of PFNs outside of the electromagnetic / electromechanical domain. The next chapter will demonstrate how linear circuit synthesis concepts used in established methods for PFNs cannot be applied to non-linear systems. An effort, therefore, will be made to formulate a methodology allowing for the analytical description and realization of a hydro-mechanical PFN.

The absence of prior art presents a dual-layered challenge; to first identify an appropriate synthesis technique, and then to provide a suitable model of the non-linear hydro-mechanical system that appropriately predicts its behav-

ior. This model will form the basis for pulse synthesis techniques. Collectively, the modeling and synthesis technique will enable the design, scaling, and deployment of effective HPPFN systems. A more in-depth description of these methods will be presented in the next chapter.

The objectives of this dissertation are first and foremost to fill the void where no prior art existed for an entire class of systems described here as hydro-pneumatic pulse forming networks, and secondly to deliver a concise methodology with which future practitioners of the art can model, size, and build effective HPPFN systems capable of useful work.

1.2 Overview of Methodology

In order to effectively implement the HPPFN apparatus, an approach is necessary that will facilitate the design, implementation, and tuning of a PFN with appropriate power output and duration. The effort will follow an approach centered around a model development of a known physical system. As is often the case with many 'one-off' concept designs, the system presented here was built and operated before sufficient insight was gained to support model development. This is indeed fortuitous, since the existence of a prototype system prior to modeling had two distinct advantages. Firstly, since the exact system components and their specifications are known, a highly accurate representation can be developed. Secondly, having an operable system capable of producing experimental data allows for incremental verification and validation as the model progresses.

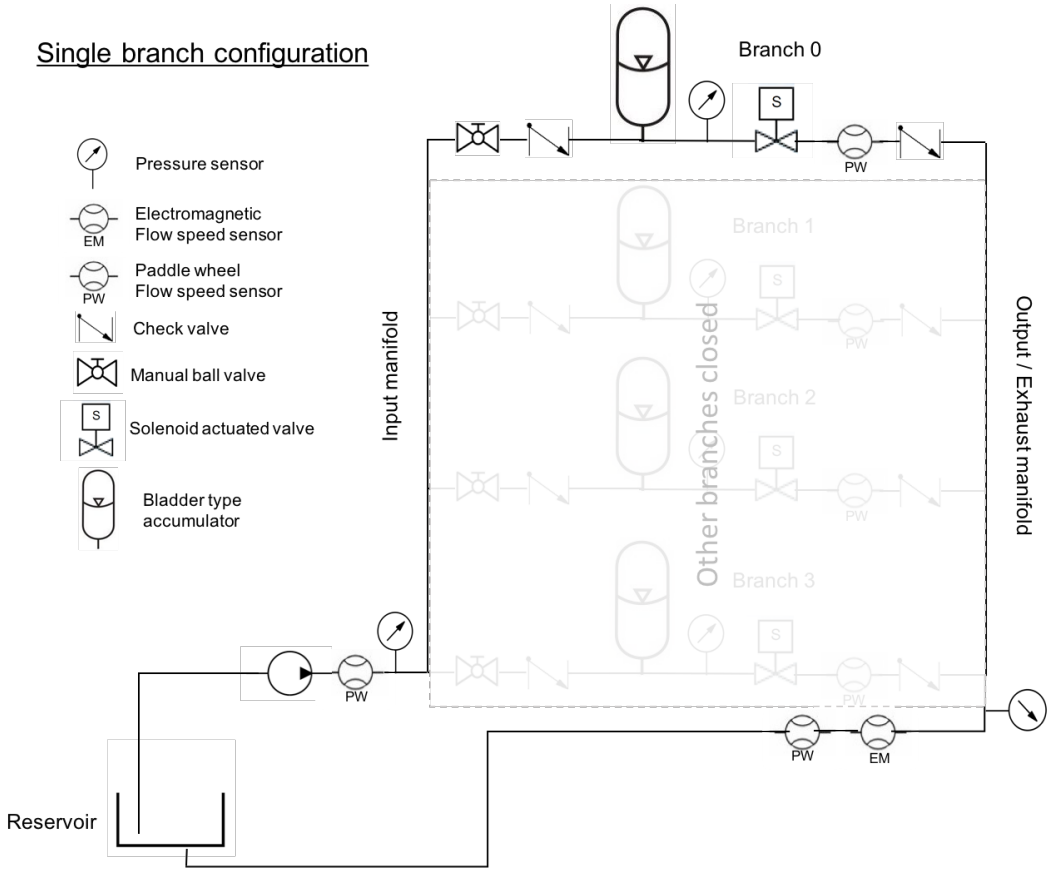

Figure 1.3: Single accumulator branch setup

The modeling effort begins with the construction of the simplest operating subsystem, an individual accumulator and its manifold branch. The manifold branch (Figure 1.3) being the run of line from the accumulator to the exit at the reservoir. This subsystem model, once tuned and verified experimentally with the physical system, is intended to be a modular piece in the formation of a multi-branch, multi-accumulator system. The modeling of the multi-branch system required both an appropriate numerical technique

to switch states, and an understanding of the fluid interaction between the individual branch flows during operation. There are numerous subtleties in the fluid interaction for the multi-branch system that required investigation before the theory could be implemented into model form. Each of these attempts to model the interaction in the multi-branch system is compared to the experimental system until a theory is found that allows the model to produce outputs with reasonable similarity. At this stage the model is tuned to best match experimental outputs. In the final stage the tuned model is verified by varying the initial conditions of the experimental system and ensuring that results of the model using these same initial conditions are repeatable and reliable.

1.3 Dissertation Overview

The next chapter presents the underlying concepts and methods used to design pulse forming networks. A brief overview is given of the history, purpose, and applications. A brief but concise introduction to pulse forming networks will follow, as well as an explanation of present modeling methods and their limitations as it applies to the current system (linear vs. nonlinear). This will provide the animus by which the modeling approach will be developed. Preliminary results from an HPPFN system, modeled in the SimHydraulics® simulation environment, is then presented that will provide initial evidence for system viability. Chapter 3 follows by providing a description of the experimental apparatus, including a detailed description of the

test bed and instrumentation that was developed. The preliminary results of the experimental system are also presented for the testbed and compared to known system outputs found in railgun literature. Chapter 4 will then present a methodical approach to the development of a simple but usable modeling, and synthesis technique which may be used to design, predict the output of, characterize, and scale, a sequentially fired hydro-pneumatic pulse forming network. This is followed by a progressive set of models of increasing complexity culminating in a model of the full system. The model will then be verified experimentally in Chapter 5 with a series of tests to verify it's operational capability as an effective HPPFN design tool. This paper will conclude with a recap of how the investigation met or failed to meet the research goals of the effort, and will follow with a discussion on proposed future work. The chapter will conclude with HPPFN systems' envisioned implementations and proposed practical application.

Chapter 2

Theory

2.1 Pulse Forming Networks

Pulse forming networks have their beginnings in the prolific era of the MIT Radiation Lab research efforts supporting the D.o.D. during the last World War. As regards this research, the seminal work was completed by Guillemin [10] in 1942. Six years later, methods for practical design and application of pulse forming networks were developed by Glasoe and Lebacqz [8]. They codified an approach for synthesis by first identifying classes of systems for which PFNs show applicability, and then by deriving unique methods for solving the set of system equations for each class, given some exceptions.

The underlying premise of the Glasoe and Lebacqz approach is to match the PFN impedance to the load impedance. One way to accomplish this is by solving Fourier series expansions with fitted functions to obtain the PFN circuit parameters. A total of five distinct network types (circuit topologies) were identified that could be used in pulse synthesis, as summarized in Figure 2.1. These were identified by the types A, B, C, D, and E, the latter two being the most difficult to solve using direct analytical methods. The operation of these systems relies completely on the natural discharge of the capacitances and/or

inductors in the ladder networks. There is no control over the individual energy store discharges other than by the initial circuit switch. In this case, the natural sequential discharge of the energy stores in the network forms the pulse by a superposition of their collective outputs. These networks are usually allowed to stay "on" until all the energy stores of a network have been discharged into the network's load.

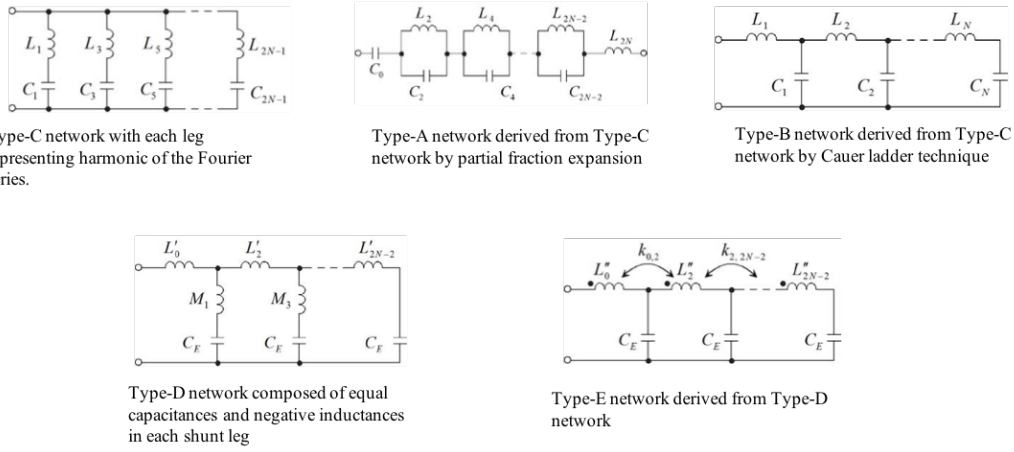

Figure 2.1: Circuits for A, B, C, D, and E type networks as presented by C. Rose [22].

The types of systems dealt with in these two seminal works and in the topical literature to date, are all electromagnetic in nature. Research in this area primarily deals with the charge and networked discharge of one of two types of storage devices: the capacitor and the inductor. As mentioned earlier, the premise of the synthesis approach was first presented by Guillemin [10] and codified by Glasoe et al. [8], and relies on linear circuit theory, which forms the basis for PFN design.

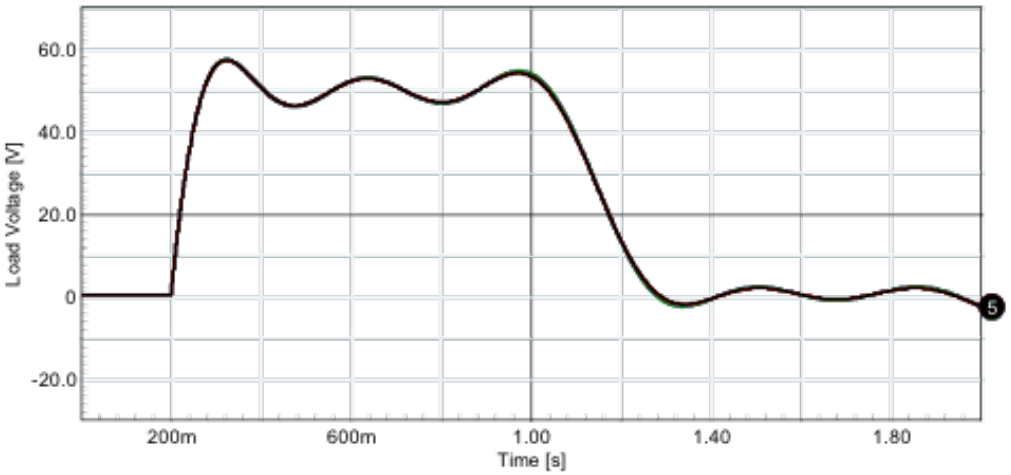

Figure 2.2: Overlay of 5 SPICE simulation PFN outputs, one each for type A, B, C, D, and E type networks from C. Rose [22]

The method that Glasoe et al. [8] espouses applies the following steps to the PFN synthesis problem:

1. Determine the system energy required for the application
2. Determine capacitance of available storage devices or desired storage device.
3. Divide total energy storage required by capacitor storage device individual storage capabilities and attain number of sections.
4. Use table (Table 6.2, page 202) in "Pulse Generators"[8] to find the design parameters.

These techniques are proven to work exceptionally well for ladder net-

works used in electromagnetic transmission and radar applications. Additionally, these systems are linear, assuming both linear source and load.

Given this well-established theory for linear PFN design, the question here remains to what extent these methods would apply to systems with non-linearities, such as for pulsed networks formed by other types of energetic components. Would it be worthwhile to even linearize such systems so that similar methods could be used? The next section incrementally deals with this question, beginning with the detailed differences between the hydro-pneumatic pulsed fluid network (HPPFN) and the (electrical) ladder network PFN. A synthesis technique will then be presented for electromagnetic launch in rail guns which has a linear source and a non-linear load. A discussion will ensue about whether this approach has potential to apply to the hydro-mechanical domain. This will logically be followed by a synthesis technique for a type of system that has a time varying source – that could be linear or non-linear in nature – and non-linear load, directly addressing the type of hydro-pneumatic systems that are of interest.

2.2 Pulse synthesis techniques

As was alluded to in the previous section, we look to the railgun PFN system to find clues as to how it's synthesis techniques might be applicable to the analogous problem in developing an HPPFN system. This assessment draws on past work reported on railgun PFN design, as well as on the author's past practical experience in this area.

There are four ways in which a railgun PFN design differs substantially from the systems first examined by Guillemin. First, load impedance is not the basis for the circuit / system design; i.e., the load impedance is not matched to the PFN impedance. Secondly, and most importantly, the non-linearity of the load and the changing load circuit length during launch precludes a closed form analytical solution. Consequently, *timing of the energy store discharges that will produce a desired pulse shape is difficult if not impossible to be analytically determined*. This problem has led to the development of a derivative PFN system known as a *sequentially-fired PFN* (or SFPFN). This class of PFN is of particular interest since it is much more controllable. Consequently, the railgun PFN requires an iterative design approach.

The third major difference between railgun and linear ladder network PFNs is that there is little communication or coupling between the energy-storing capacitor banks. In the Guillemin type PFN, timing of the discharge of a capacitive element is initiated by the previous (or neighboring) element's discharge, since there are no switches between elements. This produces a *cascading* effect completely dependent on the natural resonant characteristics (effective time constants) of the individual ladder circuits.

The fourth difference, which is closely related to the first, is that Guillemin's design technique focuses on finding the correct ladder elements such that the DC steady state current output closely matches what is desired. This is primarily based on matching the impedance of the load to that of the PFN circuit. Of course, it should also be mentioned that the load is a linear

resistor in the Guillemin method, which is not the case for railguns. Determining the impedance and knowing the desired pulse width then allows one to determine the elements of the system. In the case of a railgun PFN synthesis method used in practice, the elements of the system are not easily changed. Significant hardware design may have been invested in certain components, so a different approach must be taken. An example of a railgun PFN used at the University of Texas at Austin, Institute for Advanced Technology (UT-IAT) can be seen in Figure 2.3 below.

It is also the case that due to the large number of variables in the railgun system, including stray capacitances and inductances, as well as the non-linear nature of the load, it is not feasible to approach the synthesis using analytical methods. Experience has shown that a design approach using *iterative nonlinear simulation* is especially effective for synthesizing the desired output pulse. A detailed description of railgun PFN synthesis methods and techniques can be found in [17], [9], [21], and [6].

The resultant timings and charge values from the iterative synthesis methods constitute the essence of the SFPFN, a specific system for which controlled discharge timings enable much more control over the final pulse shape. An example from [7] of an SFPFN system and output can be seen in Figures 2.4, 2.5, and 2.6.

The HPPFN embodies, in the very least, three of the attributes of the railgun system, in that: a) the energy storage elements of the system have negligible coupling due to controlled bi-directional flow, b) there is a non-linear

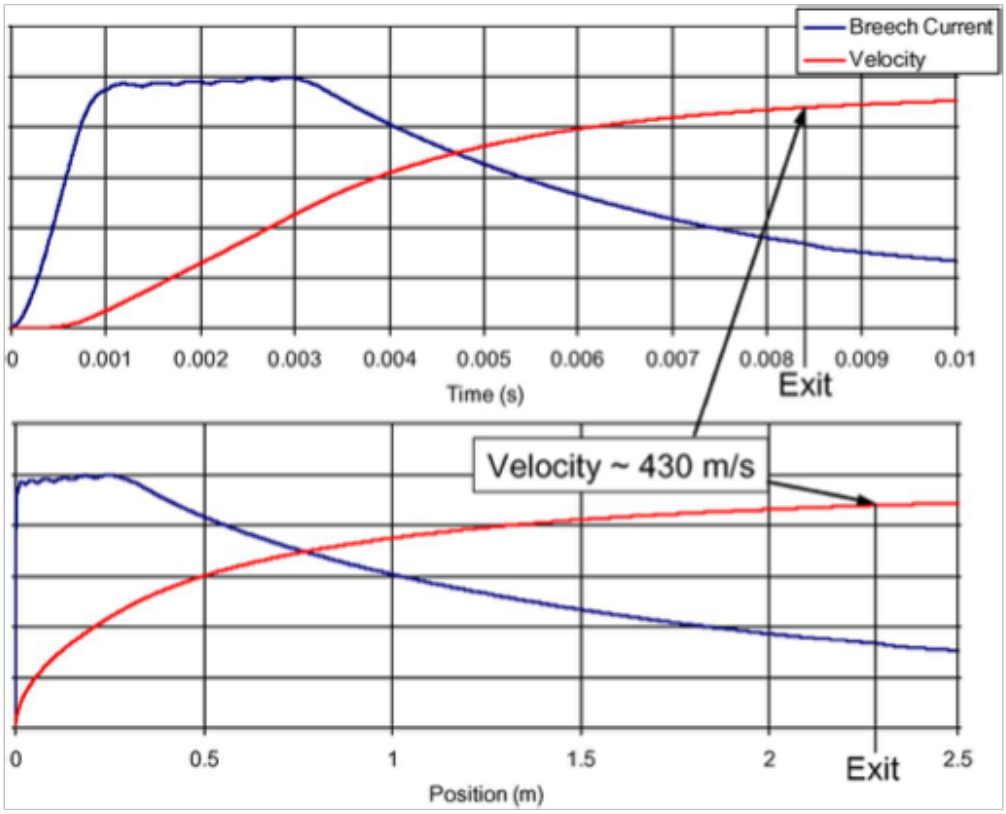

Figure 2.3: IAT Large caliber launcher (LCL) PFN output represented by output with position and output with time [4]

load (purely resistive in this case), and c) there is a capacity to precisely time energy store discharges. A significant difference, however, is that the HPPFN has *non-linear* energy stores. In the next section, the potential for using a SFPFN approach for synthesis of HPPFN pulses is examined in more detail.

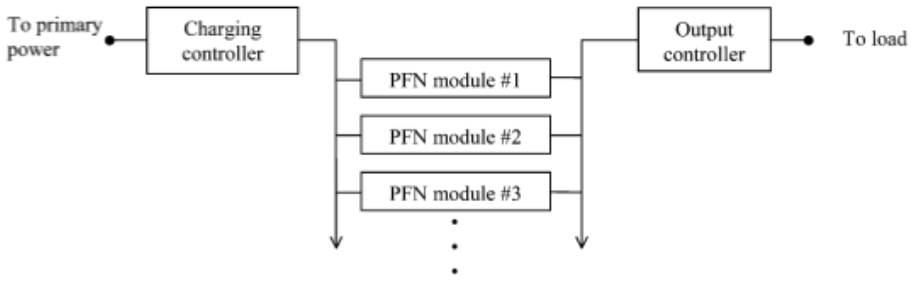

Figure 2.4: PFN block diagram of 20 module system from Engle et al. [7]

.

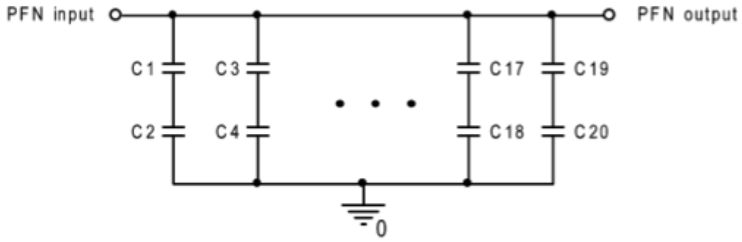

Figure 2.5: PFN module schematic illustrating single PFN module from 2.4 as presented by Engle et al. [7]

.

2.3 Application to hydro-pneumatic domain

The PFN as defined by Glasoe, et al., not only serves as a means for storing energy but also as a pulse shaping element, a means for conditioning the power flowing out of the PFN. Although most if not all of the work done using PFNs has been for sub-millisecond high power electro-magnetic applications, such as those already mentioned, the intent of this research is to investigate the extension and application of these methods to the hydro-mechanical domain. The storage of energy in the fluid-mechanical domain and the corresponding time scale for its release has many practical possible applications, such as the

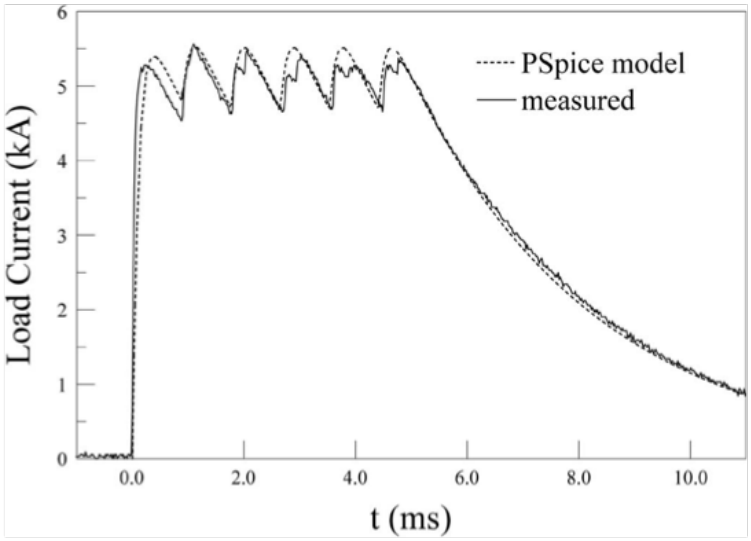

Figure 2.6: SFPFN output of 20 module system from Fig2.4 as presented by Engle et al. [7]

systems that rely on cyclic, duty-cycle-type operation, as mentioned in the introduction. While the proposed use seems conceptually appropriate, there are challenges that need to be overcome.

Although the most basic idea of Guillemin's original PFN theory is used to conceptualize the HPPFN, little can be adopted into the hydro-mechanical energy domain application, due to the highly nonlinear nature of dissipative effects in fluids and pneumatic energy storage elements. On the other hand, it has been shown that a SFPFN synthesis technique has been applied to railgun systems. So, what methods from these SFPFNs can be applied to hydro-mechanical PFN applications? The basic structure of the apparatus proposed in Chapter 1 is replicated by direct analog. This analog construction

has capacitive energy storage elements (hydraulic accumulators) connected in parallel with each other through a manifold which supplies hydraulic power to a load by being discharged in a specified sequence, the purpose of which to create an output power profile of roughly a square or trapezoidal shape as in the original PFNs.

2.3.1 Compressed-Air Energy Storage

To begin the theoretical application of the SFPFN pulse synthesis technique, it is essential to understand the heart of the HPPFN system: the hydraulic accumulator. Energy storage in the accumulator occurs through compression of a captive compressible fluid such as air by an incompressible fluid. For the system of interest, compressed-air energy storage (CAES) enables the PFN to work on time scales of interest for the proposed applications, since the inherent time scale for energy release of CAES is orders of magnitude larger than practical-sized electrical capacitors. This much longer discharge characteristic will make it more suitable as a power supply for loads that have demands lasting seconds and minutes, rather than the millisecond scale required for conventional PFN / SFPFN applications.

Assuming isothermal compression of an ideal gas the energy stored in an accumulator can be derived from the ideal gas law $PV = nRT$ and expressed as,

$$E_{stored} = P_{atm} V_o \ln \frac{V_a}{V_o} \tag{2.1}$$

for a vessel with changing volume and constant molar mass of species. Here

V_o is the pre-charge chamber volume and V_a is the final chamber volume.

Unlike the linear capacitive energy storage element in a conventional PFN, the constitutive relation for CAES is nonlinear, and for assumed adiabatic expansion is modeled by,

$$P_a = \frac{P_o \cdot V_o{}^{\gamma}}{(V_o - V_a)^{\gamma}} \tag{2.2}$$

where P_a is the pre-charge pressure, P_o is the charge pressure, and γ is the ratio of heat capacities, otherwise known as the isentropic expansion factor.

2.3.2 Preliminary results

Because of the similarities in structure between SFPFN systems and the envisioned HPPFN system, a logical conclusion would be that the pulse synthesis method used for SFPFNs may be directly applied to the HPPFN. To test this hypothesis a numerical simulation was developed early on using commercially available software tools.

Simulated experiments were conducted using the Matlab/Simulink with the SimHydraulics module (MathWorks, Inc., Natick, MA). In the preliminary investigation on the feasibility of this class of system, it was important for the primary components to be properly characterized so that the simulation models that would form the foundation of the synthesis method could be verified. The preliminary work sought to characterize a single fluid-mechanical energy storage element in a hypothetical PFN comprised only of linear elements. The linear element was chosen as a spring-type accumulator operating in its linear

region, as shown in Figure 2.7, which is a block diagram model of the system, realized using SimHydraulics.

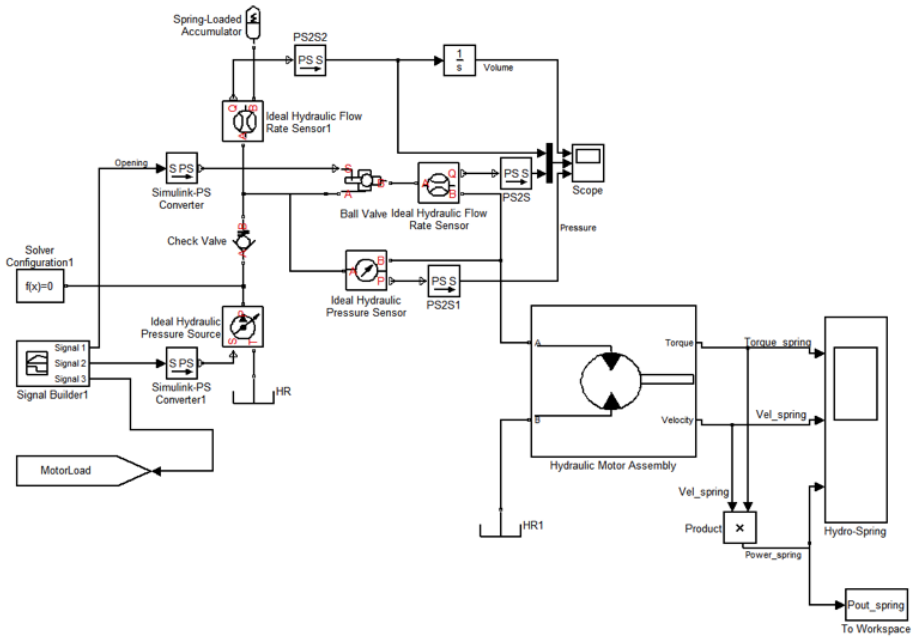

Figure 2.7: Block diagram of in SimHydraulics of a single linear spring accumulator of pre-charge volume V_{pc}. Enlarged version can be seen in Appendix A.1.

A model of the non-linear system was then constructed using a gas / air charged accumulator, Figure 2.8, found in SimHydraulics. By replacing the linear spring accumulator with a gas-charged accumulator, the resulting output could provide a basis for comparing the discharge attributes between the two cases. Results of one such comparison can be seen in Figure 2.9. The aspect of the system that was being compared was how the output differed while keeping the pre-charged volume equivalent between the different accumulators. It was

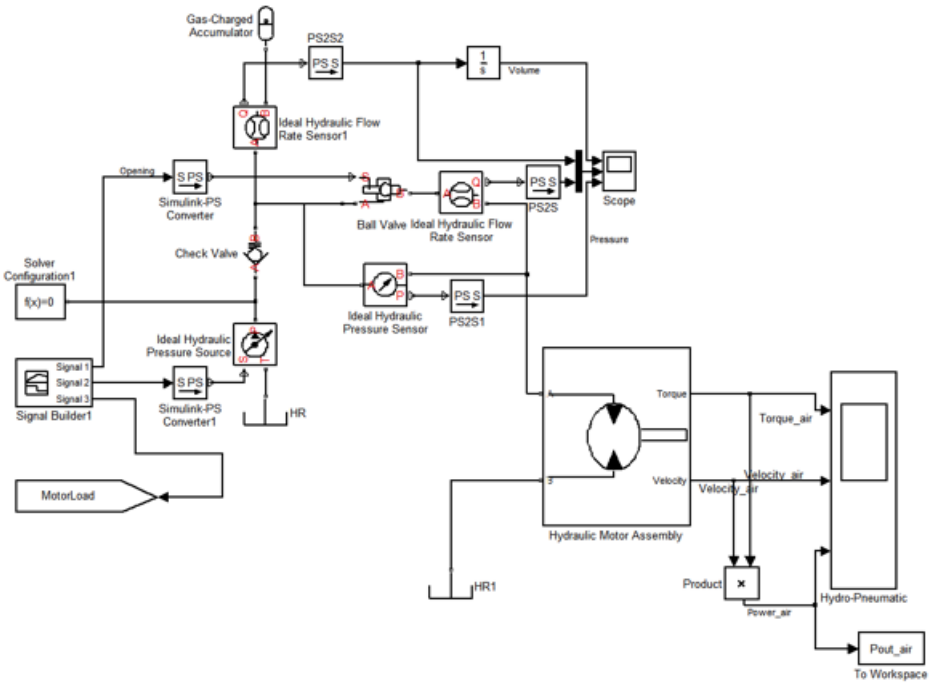

Figure 2.8: Single gas charged (non-linear) accumulator SimHydraulics model using the same pre-charge volume (V_{pc}) as linear accumulator, enlarged version can be seen in Appendix A.2

not surprising that the compressed air accumulator possessed more stored energy and produced higher power output, but what was of interest was the qualitative output.

The motivation for a comparison was to show how similar the output from the non-linear capacitive element (gas-charged accumulator) would be to that from the linear capacitive element (linear spring accumulator). This is the same type of relationship between the linear capacitors and railgun systems that motivated development of the SFPFN synthesis method for the

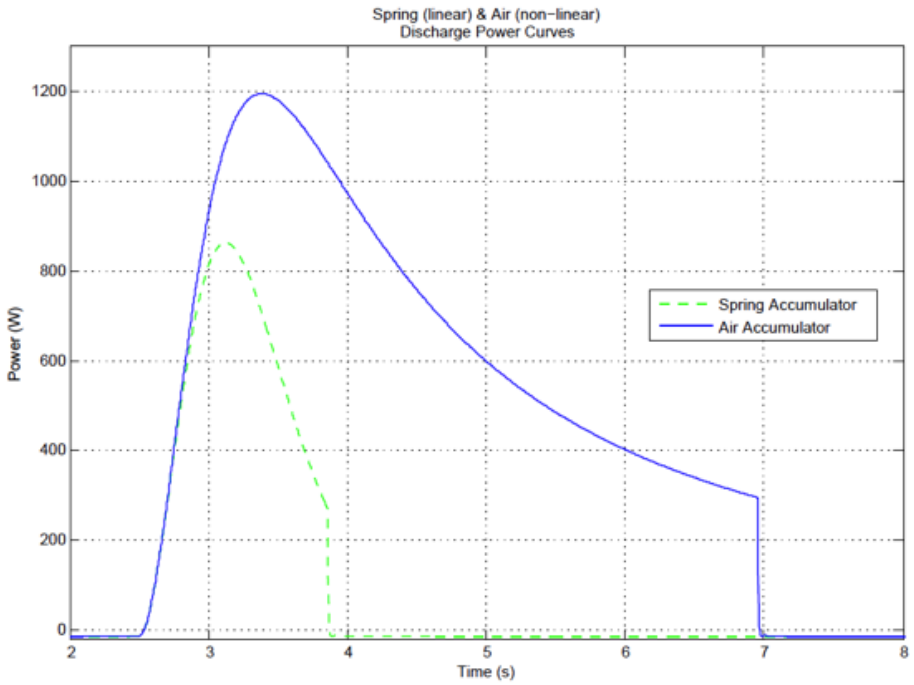

Figure 2.9: Linear accumulator vs. non-linear accumulator output

latter. As expected, the simulation results showed sufficient similarity in the output characteristics, so it was deemed that a fully non-linear SFPFN using a hydro-pneumatic model could be assessed in a model HPPFN.

The non-linear model of the gas-charged accumulator system was then implemented into a system with four such accumulators, and four command time-actuated valves. These were joined to a common pressure manifold in an attempt to form a hydraulic version of a SFPFN. The SimHydraulics block diagram for this system is shown in Figure 2.10. The output of the model was attached to a centrifugal pump model. Initial conditions for the simulation were set so that all accumulators had the same pre-charge pressure and charge

pressure. The only variation between accumulator manifold branches were the valve timings. The output of the overall system were the torque and rotational velocity of the pump, and an operation to multiply the two was used to track the total power output delivered. An iterative simulation method for SFPFN synthesis was applied, and timings were found that gave the pulsed output seen in Figure 2.11. Although using a pre-packaged simulation tool, such as SimHydraulics, provides for a convenient method of constructing prototype systems, it has significant shortcomings which hinder the users understanding of the system, and may imply expected results that may not be realizable in a physical system. The lack of transparency into the derivation of component hydraulic models keeps the user ignorant of the mechanisms that control it's behavior. This is significant when dealing with the highly non-linear behavior of said components.

2.4 Summary

The resulting output from the model developed using the SimHydraulics software showed that it may be possible to implement a real HPPFN physical system. The next step would be to create a bench top system that would prove out the concept with experimental evidence. The next chapter describes the approach taken to design, build and test such a system. The results from this preliminary design study to synthesize a PFN by experiment is used to guide the steps in formulating a more complete synthesis and design approach for a SFPFN realized in the hydro-mechanical domain.

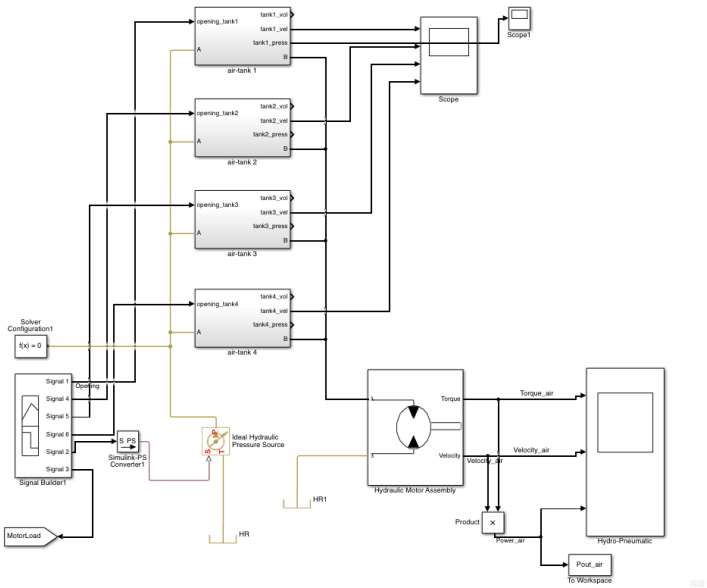

Figure 2.10: SimHydraulics model of SFPFN using four non-linear (gas-charged) accumulators, enlarged version can be seen in Appendix A.3

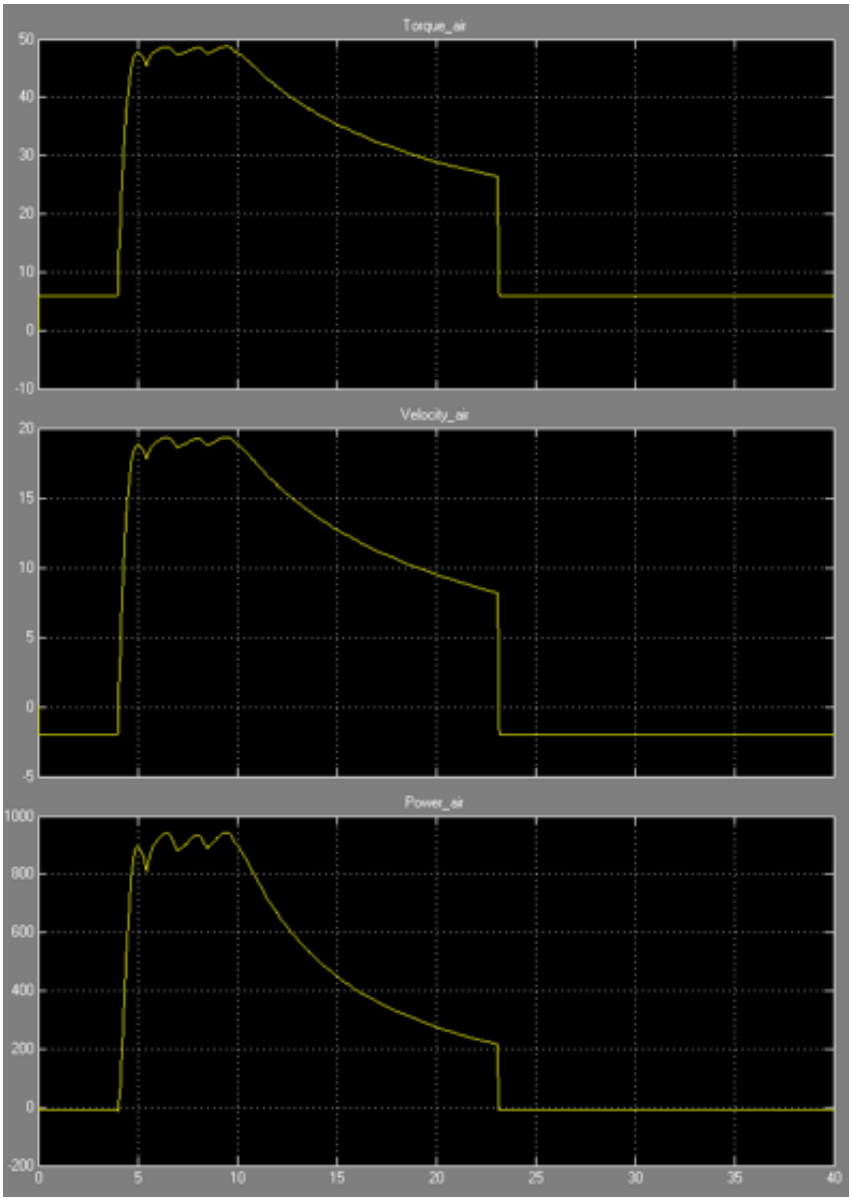

Figure 2.11: SimHydraulics simulation of SFPFN using four non-linear (gas-charged) accumulators

Chapter 3

Experimental Setup

3.1 Testbed

A laboratory testbed was constructed to investigate the feasibility of the HPPFN concept as an energy-storage and power conditioning system. The testbed was constructed primarily using off-the-shelf components, due to budget constraints, but primarily to demonstrate the ability to achieve a low-cost design effectively. All working hydraulic components were low pressure residential and RV grade plumbing fixtures with the exception of the industrial grade solenoid valves and relays. The working hydraulic components were used in conjunction with industrial / scientific grade pressure and flow sensors. Although the resulting apparatus had discharge time scales on the order of seconds rather than minutes as required by the desired applications, it was used to prove out the concept and help develop the framework necessary to design and scale larger more practically sized systems.

There were three versions of the testbed each using the same working hydraulic hardware and primary hydraulic circuit layout. The differences between the versions are presented in the table below:

Testbed version	Hydraulic	Instrumentation	DAQ
V1	Flow meter position	EM flow meter	no change
V2	raised reservoir	no change	no change
V3	accum. needle valve	no change	cRIO w/ FPGA

Table 3.1: Testbed versions

3.2 Flow circuit components

The HPPFN test bed shown, Figure 3.1, is made up of four identical branches. Each branch has a single air bladder accumulator (Shureflow, Model 182-200, 620 ml, see Appendix B.1) connected in fluid parallel, an input supply for filling, and an output branch feeding to a common pressure manifold. The system is fed from and empties into a reservoir, which acts as both the exhaust for the output and the source of fluid for the input pump.

All four accumulators are charged by fluid provided by a single diaphragm pump (Aquatec, Model 5800, 12 gpm, see Appendix B.2) via an input manifold. The pump draws water from the reservoir, which is raised above the average fluid elevation of the system as shown in Figure 3.2. From the manifold inlet, the input flow is distributed to the accumulators via manually actuated valves (1/2" NPT brass ball type) located on each input branch. This gives the ability to control which accumulators are charged and which are excluded, depending on the desired test. This design enabled the isolation of individual lines during testing to characterize losses and individual accumulator charge and discharge characteristics. A check valve (1/2" NPT, brass swing type) is placed just upstream of each ball valve on each input branch.

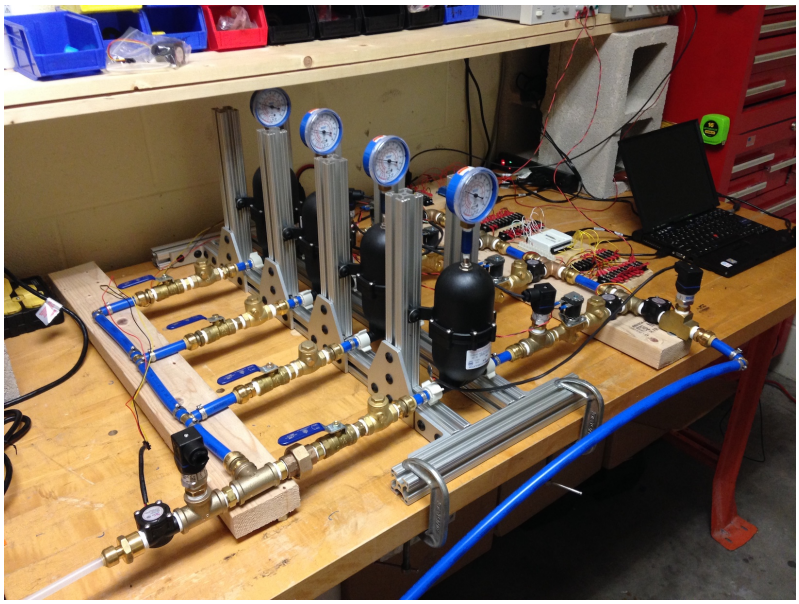

Figure 3.1: Bench-top testbed, charge side

The check valve maintains unidirectional flow, while allowing for all branches to balance pressures so long as their output valves remain closed. The input side manifold is instrumented with only one pressure sensor and one flow meter, since charging is done on a self balancing fluid network, and so it is assumed that the resultant charge pressure will be the same for the entire input manifold once pumping is completed. The input side flow meter allows for health monitoring of the pump and, when coupled with the pressure sensor, can provide a capability to monitor simulated stochastic inputs for total system "round trip" efficiency experiments.

Each accumulator was instrumented with an analog dial type pressure gauge (WIKA, 120 psi range) to aid with setting pre-charge pressure using a manual air pump, and to determine the charge pressure when pumping the

Figure 3.2: Benchtop testbed V2 configuration reservoir and Aquatec pump.

accumulator with water. A concerted effort was made during each test to ensure that initial conditions (charge and pre-charge pressures) were recorded. In the final testbed configuration, each accumulator also had a needle valve on the air bladder input (see Figure 3.4) for the purpose of accurately setting the pre-charge pressure. The intention being to reduce parameter variability. Each of the parallel lines contain check valves on the input side and output side of each accumulator facing the direction of the output to eliminate back flow into any of the accumulators during operation.

Each output branch is constructed as follows: starting at the output of the accumulator, the flow enters a short section of PEX tubing, a 1/2" brass

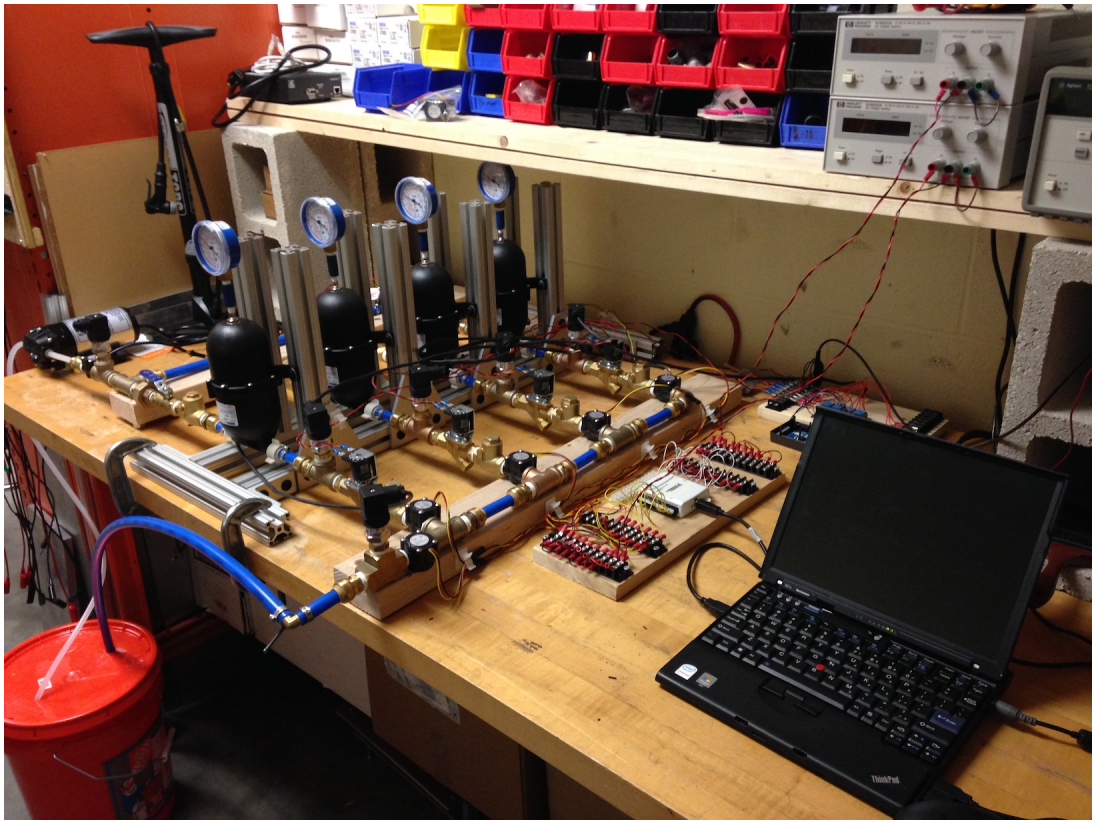

Figure 3.3: Bench-top testbed, discharge side

tee that provides a port for a pressure sensor, a solenoid valve (12V), and then a check valve of the same type as on input supply side. After the check valve, fluid flows through a paddle wheel type flow meter, before entering the manifold. The first branch connects to the manifold via a 1/2" brass 90 degree elbow, while the others via a 1/2" brass T-junction. The manifold is actually formed by interconnecting the brass elbow and T-junctions using PEX tubing (see Figure 3.1). Flow from the manifold then exits into a final paddle wheel and EM flow meter, and pressure sensor, before exiting the system down the

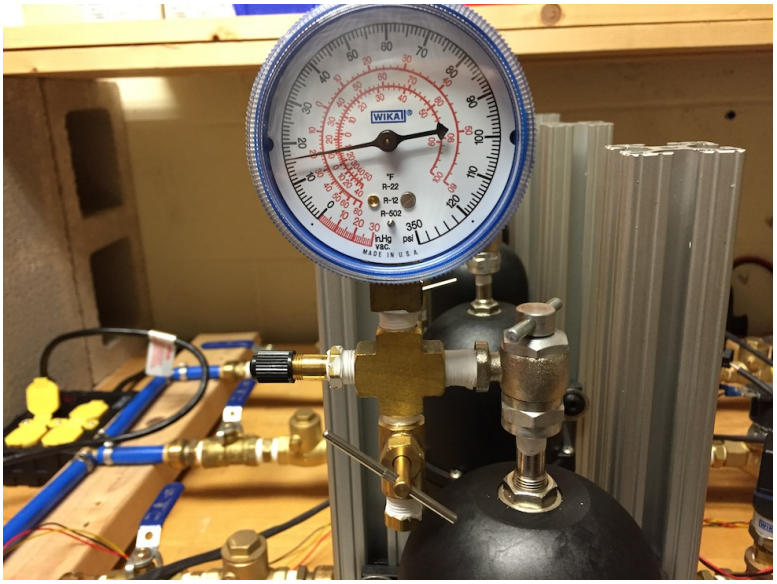

Figure 3.4: Accumulator pressure gauge and bladder needle valve

outlet line to the reservoir.

3.3 Controls

The HPPFN system power output profile is controlled by a timed accumulator discharge sequence, resulting in the superposition of outputs from each branch into the output manifold. This process effectively creates a sequentially-fired pulsed forming network (SFPFN). Timing of the sequential discharges is managed by a programmable micro-controller (Arduino, connected via USB to PC). The micro-controller digital outputs are connected to an array of DC-powered relays, to control opening of the solenoid valves in each of the HPPFN output branches.

During the initial phase of the investigation the determination of a

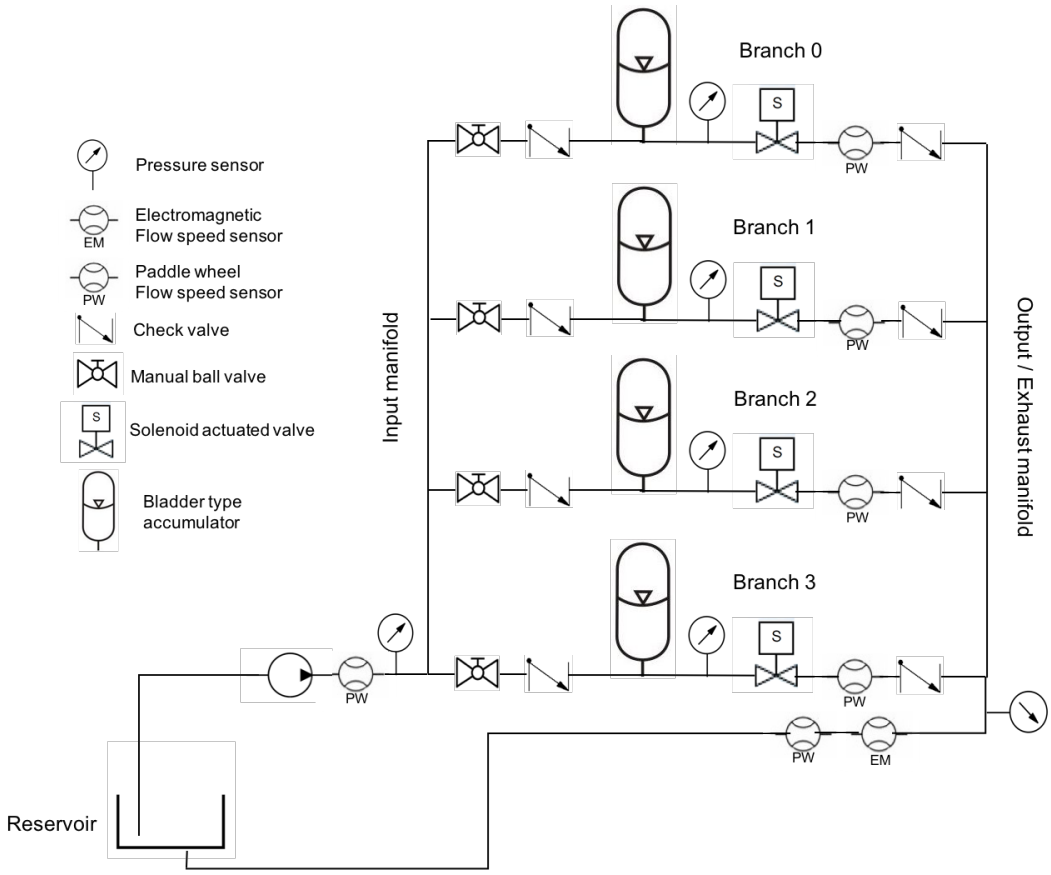

Figure 3.5: Testbed hydraulic schematic

proper timing sequence was accomplished empirically. This involved changing the discharge times in an iterative manner experimentally until a desired output pulse was attained, a process that was rather cumbersome and time consuming. For conventional SFPFNs designed for railgun technology, timing protocols are primarily determined through repetitive simulation of a well-characterized model [7].

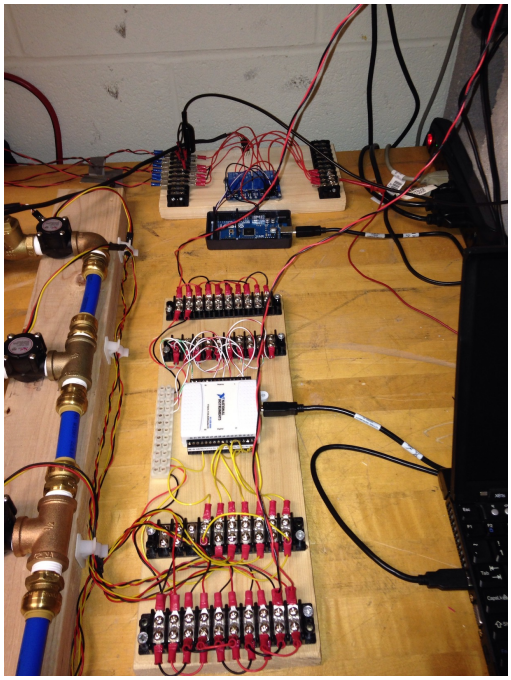

Figure 3.6: Arduino controller, controlled relay switches, and NI USB-6008 DAQ

3.4 Instrumentation and signal processing

The control instrumentation was realized using a low-cost Arduino micro-controller. The experimental testbed was also equipped with instrumentation to monitor HPPFN performance and to aid in conducting model validation studies. Significant effort was dedicated to qualifying sensors that could accurately capture the pulsatile output flow and pressure for each accumulator and for the combined system. The placement and type of sensors were also chosen to support the modeling efforts needed to develop the simulation models needed to design the HPPFN timing sequences. Each of the accumulator output lines are instrumented for both pressure and flow rate at

locations before the flow enters the output manifold, thus each branch is monitored independently. The manifold output is also instrumented for both flow and pressure. The data acquisition instrumentation was chosen to capture the time-varying pressure and flowrate signals from all of the installed sensors.

Data collection was initially conducted by means of a USB-based data acquisition system (National Instruments, Inc., Model NI USB-6008). Analog signals were collected from six pressure sensors (WIKA, model A-10, piezo-resistive type, see Appendix B.5), and digital inputs were used to monitor the digital outputs from six flow meters (e.g., seedstudio.com, G- 1/2", paddle-wheel flow sensors, hall effect type, see Appendix B.4.2). This initial setup was programmed using a virtual instrument (VI) developed in LabVIEW (National Instruments, Inc., Austin, TX). Measurements of the analog signals from the pressure sensors were found to be as expected, and matched with initial model simulation results. The pressure sensor data was consistent from test-to-test as well as in repeated calibration.

On the other hand, collecting digital data from the flow sensors was more problematic. The sensors generated very similar pulsed output profiles from one sensor to the next, however the pulsatile nature of the flow was not as effectively captured, see Figure3.7. This was evident by the rather sluggish output compared to the pressure sensors. An investigation was undertaken to assess whether the presume error was resulting from the flow meter physical response characteristics or from a limitation in the measurement and processing of digital signals from the flow sensor being used. This effort explored: a)

higher frequency response flow meter types, including those capable of analog rather than digital output, and b) pulse counting and averaging algorithms.

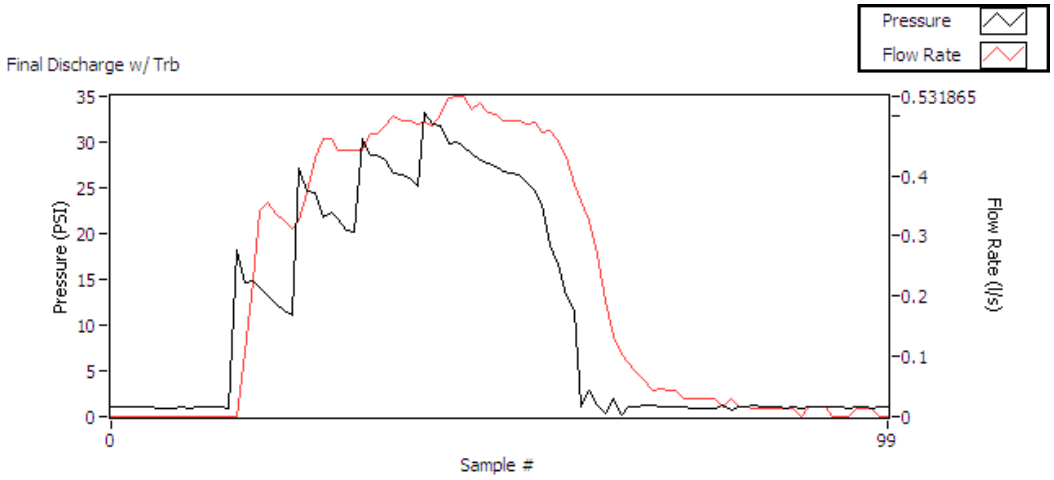

Figure 3.7: Typical output plot for NI, VI for the pressure and flow

The flow sensors that were initially sourced for this project were intentionally chosen due to low-cost and simple construction. To assess whether there was a physical limitation that prevented 'good data', testing was conducted with two additional higher-grade flow sensors that were not based on interaction with the fluid, such as a paddle-wheel or turbine. First, an electromagnetic (EM) non-contact flow meter (Omega Engineering, Inc., FMG-90 series, see Appendix B.4.1) was selected. This type of sensor detects inherent charge in the fluid without any obstruction. A single FMG-90 was installed on the output of the manifold in-line with one of the paddle-wheel flow sensors. Unlike the digital output from the latter, the EM flow meter uses a proprietary D-A converter so that the output signal can be measured using

analog channels. The EM flow meter was placed directly upstream of the paddle-wheel flow meter so that a correlation between the two outputs could be observed with as little physical variation in position as possible. In addition to the EM flow meter, an ultrasonic flow sensor (Transonic Systems, Inc.) was also used for testing. Both of these non-contact/non-obtrusive type sensors had the bandwidth to enable tracking the pulse, however the systems available could not resolve the *peak* of the pulsed flow generated by the HPPFN testbed. While these types of sensors may be suitable given a suitable dynamic range, both the EM flow meter and the ultrasonic flow sensor probe have costs that are at least two and three orders of magnitude higher, respectively, than the paddle-wheel sensor. Fortunately, these sensors revealed that there was a real limitation in the paddle-wheel sensors, and helped focus the investigation into determining whether there was an inherent dynamic response limitation in these sensors or if the problem was arising because of the data acquisition and signal processing that had been initially implemented.

As previously mentioned, the paddle-wheel flow sensors integrated throughout the HPPFN testbed were chosen because they offer a low-cost monitoring solution, especially when coupled with digital I/O on a basic USB data acquisition system. These sensors basically provide a pulsed voltage signal from a hall-effect sensing circuit, where the pulses have a period proportional to the rotational rate of the paddle wheel. There are two concerns that needed to be resolved. First, as long as the paddle wheel faithfully tracks the fluid flow velocity, the dynamic response should be sufficient. There is no manufacturer-

supplied calibration or testing results, and for the most part it is assumed that these sensors are used in steady-state flow conditions. Consequently, there was some concern as to whether the difference between measured flow rates from these sensors and those predicted could be attributed to poor dynamic response. This was reinforced by the fact that the non-contact/non-obtrusive sensors showed that the flow rates in the HPPFN had very high rates of change, similar to model-predicted results. The second concern was that the acquisition and processing of the pulsed-signal was effectively 'low-pass filtering' the pulsed signals. It is necessary to capture the signals at a sufficiently high rate, but then several cycles need to be processed to estimate an instantaneous rate. If these processes are not evaluated fully over the range of operation, there will be significant error in estimating magnitudes and dynamic response of the fluid flow rates.

An extensive period of testing and re-programming of the instrumentation control software eventually led to improved flow rate measurements. This process involved replacing the low-cost USB data acquisition with use of a real-time control platform (National Instruments, NI-cRIO, with field-programmable gate array, FPGA module installed). This change enabled a LabVIEW VI to be developed that improved the capture and counting of pulses by using the on-board FPGA. All flow meter outputs were re-routed to the FPGA instead of the NI USB-6008 DAQ. This reconfiguration proved successful, and was used for the final HPPFN testbed and for subsequent testing for model validation. Results from initial tests are provided in the next

section.

3.5 Preliminary experimental results

Once the initial setup was complete, a set of initial experiments were conducted, in the manner discussed above, to see if a reasonable pulse could be formed and results monitored for use in model validation. At this time and for this class of system, there is no established metric for the determination of pulse quality. However, the following criteria were identified and used as a qualitative basis for evaluation.

1. Evidence of superposition between branch outputs seen at output
2. Depth of gap between discharges seen on system outputs
3. Continuity of flow
4. Qualitative comparison of shape (proportion) with known SFPFN outputs

A set of iterative experiments were conducted to empirically identify a suitable discharge timing sequence capable of forming a reasonable pulse based on the defined criteria. Tests were also conducted to reveal any trends and sensitivities of timing parameters and charge pressures. Experiments conducted during this phase were completed with all accumulators charged to the same pressure and using the first testbed configuration as presented in Table 3.1.

Experimentation revealed a timing sequence that gave a reasonable pulse using the following initial conditions and timing:

Pre-charge	Charge	Discharge Δt
32 psi	60 psi	280 ms

Table 3.2: System initial conditions

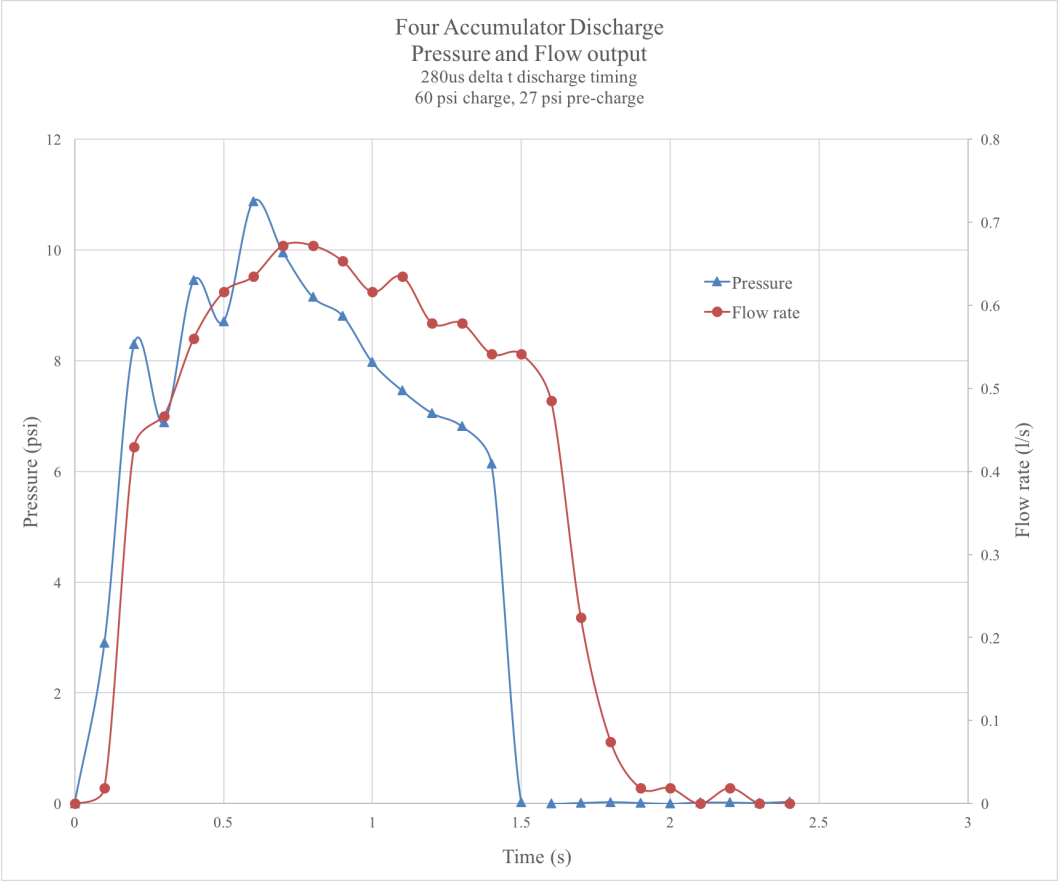

Figure 3.8: Pressure and flow output for 60psi charge pressure with 280us delta t between accumulator discharges

Based on the first three qualitative evaluation criteria, the experimental

output in Figure 3.8 shows good evidence that a proper pulse can be created.

Addressing the final qualitative criteria, a comparison was conducted against demonstrated voltage and current outputs for railgun systems from literature. The experimental pressure output comparison (Figure 3.9) was done with a voltage discharge profile from Cravey et al [3] and showed a much flatter output for an EM system as compared to the experimental HPPFN. Although not perfect, similarities in the rise time, time at amplitude, and decay can be observed. The comparison between the EM SFPFN current output and the HFPFN volumetric flow rate in Figure 3.10(a) is much more favorable.

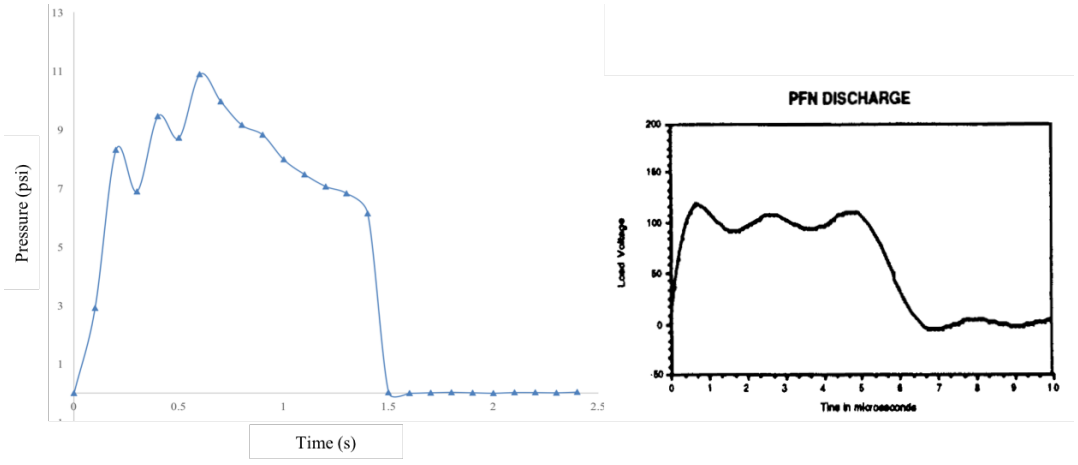

(a) (b)

Figure 3.9: Pressure and Voltage outputs for qualitative comparison: (a) HF-PFN pressure output for 60psi charge, 280us timing, and (b) measured voltage output for a transmission line PFN discharged into a matched load from Cravey et. al [3]

It should be noted that a subsequent change to the setup helped alle-

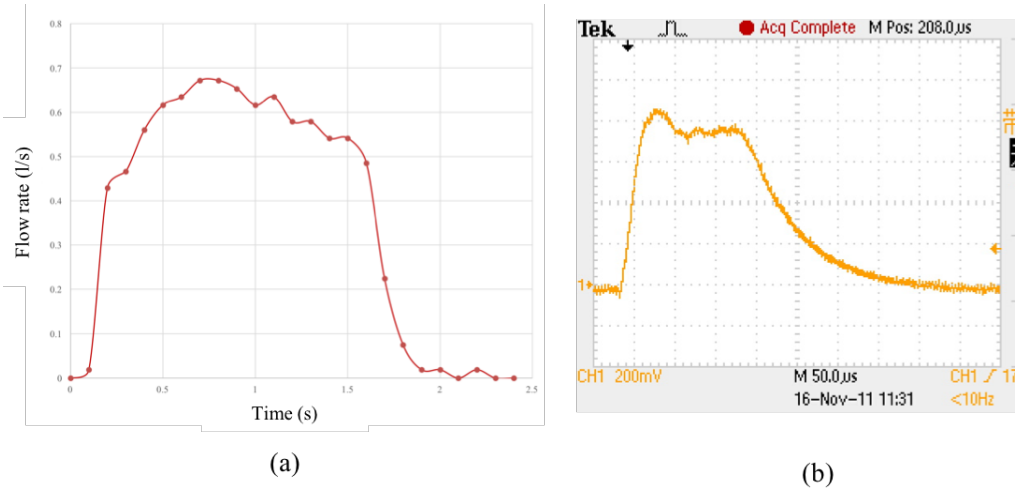

(a) (b)

Figure 3.10: Volumetric flow and current outputs for qualitative comparison: (a) HFPFN flow rate output for 60psi charge, 280us timing, and (b) measured current output for an EM SFPFN from Liu et al. [15]

viate a modeling issue that will be discussed in the following chapter. This was done to change the line initial conditions of the output manifold and exhaust line from being empty of fluid prior to discharge to completely full at all times. This ensures that the system elements are in 'fluid communication' at all times. This was accomplished simply by raising the vertical position of the reservoir tank approximately over the exhaust manifold level, as shown in Figure 3.2.

3.6 Summary

Preliminary experimental results with the experimental HPPFN showed good qualitative comparison with outputs from SFPFNs configured for railgun systems. The results also suggest there is a need to better understand the

system dynamics in a manner that a "canned" simulation tool, such as Matlab/SimHydraulics, does not allow. The inability to adjust certain modeled hydraulic elements in SimHydraulics, the subtleties of the non-linear effects on the system, and the interaction of the flows and their effects on one another, gave motivation to the development of a more fundamentally-based physical system model. The adoption of a bond graph approach enabled development of a model that would allow for better understanding of significant power flows and losses in the system. This type of model development, which provides an ability to experiment with 'structural' model changes and to change key parameters iteratively, is important when developing a new type of system, such as the HPPFN. Insight is gained into which components and associated physical variables influence efficiency and power output, for example. As such, a key goal of this project was enabled through this initial development, that of being able to create a model with sufficient fidelity to guide design, analysis, and sizing of a HPPFN system. The next chapter describes the next steps taken toward this goal.

Chapter 4

Modeling and Analysis

Preliminary proof of concept of the HPPFN system was demonstrated using SimHydraulics® in Matlab/Simulink®. Since SimHydraulics® includes built-in models for components used to form the HPPFN described in the apparatus section, its use facilitated early-stage modeling of the system. Commercial simulation packages are useful in this way since they allow an engineer to simply configure a system using component-level models, provided proper parameterization and initial conditions are specified. Results in Chapter 3 provide reasonable insight, and demonstrated that the HPPFN concept was at least theoretically valid. With these results in hand, an effort was undertaken to fabricate and test a bench-top system to validate the initial model findings. Further, a more fundamental model was deemed essential in order to study how the HPPFN system could be scaled and/or reconfigured for other applications. In combination with the model basis, a validation process was undertaken, beginning with preliminary experiments designed to demonstrate formation of pulses with desired amplitude and duration.

4.1 Modeling Approach

The preliminary models formulated using SimHydraulics® were found to be useful and efficient for quickly assessing the HPPFN concept. However, there are limitations to using these types of off-the-shelf tools. For example, less insight is gained about the role of key components on the response behavior observed experimentally. Also, having less transparency and control over how the system equations are formulated and solved often translates into less understanding about how changes in the system relate to desired system response behavior. For these reasons, a more fundamental approach based on first principles and on bond graph formulation of state space models was adopted[1, 13]. The level of detail required to apply this approach helps build intuition, particularly by using causality to understand component interplay within systems of this type.

Formulation of the HPPFN models was undertaken using the bond graph approach with the work by Dransfield[5] providing specific insight into modeling of hydraulic systems and their control. This was helpful in formulating a model for the logical and sequential operation of the system.

Modeling the HPPFN requires identifying model elements needed to represent the most significant effects in the system. It is clear that certain principle components of the experimental system, such as the bladder type hydraulic accumulator which represents the key energy storage element, must be included. A challenge with these types of high-performance hydraulic systems, however, is to identify and parameterize other elements that are not as

tangible. Various components can introduce inertia and resistive (loss) effects into this system. These model elements then need to be configured as a system representing different configurations studied as part of the HPPFN development. For example, a single accumulator configuration and output branch was used for model tuning and validation. Emphasis was placed on the branch furthest from the HPPFN output, with this branched labeled '0'. Model studies focused on determining what 'model reticulations' best reflected observed experimental data for specified operating conditions (i.e., initial accumulator charge pressure).

The intent of these model studies was to establish a validated 'branch module'. This was possible only by tuning key valve characteristics, for example, which are generally flow dependent. Given this result, the HPPFN hydraulic output circuit can then be confidently formulated, using identical 'tuned branches'. The remainder of this chapter describes this process. It was found that in order to reliably predict discharge phenomena it was necessary to understand proper ways to model joining multiple branch outputs. Hence, manifold junction mass flow theory is discussed, as well as ways to properly sequence the superposition of manifold flows to accurately predict output discharge. These methods were found useful in constructing a model that can be used to represent certain operating events central to HPPFN operation. As such, the model simulation results were found to match key phenomenology evident in the experimental data. The chapter concludes with a description of the model tuning used to match experimental output, and a brief discussion

on the results is presented.

4.2 Simplified branch model

4.2.1 Accumulator model

Accumulators are well-characterized, energy-storage and pressure-conditioning components. A model implementation using bond graphs and particularly in a form useful for predicting the behavior exhibited as part of a pulsed-power network has few references, but a considerable number of non-bond graph references exist for accumulator power systems models. In the text by Dransfield[5], the accumulator bond graph is presented in two manners: a) a simple capacitance model (Figure4.1) and, b) as an RC model (Figure4.1) which incorporates generalized internal losses represented by a resistance R. This accumulator model is based on a gas over liquid accumulator.

Assumptions for the simplified model will be that the system operates under standard temperature and pressure (STP) conditions at all times, all valves actuate as ideal valves, all hose elements are rigid, the fluid (water) is an incompressible Newtonian fluid with linear resistive flow models, the system reservoir is an ideal pressure source, and lastly cavitation never occurs in any part of the system.

Dransfield proposes a generic compliance represented by the bulk modulus of the working fluid which was used for the sake of simplicity as the relation that is presented is linear in nature. However, for the purposes of this investigation, the accumulator compliance is better represented by an ideal

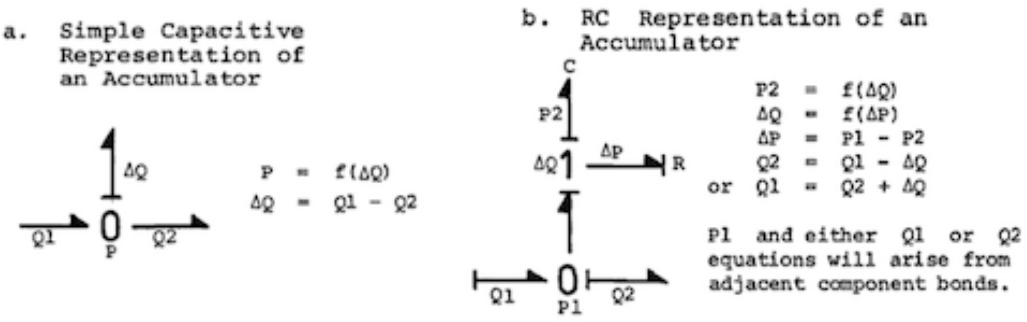

Figure 4.1: Accumulator bond graphs from Dransfield [5]

gas pressure-volume relationship since the majority of the energy stored is in the compression of the air rather than the fluid (water) in the lines or the accumulator. The basic structure of the model takes the form shown in Figure 4.2. It should be noted that the volume that is being tracked in the current case is the air volume and thus the sign convention for the volume will be opposite that of Dransfield who tracks the fluid volume in his model. The simple

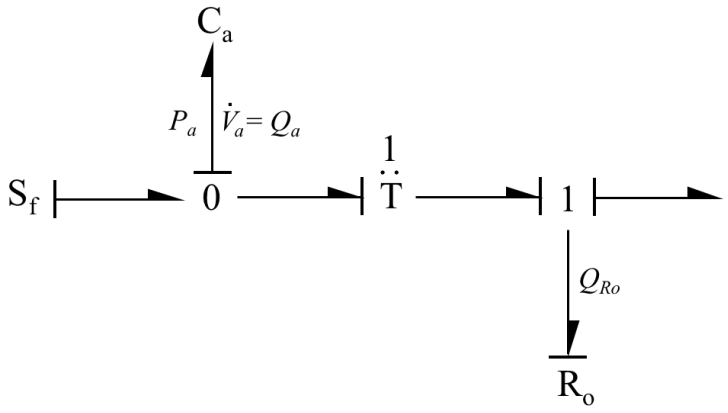

Figure 4.2: Simple hydraulic accumulator BG model

model used Figure 4.2, slightly deviates from the Dransfield representation by

keeping the common effort (zero) junction at the capacitance of Figure4.1 (a) on the RC model in (b). This is done in order to keep the port available for the addition of a flow source S_F, to charge the accumulator as needed. Although unnecessary but for the sake of completeness, a transformer T is added to describe the coupling between the pneumatic and hydraulic fluids. Since the interface between the air and the water in the current case both share the same contact area, the transformer modulus would be the ratio of cross sectional areas, $A_{cs:air}$ / $A_{cs:water} = 1$.

The C_a element represents the capacitance of the air charged accumulator and is expressed by the non-linear constitutive relation, derived from the ideal gas law, by:

$$C_a : P_a(V_a) = \frac{P_o \cdot {V_o}^{\gamma}}{\delta V_a^{\gamma}} \tag{4.1}$$

where V_o is the accumulator pre-charge volume and δV_a is the differential change in accumulator volume V_a expressed as,

$$\delta V_a = (V_o - V_a). \tag{4.2}$$

The solenoid valve used for the bench top has a relatively short operational time constant, on the order of 300 milliseconds. Although it is common to develop valve models with finite time opening characteristics, especially for larger systems (e.g., hydro-mechanical power systems, etc.), it was found that for the HPPFN scale very small variations in opening parameters produced very large effects on the output during model simulations. This made it very

difficult to validate the model. It was found that an *ideal valve assumption* worked very well for the HPPFN model.

Initial testing with a single accumulator branch indicated that when the accumulator is allowed to fully discharge, an additional nonlinear effect is evident that defines two distinct operational modes. When the accumulator has expended all its fluid, there is a 'brake-like' phenomena on the flow, attributed to the rubber bladder. This effect is reflected in the pressure measured in the discharge flow as shown in Figure4.3. The knee in the pressure plot indicates when the bladder elasticity begins to take effect, acting against the momentum of the water evacuating the accumulator. It is postulated that the momentum of the evacuating water tends to 'pull' the bladder away from its unstressed point, possibly into the accumulator outlet orifice.

The limit-state behavior of the nearly evacuated accumulator bladder can be modeled by an effective capacitance, C_b. This capacitance will be represented by the constitutive equation,

$$\begin{aligned} P_b &= (1/C_b)\delta V_b \\ C_b &= 1/k_b \end{aligned} \tag{4.3}$$

where δV_b is the differential change in bladder volume, equivalent to the differential accumulator volume δV_a, and C_b describes the effective capacitance that engages when the bladder enters its limit-state. The pressure-volume relation will be assumed to be linear due to the relatively small deflection encountered. The bond graph shown in Figure 4.4 shows how this element is integrated into the accumulator model.

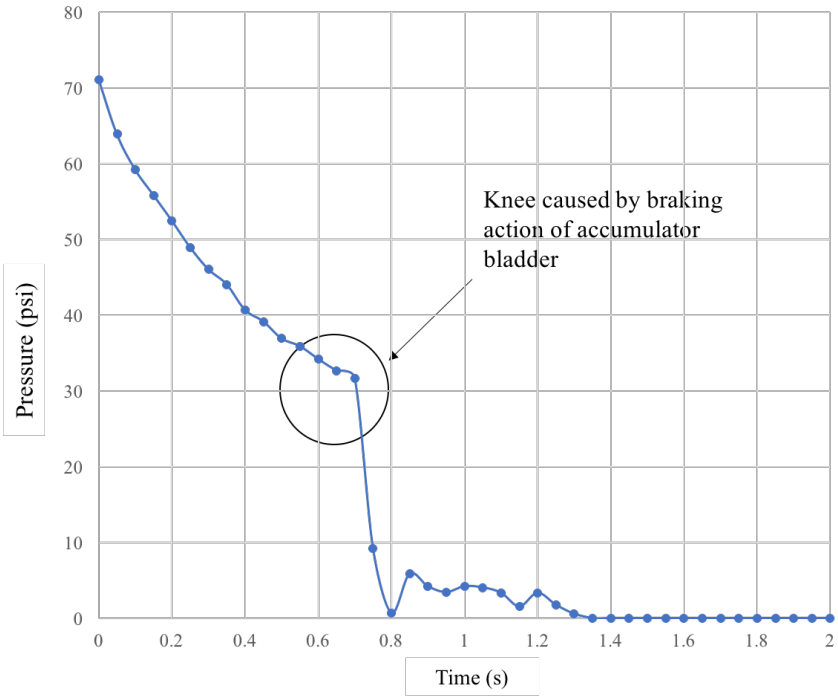

Figure 4.3: Sample experimental data from single branch discharge for pressure sensor P_{ps0} of branch 0.

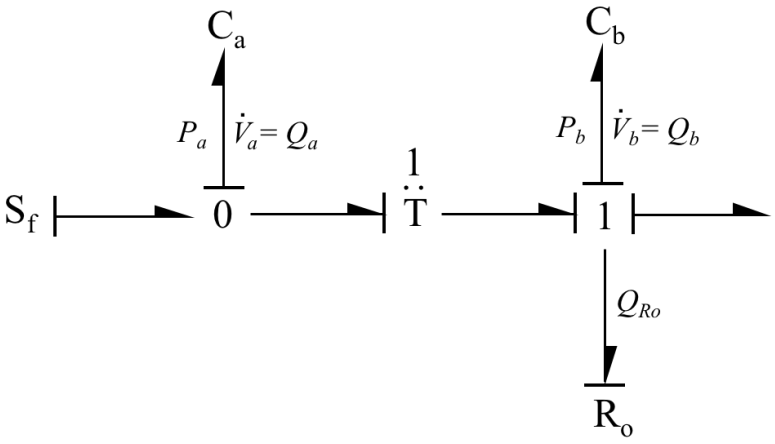

Figure 4.4: Hydraulic accumulator with bladder capacitance BG model

As discussed above the action of the bladder does not effect the system until the accumulator is fully exhausted of water so the bladder capacitance is essentially dormant until this point in the discharge cycle. Implementation of this nonlinear effect is addressed later in a discussion on model sequencing. Care must be taken in introducing this type of effect since it can introduced computational complexity.

4.2.2 Fluid inertia

Due to the aspect ratio of the line, L_{line}/ID_{line}, it is necessary to take into consideration the inertia of the fluid. For a single branch, a single lumped inertia, I_{f0}, is used to represent the sum of I_0, for the fluid in the branch up to the exhaust manifold and I_m, the manifold inertia. The inertia, I_0,

$$I_0 = \rho_{water} \frac{L_{branch}}{A_{CSline}} \tag{4.4}$$

relates the branch output flow and the fluid momentum, γ_0, in the constitutive equation,

$$I_0 : Q_0 = \gamma_0 \frac{A_{CSline}}{\rho_{water}.L_{branch}} \tag{4.5}$$

The second of the two inertias, I_m, represents the inertia of the fluid in the exhaust manifold up to the outlet,

$$I_m = \rho_{water} \frac{L_{manifold}}{A_{CSline}} \tag{4.6}$$

As discussed for the purposes of this developmental simplified model, all fluid inertias are lumped into I_{f0} being represented by:

$$I_{f0} = \rho_{water} \frac{L_{f0}}{A_{CSline}} \tag{4.7}$$

Where L_{f0} is the fluid path length from accumulator outlet to the outlet at the reservoir.

4.2.3 Fluid path resistive effects

For the simple branch model there are resistive effects in the lines that need to be accounted for in the branch model. One represents the hydraulic losses from the outlet of the accumulator to the junction of the branch and the exhaust manifold, and another from this junction to the exhaust manifold outlet. The overall pressure drop is commonly associated with a total 'head' losses, for example,

$$H_{total} = \sum_{1}^{n} H_n \tag{4.8}$$

so that,

$$P_R = H_R \cdot \rho \cdot g \tag{4.9}$$

The flow factors K_n presented here are those corresponding to the laminar flow regime. Generally, these models for fluid losses should consider whether the flow is turbulent and change head loss coefficients accordingly. However, in this case, these losses are not as significant as those due to the valves and junctions. This head loss form is convenient because it allows additional effects from other components to now be integrated in a lumped form, by considering each effect separately. Referencing Figure 4.5, the net branch resistive effects include head losses due to the following effects:

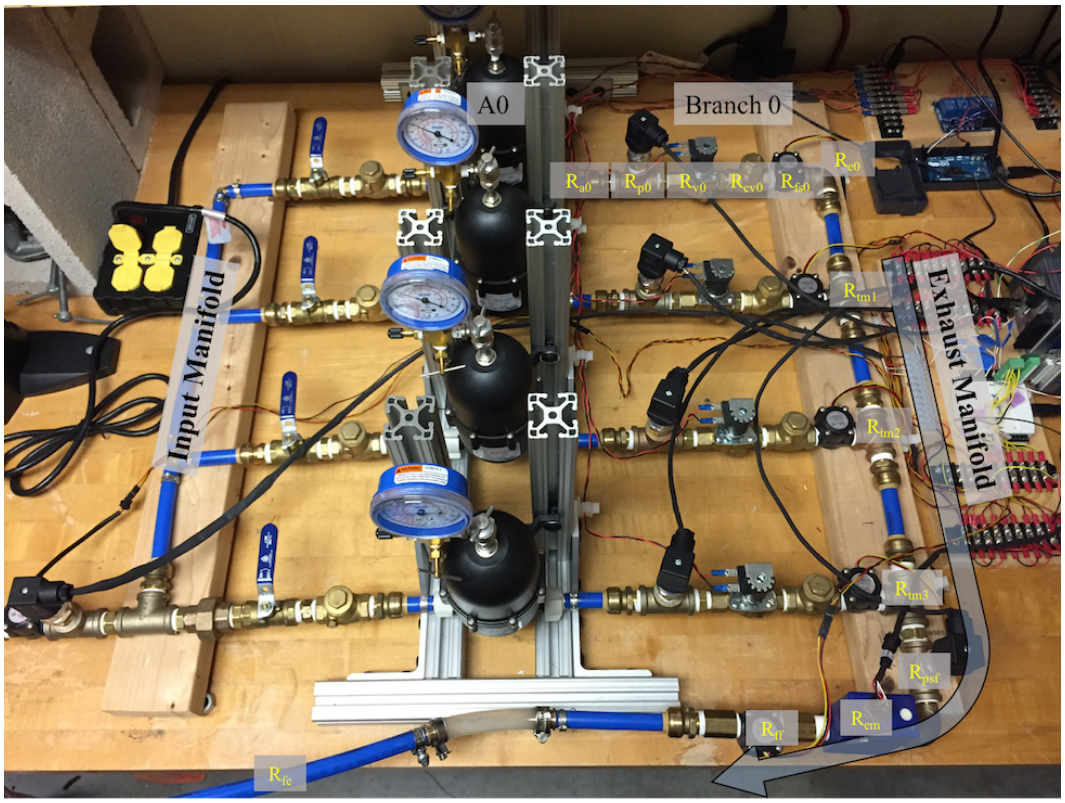

Figure 4.5: Bench top system with resistive elements labeled for branch 0 model

1. Accumulator outlet head loss expressed by:

$$H_{ra0} = \frac{K_{pe} \cdot Q_{a0}^2}{2g \cdot A_{ae}} \tag{4.10}$$

where, K_{pe} is the flow factor for an outlet orifice, Q_{a0} is the flow rate out of the accumulator and, A_{ae} is the accumulator outlet orifice cross sectional area.

2. 1/2" brass tee housing pressure sensor head loss expressed by:

$$H_{p0} = \frac{K_{p0} \cdot Q_{a0}^2}{2g \cdot A_{pex}} \tag{4.11}$$

where, K_{p0} is the flow factor for brass tee, Q_{a0} is the flow rate out of the accumulator and, A_{pex} is the inner cross sectional area of the branch (PEX line).

3. 1/2" brass solenoid control valve head loss expressed by:

$$H_{v0} = \frac{K_{v0} \cdot Q_{a0}^2}{2g \cdot A_{pex}} \tag{4.12}$$

where, K_{v0} is the flow factor for a brass gate valve.

4. 1/2" Gate type check valve head losses expressed by:

$$H_{cv0} = \frac{K_{cv0} \cdot Q_{a0}^2}{2g \cdot A_{pex}} \tag{4.13}$$

where, K_{cv0} is the flow factor for a brass gate type check valve.

5. 1/2" port paddle wheel flow sensor head losses (estimate):

$$H_{fs0} = \frac{K_{fs0} \cdot Q_{a0}^2}{2g \cdot A_{pex}} \tag{4.14}$$

where, K_{fs0} is the flow factor for the paddle wheel flow sensor.

Thus the lumped resistance R_0 is comprised of the sum of the headlosses in the branch given by:

$$H_{r0} = H_{ra0} + H_{p0} + H_{v0} + H_{cv0} + H_{fs0} \tag{4.15}$$

The pressure drop due to resistive losses can now be expressed as,

$$R_0 : P_{r0} = H_{r0} \cdot \rho \cdot g \tag{4.16}$$

Similarly, the second lumped resistive element R_m represents the fitting, instrument, line, and exhaust losses of the exhaust manifold. These are all losses from the end of branch 0 to the outlet of the exhaust manifold and is based on the sum of the head losses given by the following:

$$H_{rm} = H_{e0} + H_{tm1} + H_{tm2} + H_{tm3} + H_{psf} + H_{ef} \tag{4.17}$$

Where H_{e0}, H_{tm1}, H_{tm2}, H_{tm3}, H_{psf} and, H_{ef} represent the fitting losses for the tee junctions and elbows on the manifold. Using this equation we can express the pressure drop due to resistive losses in the exhaust manifold as,

$$R_m : P_{rm} = H_{rm} \cdot \rho \cdot g \tag{4.18}$$

Finally, the last resistance element, is the exit resistance expressed as,

$$R_e : P_{re} = H_{re} \cdot \rho \cdot g \tag{4.19}$$

where H_{re} is the headloss along the section just downstream of the exhaust manifold outlet pressure sensor to the outlet orifice in the reservoir and is represented by:

$$H_{re} = H_{ef} + H_{em} + H_{ff} + H_{fe} \tag{4.20}$$

Where H_{em}, H_{ff} and, H_{fe} represent the flow meter fitting losses and exit loss respectively.

4.2.4 Sensor model junctions

To better compare simulation with experimental output, it is useful to identify ideal junctions at points in the system where sensors are placed.

For example, two pressure sensors can be modeled ideally by drawing a signal bond from a common effort junction. Although not necessary, these 'sensor junctions' allow for a much more direct correlation between the model variables and experimentally measured signals.

The two port variables introduced for the HPPFN include P_{s0}, the pressure sensor output for accumulator branch, and P_{sf}, the exhaust manifold outlet pressure sensor. These two output pressure signals are used in model verification as well as in tuning flow resistance parameters in a much more effective manner.

4.2.5 Simple branch Bond graph model

Now that the components of the simplified branch model have been identified the bond graph for the single branch system takes the form given in Figure 4.6. Two forms are shown in this figure, the latter indicating the effect of the bladder for cases where the accumulators are driven to a limit state.

4.2.6 Simple branch model state equations

The state equations are derived following standard bond graph methods [1, 13]. Beginning with the first bond graph configuration representing the system without the bladder influence, Figure 4.6(a), we recognize that there are two states in the system,

$$x = \begin{bmatrix} v_{a0} \\ \gamma_{f0} \end{bmatrix} \tag{4.21}$$

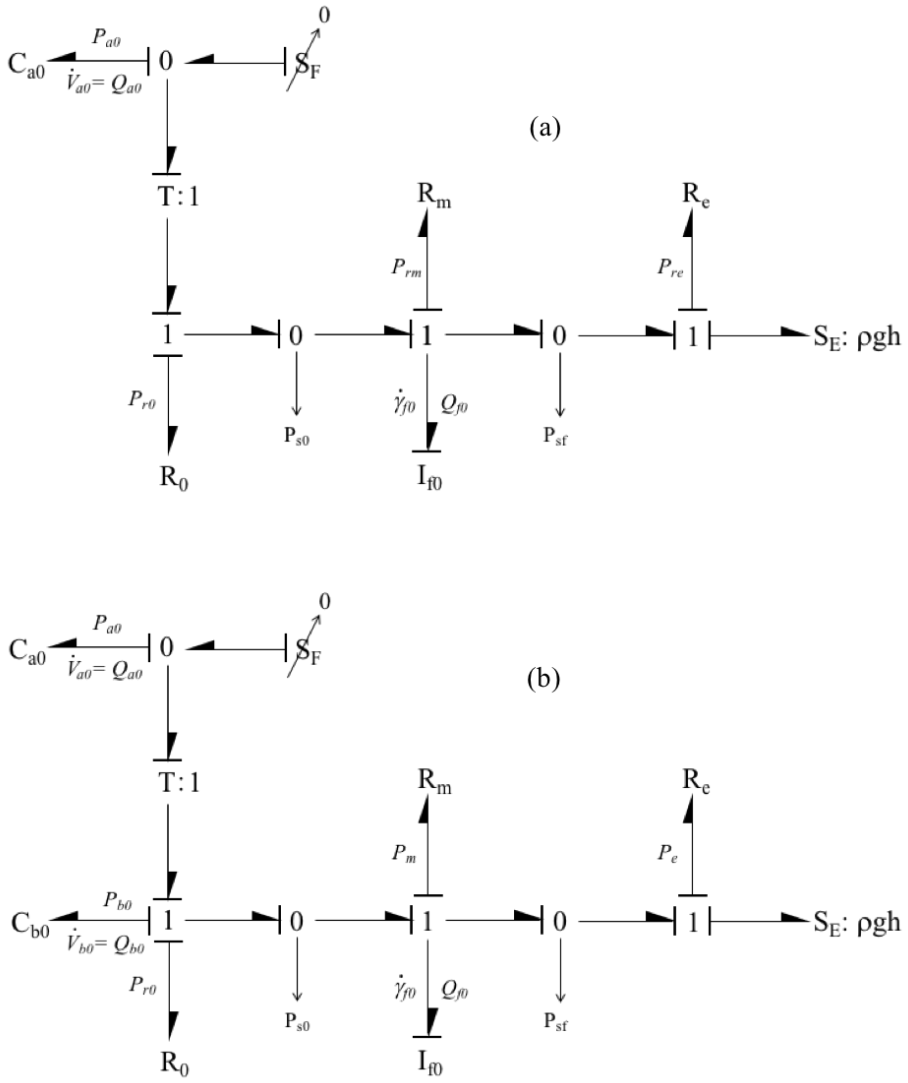

Figure 4.6: Bond graph of simple branch model, (a) without bladder capacitance, (b) with bladder compliance

where v_{a0} is the state variable, representing the accumulator's differential volume and γ_{f0} is the state variable for the fluid momentum. The resulting state

equations are,

$$C_{a0} : \dot{v}_{a0} = Q_{a0} = Q_{f0} = \gamma_{f0} \cdot \frac{\rho_{h_2o} \cdot A_{pex}}{L_{f0}} \tag{4.22}$$

$$I_{f0} : \dot{\gamma}_{f0} = P_{a0} - P_{r0} - P_{rm} - P_{re} - P_{se} \tag{4.23}$$

where,

$$\begin{aligned} P_{a0} &= P_{c0} \cdot \frac{{v_{c0}}^{\gamma}}{{v_{a0}}^{\gamma}} \\ P_{r0} &= H_{r0} \cdot \rho_{h_2o} \cdot g \\ P_{rm} &= H_r m \cdot \rho_{h_2o} \cdot g \\ P_{re} &= H_{re} \cdot \rho_{h_2o} \cdot g \end{aligned} \tag{4.24}$$

In these equations, L_{f0} is the path length of the flow from accumulator to outlet, P_{c0} and v_{c0} are as defined in section 4.2.1, and the head losses H_{r0}, H_{rm}, and H_{re} are as defined in section 4.2.3. The head losses presented are inter-related to the momentum state γ_{f0} in so much as increasing the fluid momentum will also increase the pressure head loss and in turn work against the momentum. This is evident in the pressure sum given in the state equation for γ_{f0}. The final form of the state equations are:

$$\begin{bmatrix} \dot{v}_{a0} \\ \dot{\gamma}_{f0} \end{bmatrix} = \begin{bmatrix} \gamma_{f0} \cdot \frac{\rho_{h_2o} \cdot A_{pex}}{L_{f0}} \\ P_{c0} \cdot \frac{{v_{c0}}^{\gamma}}{{v_{a0}}^{\gamma}} + (H_{r0} + H_{rm} + H_{re}) \cdot \rho_{h_2o} \cdot g \end{bmatrix} \tag{4.25}$$

As previously stated, the instant the accumulator has fully discharged, i.e. when $v_{a0} = v_{c0}$, the bladder begins to influence the flow and the bond graph of the system now changes to include the capacitive storage of the bladder as seen in Figure 4.6b, adding one more storage element to the system, giving

the following new set of states:

$$\mathbf{x} = \begin{bmatrix} v_{a0} \\ v_{b0} \\ \gamma_{f0} \end{bmatrix} \tag{4.26}$$

Following the same procedure used to derive the state equations for bond graph of system (a) gives the following,

$$C_{a0} : \dot{v}_{a0} = Q_{a0} = Q_{f0} = \gamma_{f0} \cdot \frac{\rho_{h_2o} \cdot A_{pex}}{L_{f0}} \tag{4.27}$$

$$C_{b0} : \dot{v}_{b0} = Q_{a0} = Q_{f0} = \gamma_{f0} \cdot \frac{\rho_{h_2o} \cdot A_{pex}}{L_{f0}} \tag{4.28}$$

$$I_{f0} : \dot{\gamma}_{f0} = P_{a0} - P_{b0} - P_{r0} - P_{rm} - P_{re} - P_{se} \tag{4.29}$$

$$\begin{aligned} P_{a0} &= P_{c0} \cdot \frac{{v_{c0}}^{\gamma}}{{v_{a0}}^{\gamma}} \\ P_{b0} &= k_{b0} \cdot v_{b0} \\ P_{r0} &= H_{r0} \cdot \rho_{h_2o} \cdot g \\ P_{rm} &= H_r m \cdot \rho_{h_2o} \cdot g \\ P_{re} &= H_{re} \cdot \rho_{h_2o} \cdot g \end{aligned} \tag{4.30}$$

The final form of the state equation for this mode is,

$$\begin{bmatrix} \dot{v}_{a0} \\ \dot{v}_{b0} \\ \dot{\gamma}_{f0} \end{bmatrix} = \begin{bmatrix} \gamma_{f0} \cdot \frac{\rho_{h_2o} \cdot A_{pex}}{L_{f0}} \\ \gamma_{f0} \cdot \frac{\rho_{h_2o} \cdot A_{pex}}{L_{f0}} \\ P_{c0} \cdot \frac{{v_{c0}}^{\gamma}}{{v_{a0}}^{\gamma}} + k_{b0} \cdot v_{b0} + (H_{r0} + H_{rm} + H_{re}) \cdot \rho_{h_2o} \cdot g \end{bmatrix} \tag{4.31}$$

Where the head losses here are once again related to the momentum variable as described in the previous derivation.

4.2.7 Simulation with mode change

A simulation code was developed with a 'mode' change to capture the two distinct models in Figure 4.6. An alternative approach is to use a single, nonlinear model for the bladder limit-state, however, such a model can introduced significant computational stiffness. For this reason, an event-based simulation was developed that switches between models based on predetermined events or triggers. These events are usually state variables that are tracked as the simulation runs. Once the a condition is satisfied, the simulation is paused and a new model is used in the simulation with specified initial conditions (passed from the previous model to satisfy energy constraints, for example). This event-based simulation code was used for model testing and tuning as described in the following.

4.2.8 Simple model tuning

An arbitrary operating point was chosen that fell within the acceptable operating parameters of the accumulator. The operating point was chosen as an accumulator pre-charge pressure of $P_0 = 35$ psi, and an accumulator charge pressure of $P_{c0} = 70$ psi (gauge). These operating conditions represent the average operating parameters for several experiments, due to measurement error during charging of the accumulator. This error was approximately ± 3 psi. Using the valves on the input manifold to isolate the chosen branch (branch 0) allowed only the accumulator of branch 0 to be charged and discharged. Using this isolated branch, multiple experiments were conducted to get an average

value output for the operating condition chosen.

The two-stage model was simulated, replicating the experimental operating conditions. A built-in Matlab solver using events options was used for these simulation studies. A principal goal of these simulation tests was to determine the unknown bladder compliance C_b and the unknown fluid line resistance terms. Each resistance value was assigned a scaling parameter to be tuned. These scaling factors gave an indication as to how much the lumped resistance approximations were off once the model had been tuned. Tuning was accomplished by iteratively changing one tuning parameter at a time. Changing one parameter at a time provided insight into its effect and sensitivity on the system. By focusing on a single branch in this way, it was possible to determine the parameters through successive iterations, without relying on more complex parameter fitting algorithms. It was hypothesized that the remaining lines could be parameterized using the same values found for the test branch.

4.2.9 Tuning parameter sensitivities

To investigate the tuning parameter sensitivities an approach was taken to methodically change only one variable at a time during numerical excursions, while keeping the initial conditions the same. The tuning parameter that had the greatest sensitivity to changing the shape characteristic of the system output was the bladder stiffness, C_b. This parameter had the effect of increasing the negative slope of the second stage output (after the knee) in the simulated pressure output. The higher the value lower compliance, the

lower the slope value. This trend agrees with the assumption that the bladder acts to retard the inertia of the system during the second stage (i.e., when the bladder engages).

The lumped branch flow resistance parameter, R_0, had the effect of moving the position of the knee with time and amplitude. Increasing the R_0 scaling parameter moves the knee of the discharge to the right (delays) and decreases the amplitude of the simulated pressure. Decreasing the scaling parameter has the opposite effect. Additionally, there is an effect of drawing-in the middle of the first stage output curve in the manner demonstrated in Figure 4.7. During model tuning this variable proved to be most useful for coarse tuning the knee position in time and its amplitude.

The lumped manifold flow resistance parameter, R_m, had a similar effect as R_0 on the knee position in time, with increasing scaling parameter. In contrast this parameter had a much smaller influence on the amplitude at which the knee occurred than did R_0. Of the three resistive tuning parameters, R_m had the least influence on the output of the simulation corresponding to the branch pressure as would be measured by its' pressure sensor port. It did however have a much greater influence on the exhaust manifold outlet pressure as seen on the second row of Figure 4.8. Increasing the scaling factor had the effect of dropping the magnitude of the discharge pressure.

The final of the three resistance parameters, R_e, showed negligible effect on the pressure output corresponding to the position of branch 0 pressure sensor. The output pressure did show evidence of influence by an increased

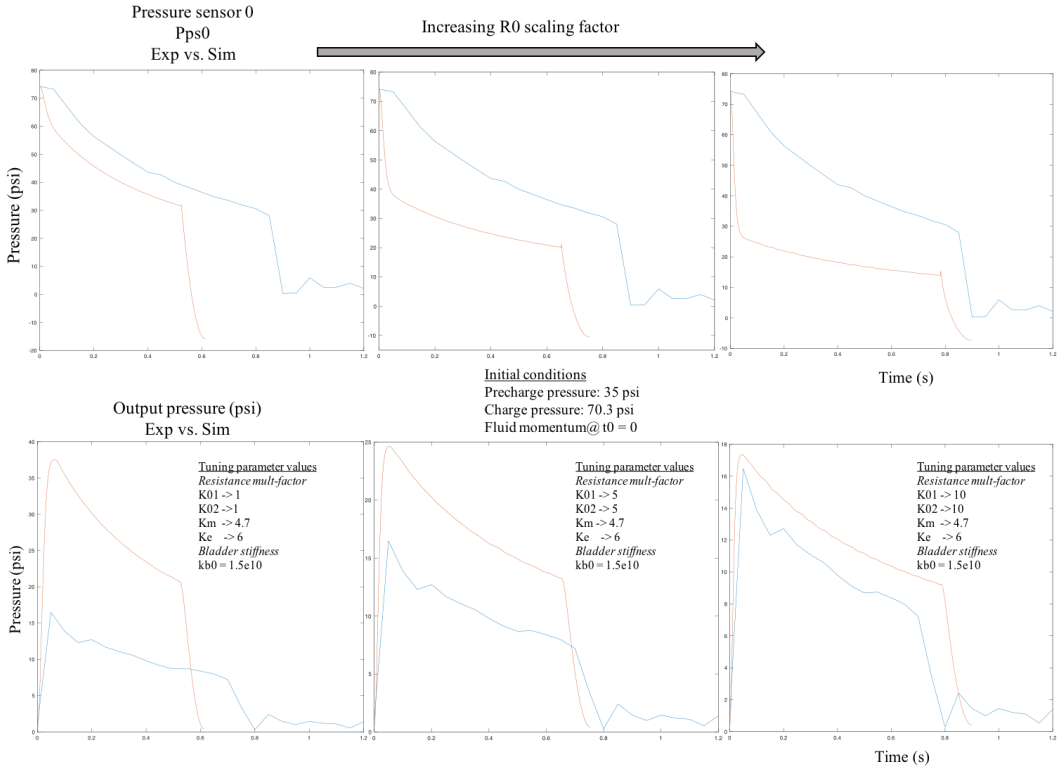

Figure 4.7: Model sensitivity to R_0, red trace is simulation and blue is experimental

scaling factor causing an increase in peak pressure, as seen in Figure 4.9. This later proved to be the tuning parameter that was most useful for fine tuning the output pressure curve.

4.3 Extended single-branch model

Given a reliable and validated modeling basis for a single branch, it can be used to model a multi-branch HPPFN system. For the experimental HPPFN, this is accomplished by adding identical line sections to more ac-

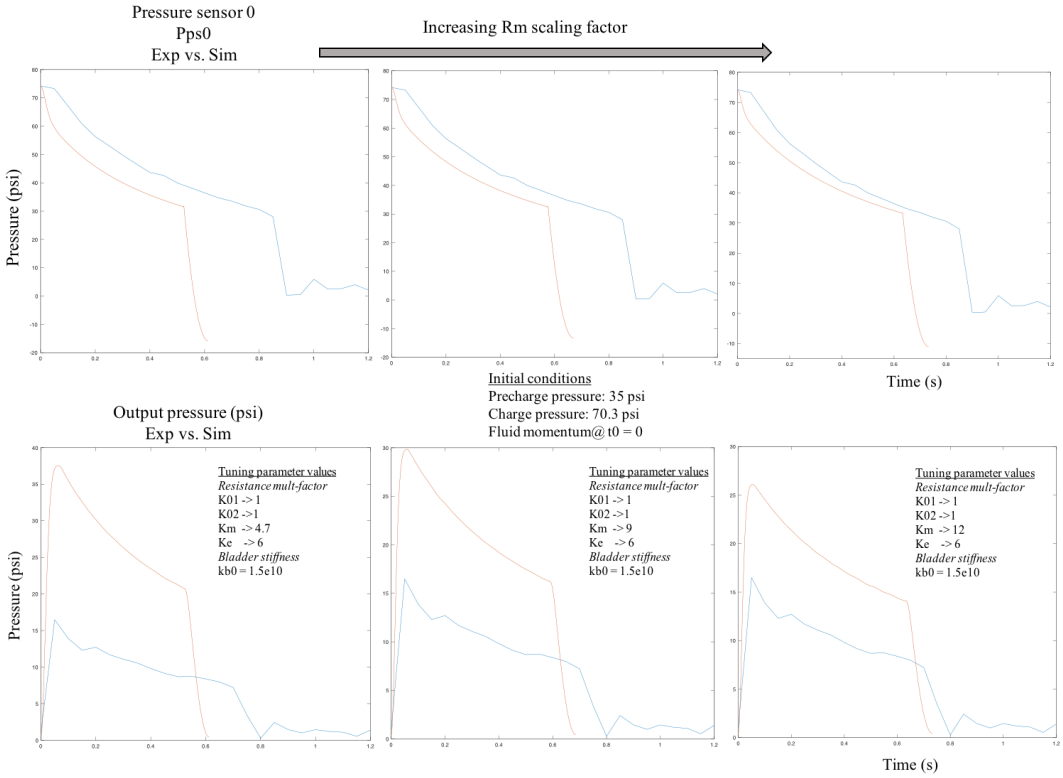

Figure 4.8: Model sensitivity to R_m, red trace is simulation and blue is experimental

curately represent the other three accumulator branch models. The goal is to form a composite model with the ability to simulate the key physical effects and sequence of events that accurately represent the dynamic fluid and mechanical interactions of the HPPFN system.

The assumptions for the composite model are the same as those used for the simple model, namely that all valves actuate ideally, each line of fluid (water) is assumed to be an incompressible Newtonian fluid flowing in rigid pipes, the system is operated under STP conditions, and the reservoir is modeled as

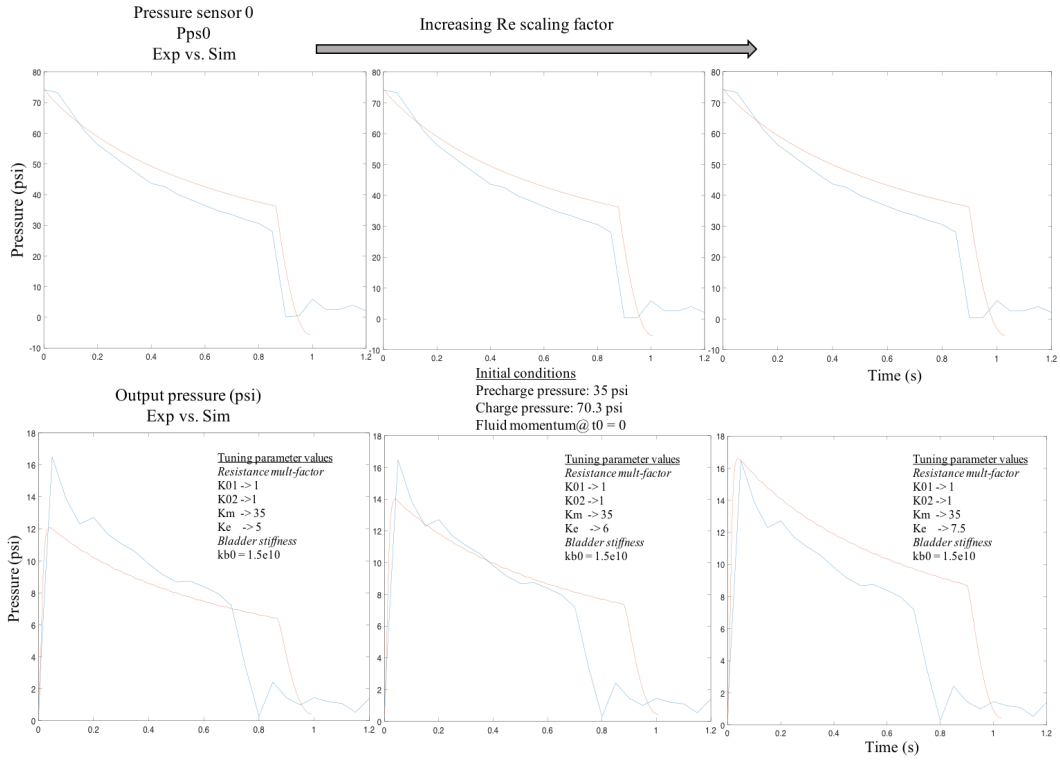

Figure 4.9: Model sensitivity to R_e, red trace is simulation and blue is experimental

an ideal effort source.

Using the simple branch model as a basis for branch 0, an *exhaust manifold* is now represented explicitly by five sections which correspond to four exhaust manifold sections and a final fluid line running from the manifold to the reservoir. As in the simple model, signal ports represent outputs from testbed pressure sensors used for comparisons with model simulation results. The composite model also operates in two modes, the first mode being without the influence of the bladder capacitance, and the second mode with the bladder

capacitance engaged. The condition for the mode switch is the instant when the final accumulator is evacuated of all water. It should also be noted that I_{f0} from the simple model is now split into two distinct fluid inertias, with fluid inertia associated with the manifold, I_m, now in derivative causality in the composite model. The bond graphs for the first and second modes are as shown in Figures 4.10 and Figure 4.11, respectively.

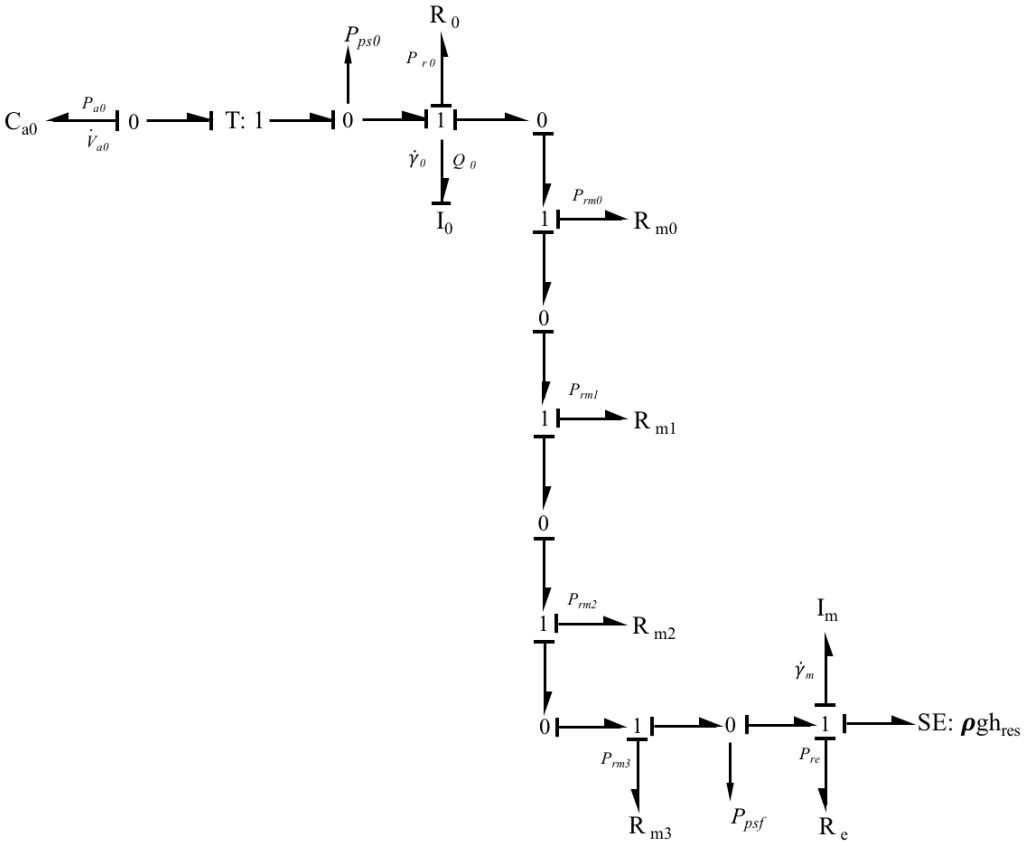

Figure 4.10: First mode extended branch 0 bond graph model

Beginning with the first mode and recognizing the storage elements in

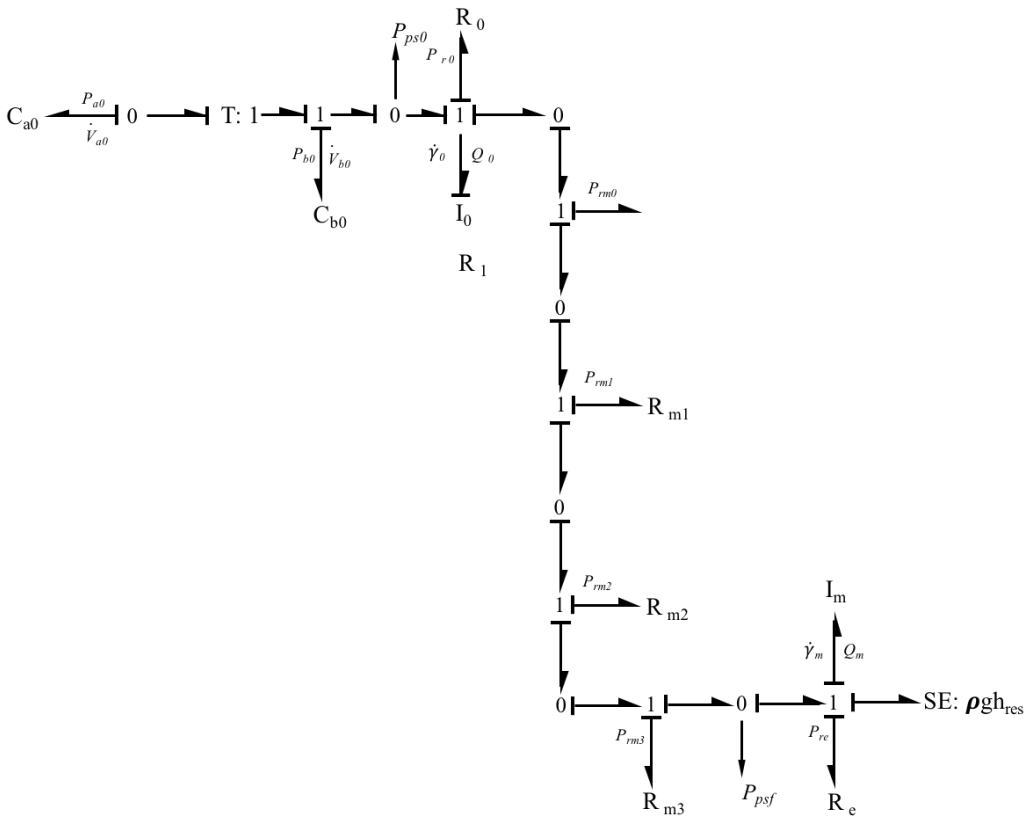

Figure 4.11: Second mode extended branch 0 bond graph model

the system, gives only two states (detailed derivation available in Appendix C.1),

$$x = \begin{bmatrix} v_{a0} \\ \gamma_0 \end{bmatrix} \tag{4.32}$$

Following standard formulation procedures to find the state equations for each independent energy storing element,

$$C_{a0} : \dot{v}_{a0} = Q_{a0} = Q_0 = \gamma_0 \cdot \frac{\rho_{h_2o} \cdot A_{pex}}{l_0} \tag{4.33}$$

$$I_0 : \dot{\gamma}_0 = P_{a0} - P_{r0} - P_{m0} - P_{m1} - P_{m2} - P_{m3} - P_{re} - \dot{\gamma}_m - P_{se} \tag{4.34}$$

where P_{a0} and P_{se} are as previously given, and P_{r0}, P_{m0}, P_{m1}, P_{m2}, and P_{m3} are the pressure drops due to the respective line section resistive elements. A lumped parameter resistance is used for the final resistance element, R_e, comprising in part the sum of the flow resistance parameter values for the tee housing, the output pressure sensor, the EM flow sensor, the final flow sensor, and the outlet. Identifying valid model forms and parameterization for these loss effects is a key effort in formulating a validated model of the HPPFN system. The equations representing all these resistive pressure losses are presented in more detail in Appendix C.1, where a detailed state equation derivation for this system is also provided.

The *derivative causality* on the manifold fluid inertia, I_m, represents the fluid in the line from the termination of branch 0 to the outlet of the system at the reservoir. This dependent inertia is coupled with the branch inertia by the relation,

$$\gamma_m : \gamma_0/I_0 = \gamma_m/I_m \rightarrow \gamma_m = \gamma_0 \cdot I_m/I_0 \tag{4.35}$$

from which follows that the rate of change of the manifold fluid momentum can be described by,

$$\dot{\gamma}_m = \dot{\gamma}_0 \cdot I_m/I_0 \tag{4.36}$$

The final form of the state equations for the first mode of the model is now given by,

$$\begin{aligned} \dot{v}_{a0} &= \gamma_0 \cdot \frac{\rho_{h_2o} \cdot A_{pex}}{l_0} \\ \dot{\gamma}_0 &= P_{a0} - P_{r0} - P_{m0} - P_{m1} - P_{m2} - P_{m3} - P_{re} - \dot{\gamma}_m - P_{se} \end{aligned} \tag{4.37}$$

where $\dot{\gamma}_m$ is replaced by the relation in 4.36.

Similarly, as in the single branch model, the second mode adds another capacitance and thus adds one more state giving the states (detailed derivation available in Appendix C.2),

$$x = \begin{bmatrix} v_{a0} \\ v_{b0} \\ \gamma_0 \end{bmatrix} \tag{4.38}$$

Using the same methods to formulate the state equations as in mode 1 for mode 2 results in the following,

$$\begin{aligned} \dot{v}_{a0} &= \gamma_0 \cdot \frac{\rho_{h_2o} \cdot A_{pex}}{l_0} \\ \dot{v}_{b0} &= \gamma_0 \cdot \frac{\rho_{h_2o} \cdot A_{pex}}{l_0} \\ \dot{\gamma}_0 &= P_{a0} - P_{b0} - P_{r0} - P_{m0} - P_{m1} - P_{m2} - P_{m3} - P_{re} - \dot{\gamma}_m - P_{se} \end{aligned} \tag{4.39}$$

The detailed derivation is given in Appendix C2, where as with the extended model's first mode, expressions for the resistive pressure drops are presented in explicit form.

4.3.1 Extended branch model tuning

The experience gained in tuning a single branch model allows for efficient tuning of the extended branch model, since significant insight is gained into the effect of tuning parameters on system response. The effect of the *dependent* inertia term, I_m, however, can have an effect on the system response. Using (tuned) parameter values from the single branch model will likely not result in a predicted output that matches the experimental data, thus requiring additional iterative tuning of the extended model.

The iterative process resulted in a new set of tuning parameters that resulted in the model output presented in Figure 4.12. These plots represent the results of using the tuning parameter values for the resistive element scaling factors: $R_0 = 6.5$, all R_m's $= 6$, and $R_e = 3.6$. With the exception of an approximately 12% peak amplitude difference near the beginning of the discharge cycle, the results of the tuning process show favorable comparison with test data for the majority of the output pressure curve. The branch 0 pressure curve showed more deviation in the simulation with the knee of the pressure drop occurring approximately 11% sooner, but matched well with the amplitude of the testbed data.

4.4 Multi-branch model

Given a validated extended single-branch model, the other accumulator discharge branches can be added to form the full multi-branch HPPFN system model. Recall that the extended single-branch model was developed with the intention of "plugging in" the other accumulator branches. The process is a bit more involved. A sequence of operations must first be introduced that will properly represent how fluid flow should interact at junctions. Unlike the majority of electrical PFN 'nodes', where ideal power flow junctions are sufficient to represent the interaction of *parallel* electrical power paths, this is not necessarily the case for fluid systems. The following subsection briefly presents background on the theory of flow interaction in manifolds, which motivated the approach taken to formulate the logic and event sequencing

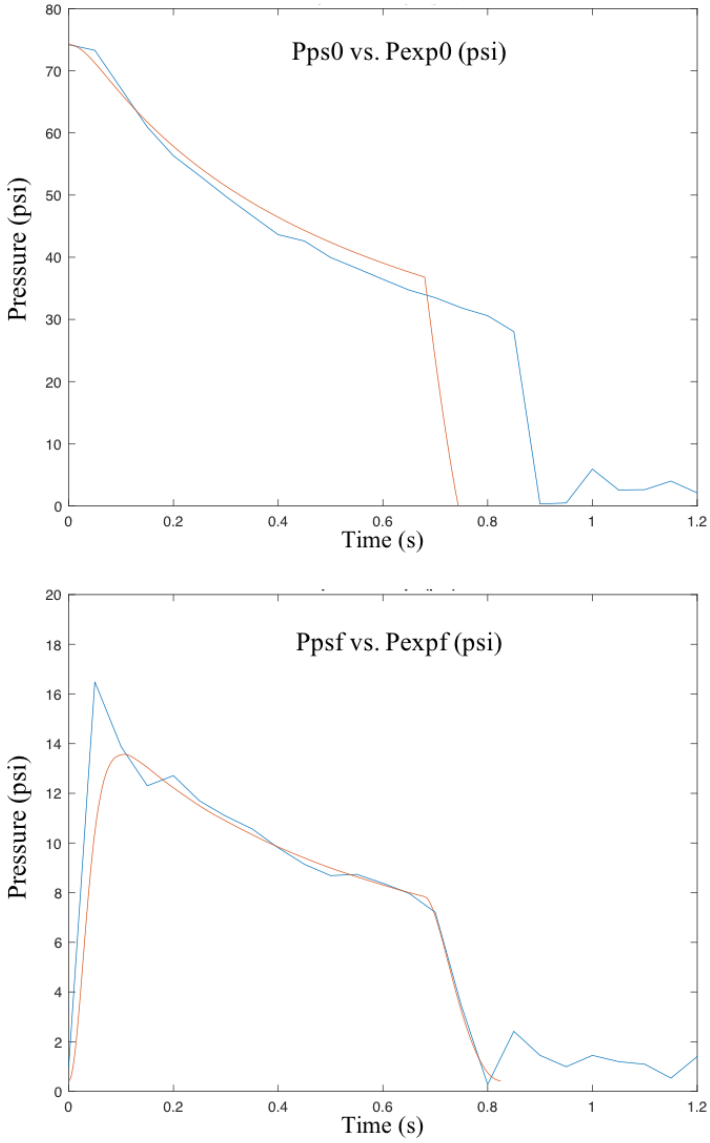

Figure 4.12: Extended branch model output plotted with experimental data for comparison: red = model, blue = experimental

used in the HPPFN model.

4.4.1 Manifold flow interaction

There are various ways to represent how flows interact at hydraulic junctions. In many cases, the fluid flow junctions, such as that shown in Figure 4.13(a), are treated as ideal potential junctions where pressure is common, $p_1 = p_2 = p_3$, and continuity for incompressible flow gives, $Q_1 + Q_2 + Q_3 = 0$, for the sign convention shown. Breedveld [2] addresses the fact that ideal junctions are not realistic for many hydraulic junctions by using the gyrator structure shown in Figures 4.13(b) and (c). Breedveld's approach reflects the more fundamental treatment addressed early on for systems applications by Katz [14].

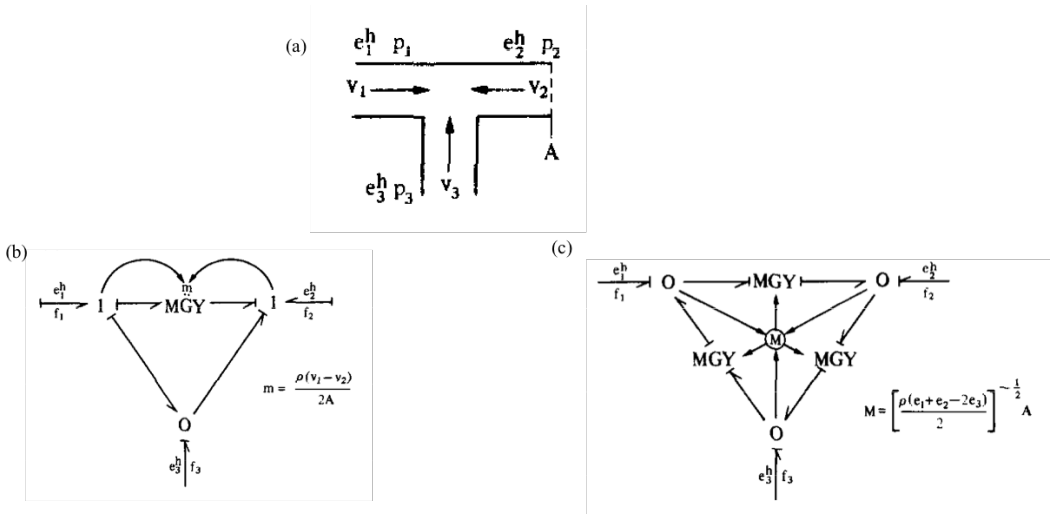

Figure 4.13: Breedveld's 3-port gyrator structures for modeling fluid junction from [2]; a) fluid junction represented by (b) decomposition of junction by flow causality, and c) decomposition based on effort (pressure).

Figure 4.14 is adapted from [14], and summarizes how ideal flow interactions can incorporate dynamic fluid effects, especially highlighting how

there can be differences based on whether the flow is separating or mixing at the junction.

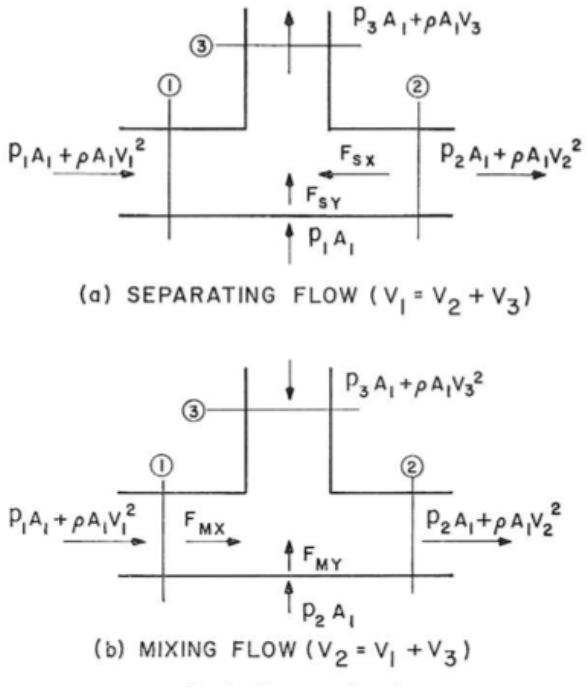

Figure 4.14: Katz's fluid junction scenarios from [14].

Katz provides a systematic framework with which to address the logic structure required for a model during simulation, providing a much more direct (and less complex) approach for the general reader than that presented by Breedveld, although the latter might be preferred by the bond graph specialist. Willson [24] and Willson and Traver [23], for example, followed the work of Breedveld in their work on liquid piston engine dynamics modeling and simulation. In any case, the fundamental methods of Katz were used to facilitate the simulation model development in this study.

Consider an adaptation of Katz as an addendum to his theory on flow mixing. So long as the pressure of the flow from port 3 of the junction, as shown in Figure 4.14(b), is greater than the incoming flow from port 1, the flow from port 3 will dominate and cause a vortex boundary to form at 1, thereby reducing or eliminating most flow contribution from that port and fully redirecting the flow of port 3 out to port 2. This can be considered similar to the action of a check valve, without the mechanical valving action. For this to be functionally to be valid, it must be assumed that *back flow* is not possible in any of the junctions. This is the case for the HPPFN testbed system, since each accumulator-branch includes a check valve upstream to the respective inlet to the exhaust manifold.

4.4.2 HPPFN system BG

For the first mode, as in the extended model, each branch will consist of only one **C** element (accumulator), one lumped **R** element for the branch line, and one **I** element representing the branch fluid inertia. The second mode will likewise be similar to that used in the extended model, and will consist of the elements of the first mode plus the addition of the accumulator bladder capacitance. Each branch will also retain a signal port to represent the pressure sensor location in the test bed branch.

A full derivation of the state equations for the multi-branch model can be found in Appendix C3. The bond graphs of Figures 4.15 and 4.16 were used to derive the state equations for both the first and second modes, respectively.

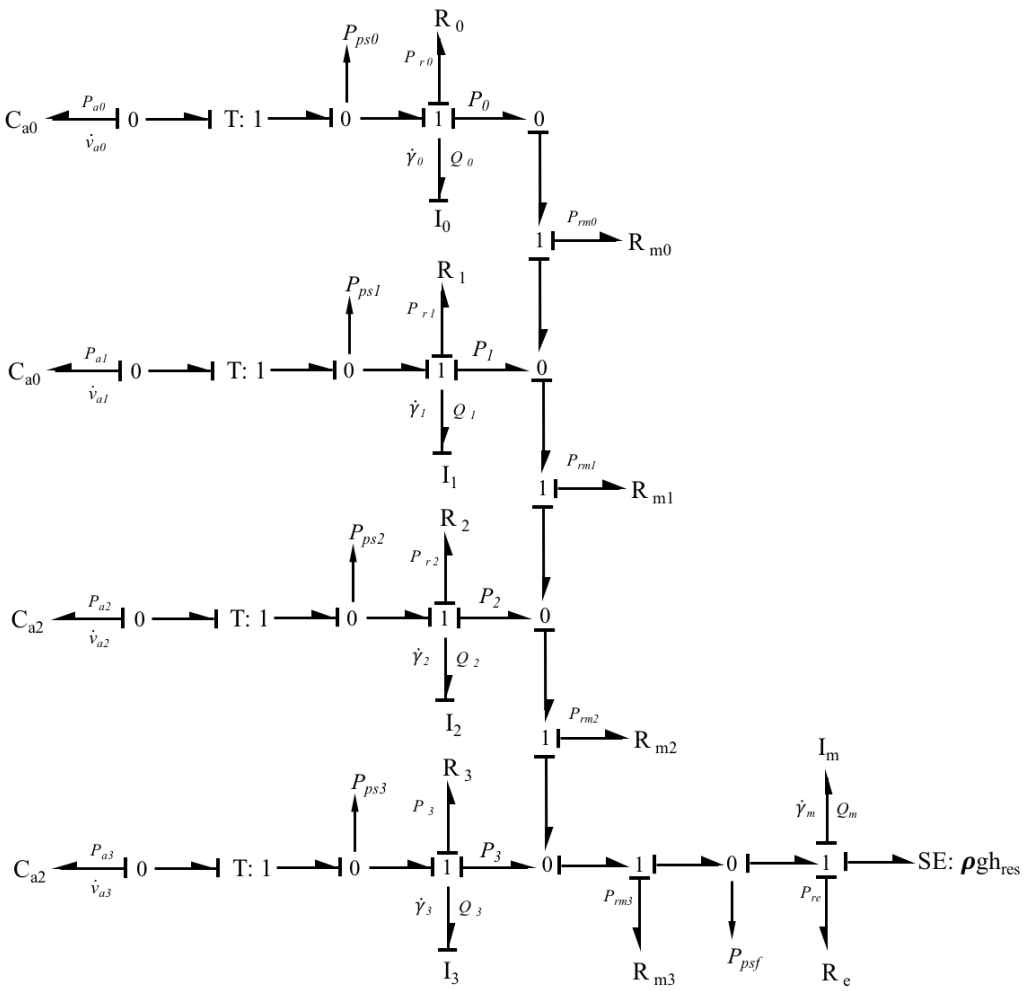

Figure 4.15: HPPFN 1st mode bond graph

From the first mode multi-branch bond graph, the system states are,

$$\mathbf{x} = \begin{bmatrix} v_{a0} \\ \gamma_o \\ v_{a1} \\ \gamma_1 \\ v_{a2} \\ \gamma_2 \\ v_{a3} \\ \gamma_3 \end{bmatrix} \tag{4.40}$$

In the bond graph for Figure 4.15, we once again find that the manifold inertia is in derivative causality. This causes a coupling that is expressed similar to that of the extended single-branch model, except there are now multiple branches and the coupling extends across more states. To provide a proper expression for the inertia, a matrix operation must now be performed on the generalized expression. A detailed derivation of the expression for multi-branch $\dot{\gamma}_m$ is provided in Appendix C.3.1. Using the bond graph with the standard equation formulation techniques, the state equations are found for the first mode model (see Appendix C.3.2 - C.3.5 for a detailed derivation) as,

$$\begin{aligned}
\dot{v}_{a0} &= Q_{a0} = Q_{f0} = \gamma_0 \cdot \frac{\rho_{h_2o} \cdot A_{pex}}{l_0} \\
\dot{\gamma}_0 &= P_{a0} - P_{r0} - P_0 \\
\dot{v}_{a1} &= Q_{a1} = Q_{f1} = \gamma_1 \cdot \frac{\rho_{h_2o} \cdot A_{pex}}{l_0} \\
\dot{\gamma}_1 &= P_{a1} - P_{r1} - P_1 \\
\dot{v}_{a2} &= Q_{a2} = Q_{f2} = \gamma_2 \cdot \frac{\rho_{h_2o} \cdot A_{pex}}{l_0} \\
\dot{\gamma}_2 &= P_{a2} - P_{r2} - P_2 \\
\dot{v}_{a3} &= Q_{a3} = Q_{f3} = \gamma_3 \cdot \frac{\rho_{h_2o} \cdot A_{pex}}{l_0} \\
\dot{\gamma}_3 &= P_{a3} - P_{r3} - P_3
\end{aligned} \tag{4.41}$$

and the pressure signal equations are,

$$
\begin{aligned}
P_{ps0} &= P_{rm0} - P_{r0} \\
P_{ps1} &= P_{rm1} - P_{r1} \\
P_{ps2} &= P_{rm2} - P_{r2} \\
P_{ps3} &= P_{rm3} - P_{r3} \\
P_{psf} &= P_{re} + I_m \cdot ((\dot{\gamma}_0/I_0) + (\dot{\gamma}_1/I_1) + (\dot{\gamma}_2/I_2) + (\dot{\gamma}_3/I_3)) + P_{SE}
\end{aligned}
\tag{4.42}
$$

Adding the bladder capacitance in second mode of the model to each line increases the number of states of the model by four, one for each accumulator branches as seen in Figure 4.16 below.

Recognizing all energy storage elements in second mode multi-branch bond graph model yields the states (see Appendix C.4 for detailed derivation),

$$
x = \begin{bmatrix}
v_{a0} \\ v_{b0} \\ \gamma_o \\
v_{a1} \\ v_{b1} \\ \gamma_1 \\
v_{a2} \\ v_{b2} \\ \gamma_2 \\
v_{a3} \\ v_{b3} \\ \gamma_3
\end{bmatrix}
\tag{4.43}
$$

Again, following the standard procedures to obtain the state equations yields

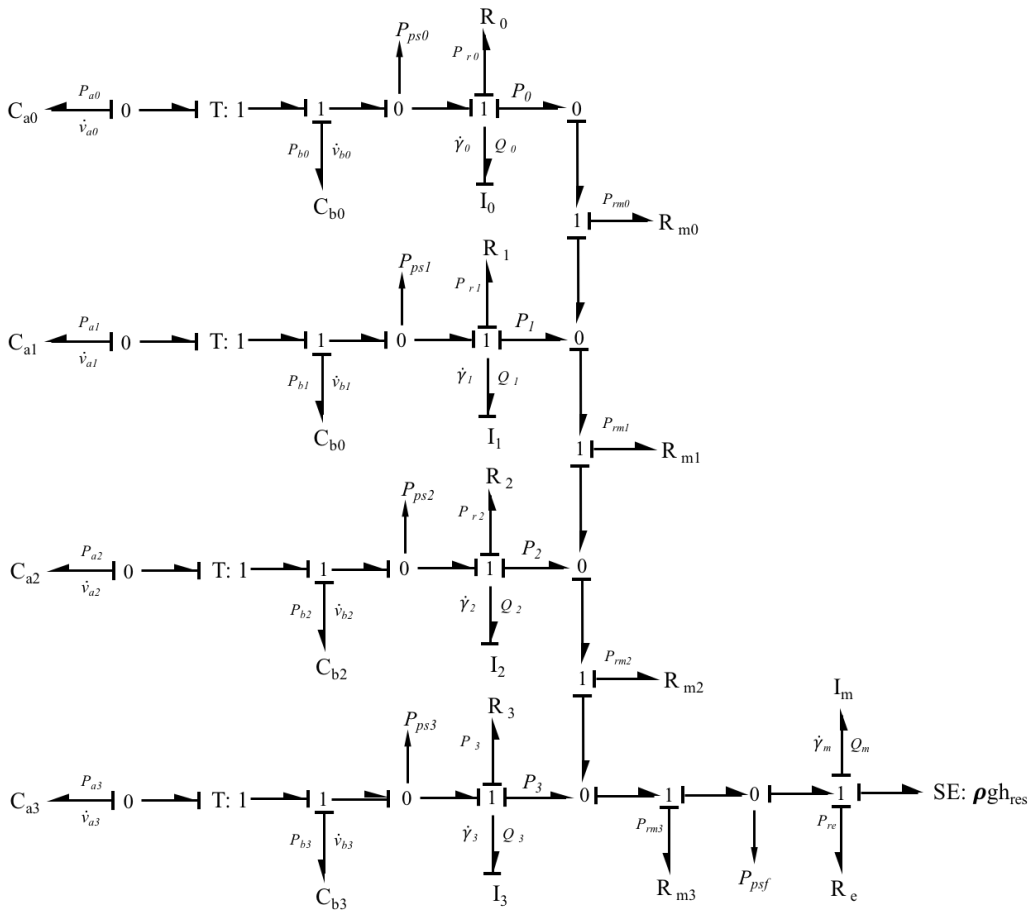

Figure 4.16: HPPFN stage 2 bond graph

the state equations for the second mode model as,

$$\begin{aligned} \dot{v}_{a0} &= \gamma_0 \cdot \frac{\rho_{h_2o} \cdot A_{pex}}{l_0} \\ \dot{v}_{b0} &= \gamma_0 \cdot \frac{\rho_{h_2o} \cdot A_{pex}}{l_0} \\ \dot{\gamma}_0 &= P_{a0} - P_{b0} - P_{r0} - P_0 \end{aligned} \tag{4.44}$$

state equations continued as,

$$\begin{aligned}
\dot{v}_{a1} &= Q_{a1} = Q_{f1} = \gamma_1 \cdot \frac{\rho_{h_2o} \cdot A_{pex}}{l_0} \\
\dot{v}_{b1} &= \gamma_1 \cdot \frac{\rho_{h_2o} \cdot A_{pex}}{l_1} \\
\dot{\gamma}_1 &= P_{a1} - P_{b1} - P_{r1} - P_1 \\
\dot{v}_{a2} &= Q_{a2} = Q_{f2} = \gamma_2 \cdot \frac{\rho_{h_2o} \cdot A_{pex}}{l_0} \\
\dot{v}_{b2} &= \gamma_2 \cdot \frac{\rho_{h_2o} \cdot A_{pex}}{l_2} \\
\dot{\gamma}_2 &= P_{a2} - P_{b2} - P_{r2} - P_2 \\
\dot{v}_{a3} &= Q_{a3} = Q_{f3} = \gamma_3 \cdot \frac{\rho_{h_2o} \cdot A_{pex}}{l_0} \\
\dot{v}_{b3} &= \gamma_3 \cdot \frac{\rho_{h_2o} \cdot A_{pex}}{l_3} \\
\dot{\gamma}_3 &= P_{a3} - P_{b3} - P_{r3} - P_3
\end{aligned} \tag{4.45}$$

and measured pressure signal equations are,

$$\begin{aligned}
P_{ps0} &= P_{rm0} - P_{r0} \\
P_{ps1} &= P_{rm1} - P_{r1} \\
P_{ps2} &= P_{rm2} - P_{r2} \\
P_{ps3} &= P_{rm3} - P_{r3} \\
P_{psf} &= P_{re} + I_m \cdot ((\dot{\gamma}_0/I_0) + (\dot{\gamma}_1/I_1) + (\dot{\gamma}_2/I_2) + (\dot{\gamma}_3/I_3)) + P_{SE}
\end{aligned} \tag{4.46}$$

It should be noted that while the pressure P_{psf} in both modes includes the terms,

$$I_m \cdot ((\dot{\gamma}_0/I_0) + (\dot{\gamma}_1/I_1) + (\dot{\gamma}_2/I_2) + (\dot{\gamma}_3/I_3)) \tag{4.47}$$

these pressure effects are not physically measurable, and are thus not included when simulation and testing results are compared. The pressure detected by

the sensors can be more faithfully represented by the pressure associated with the resistive effect, R_e.

The state equations sets for the two modes were implemented into computational code (see Appendix D). The following section describes how this computational code is formed to properly capture the HPPFN operation.

4.4.3 Branch sequencing logic

It is necessary to include branch sequencing logic to properly simulate the how the HPPFN testbed system discharges with controlled valve timing. The sequencing of events is structured with logical switches, however the theory of fluid interaction at the hydraulic junctions as presented in 4.4.1 is included. The method used to properly implement discharge timing is also described.

In HPPFN operation, the accumulator branches are activated with a proper timing sequence. As the accumulators discharge, and fluid upstream from the branch discharging is diminished, so the manifold inertia will be incrementally decreased by the length of manifold section between the discharging accumulator and the upstream accumulator.

One way to model this type of physical phenomena is to build a simulation model with a sequence of events and associated switch logic defined as follows:

1. Full model is implemented for all lines and branches without bladder

in model mode 1. The manifold inertia will reflect the full length of manifold, and accumulators will be fired with a predetermined firing sequence. All accumulators should initiate discharge during this stage.

2. When the state variable γ_0 for branch 0 fluid inertia is made zero, the branch is functionally eliminated, up until which time the inertia is non-zero. The manifold inertia will then reflect the length of manifold from branch 1 to the outlet. This process is repeated for each successive branch until branch 3 is reached. In theory this results from both the check valves of the individual branches and the 3-port junction phenomena presented previously.

3. Once the line pressure in branch 3 is reached with the other branches, flow begins once more out of those branches, starting with the branch that has been left with the highest residual pressure from the preceding process. This occurs until a trigger point is reached for branch 3 to begin the second mode.

4. At this point all branches will be shifted to the second mode branch model, which includes the bladder capacitances, and the model will run until the final accumulator branch (branch 3) has fully been evacuated of all fluid.

There are two key points that should be reiterated as they are critical to the model's functionality. First, none of the second mode branch models take

effect until the final accumulator (branch 3 accumulator), reaches a discharge volume equal to it's initial charge volume; i.e., until it is 'empty'. Second, as was stated in the theory of operation, a higher pressure flow into a three way junction should always result in the lower pressure port ceasing to contribute flow until the pressures at the junction are at least equalized. It was found that by adhering to these two points, the model simulations were able to reproduce certain key trends observed in data measured from the HPPFN testbed.

4.5 Model assessment criteria

Model performance will be based on a qualitative assessment derived roughly from the HPPFN performance parameters discussed in Chapter 2. Here, specific elements and features of the outputs are qualitatively compared using the following output pressure and flowrate attributes:

1. Output curve feature position in time
2. Output curve feature amplitude
3. Output curve feature shape
4. Comparison of overall system efficiency
5. Comparison of average system power output

The output curve features that will be used for this assessment are defined in Figure 4.17.

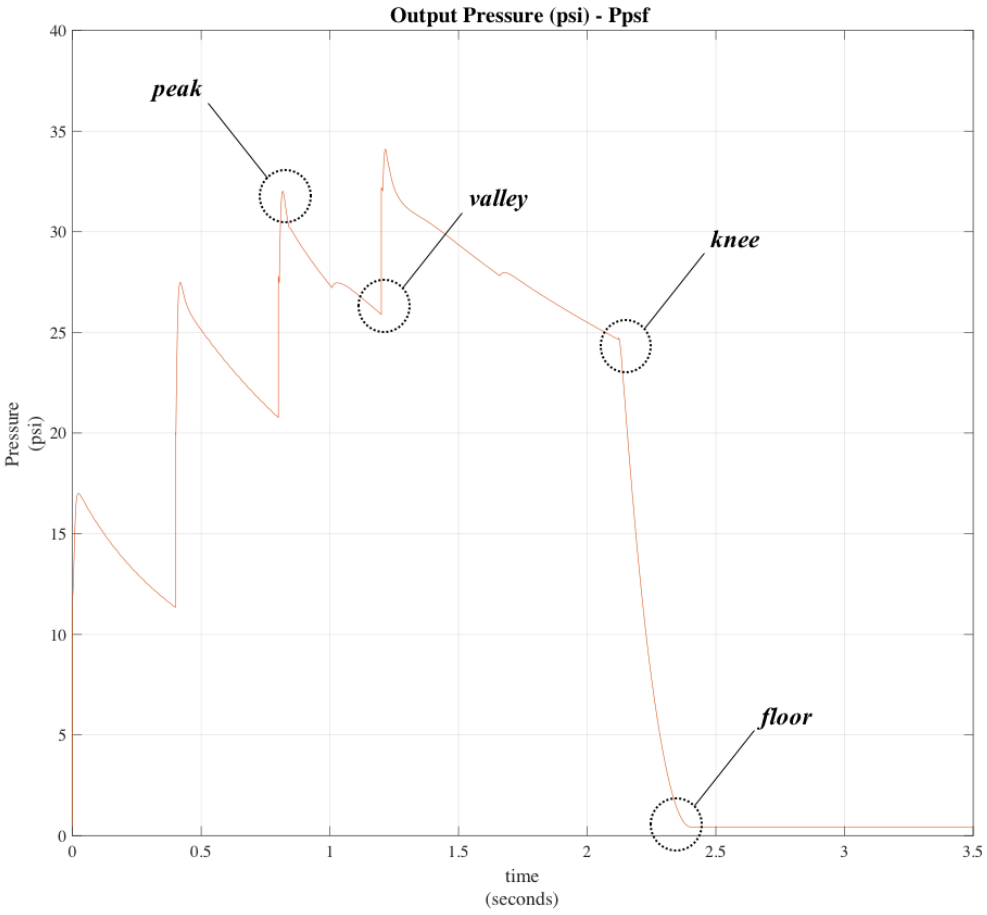

Figure 4.17: Output curve features used for similitude analysis

The comparison of the average power output and the discharge efficiency describe overall system performance. These may also be used to provide insight that can help optimize system performance when the iterative simulation methods developed are adopted into an automated optimization tool.

4.6 Model performance

The given assessment criteria were used to compare the experimental and the multi-branch model outputs. As in the previous model comparisons, the same initial conditions were used in both. The tuned model parameters from the extended-branch model were used with each of the branches in the multi-branch model. Some minor re-tuning was required to attain the results presented in Figures 4.18, 4.19, and 4.20. The M-file code used to conduct the simulation can be found in Appendix D.2.

The tuned flow output had an average difference in pulse peak amplitude of approximately 15% and showed reasonable similarity in feature position (in time), resulting in a total length of pulse that is very similar to that found experimentally. The initial pulse in the model output has a faster rise time than the experimental, but in contrast the pulse shows good similarity in pulse decay and drop off. Even though the magnitude of the features in the experimental data is smaller than the simulation, there is reasonably good agreement.

The tuned pressure output had an average difference in pulse peak amplitude of approximately 5% and showed almost identical feature position and total pulse length and form. The model-predicted pressure pulse is slightly more abrupt than the experimental. The overall pulse form is almost identical, providing some confidence in the model assumptions and sequencing.

Efficiency and overall energy expenditure differences are a bit more

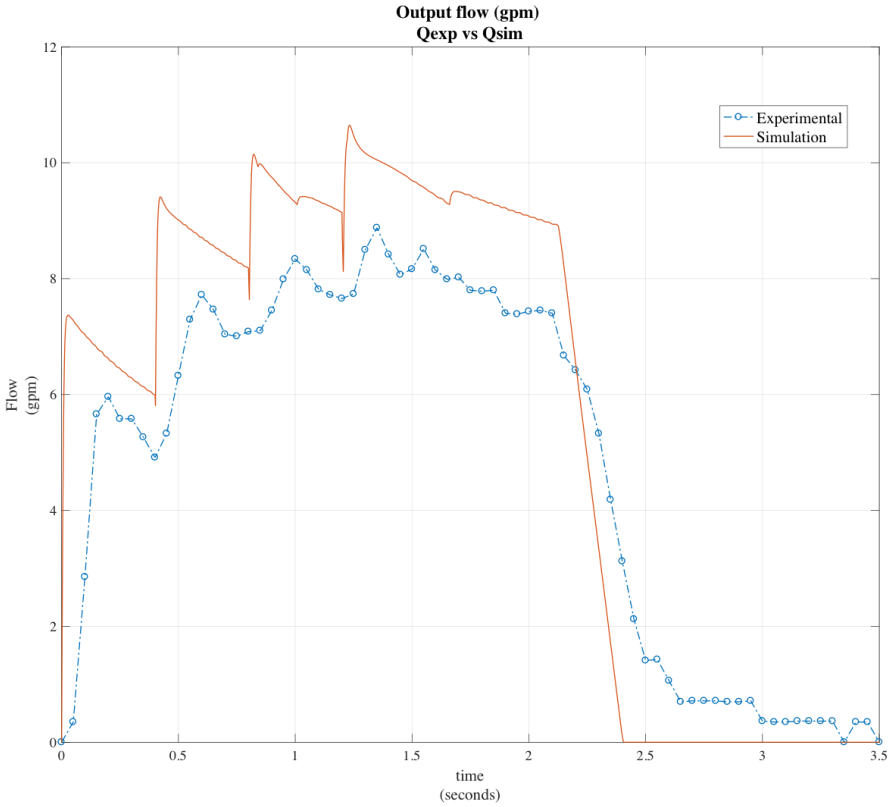

Figure 4.18: Tuned HPPFN model flow output comparison

pronounced. The power output comparison will magnify any model disparities since it is the product of the pressure and flow outputs. Studying the plots, the most obvious difference in the two outputs is the abrupt jumps in power predicted by the simulation. The more gradual jumps in the experimental data are more a result of the flow component of the power, as was seen in the flow output plot. The flow output may be lagging due to either measurement latency of the experimental system or an underestimation in the model's flow resistances. Overall combined pulse length and number of features show good

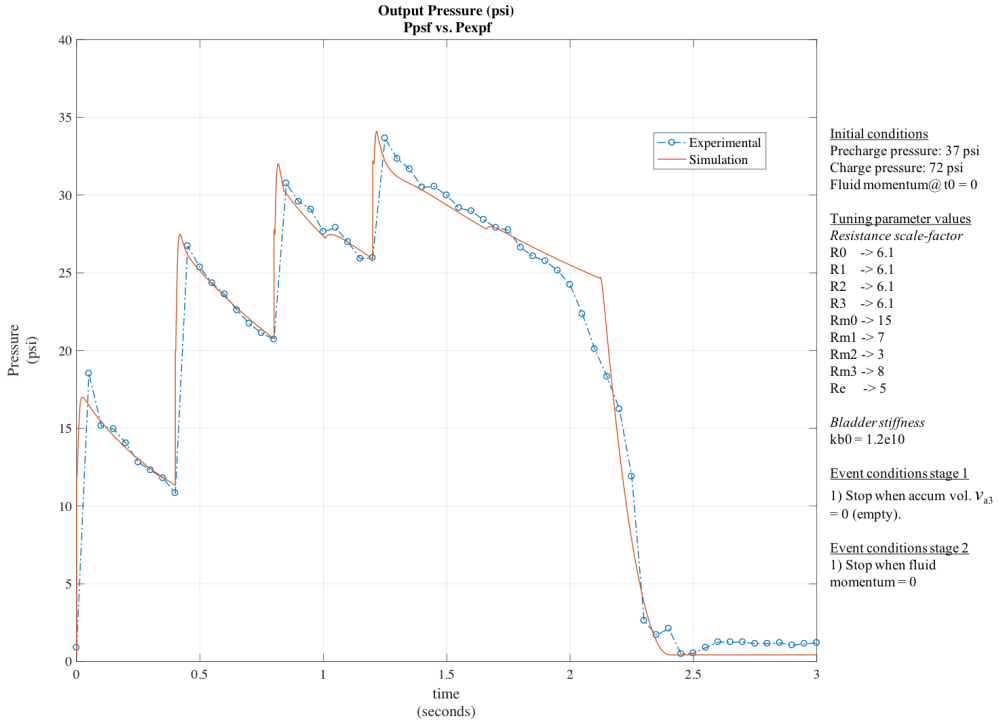

Figure 4.19: Tuned HPPFN model pressure output

comparison. The efficiency difference is about 9%, with the simulation over predicting. The total energy gives a larger difference of 30%. This is due to the difference in a number of features in the simulation having sharper corners and larger amplitudes. Based on the data, there is an average power out for the experimental versus the simulated system of 42 W versus 82 W, indicating a rather large percentage difference of approximately 50%. Output data is provided in tabular form in Appendix E.2.

In summary, the tuned model shows relatively good agreement with the experimental data, especially the pressure output. The tuned timing was

attained using a process that involved bringing the knees of the outputs as close together in time and amplitude, then matching the peaks and valleys of the outputs. This was done using the system tuning parameters in an iterative fashion. The resulting model gave a qualitative comparison with reasonably good agreement with experimental results in the phenomenology of all three outputs.

In the next chapter, the model is further evaluated as a design synthesis tool. Once the model is shown to give valid results, it can be used to determine the discharge timing for the testbed at the tuned operating condition. Furthermore, tests can be conducted at the tuned condition and with varying discharge times to investigate the ability of the model to properly predict the behavior of the output pressure and flow as compared to testbed data for the same discharge timing.

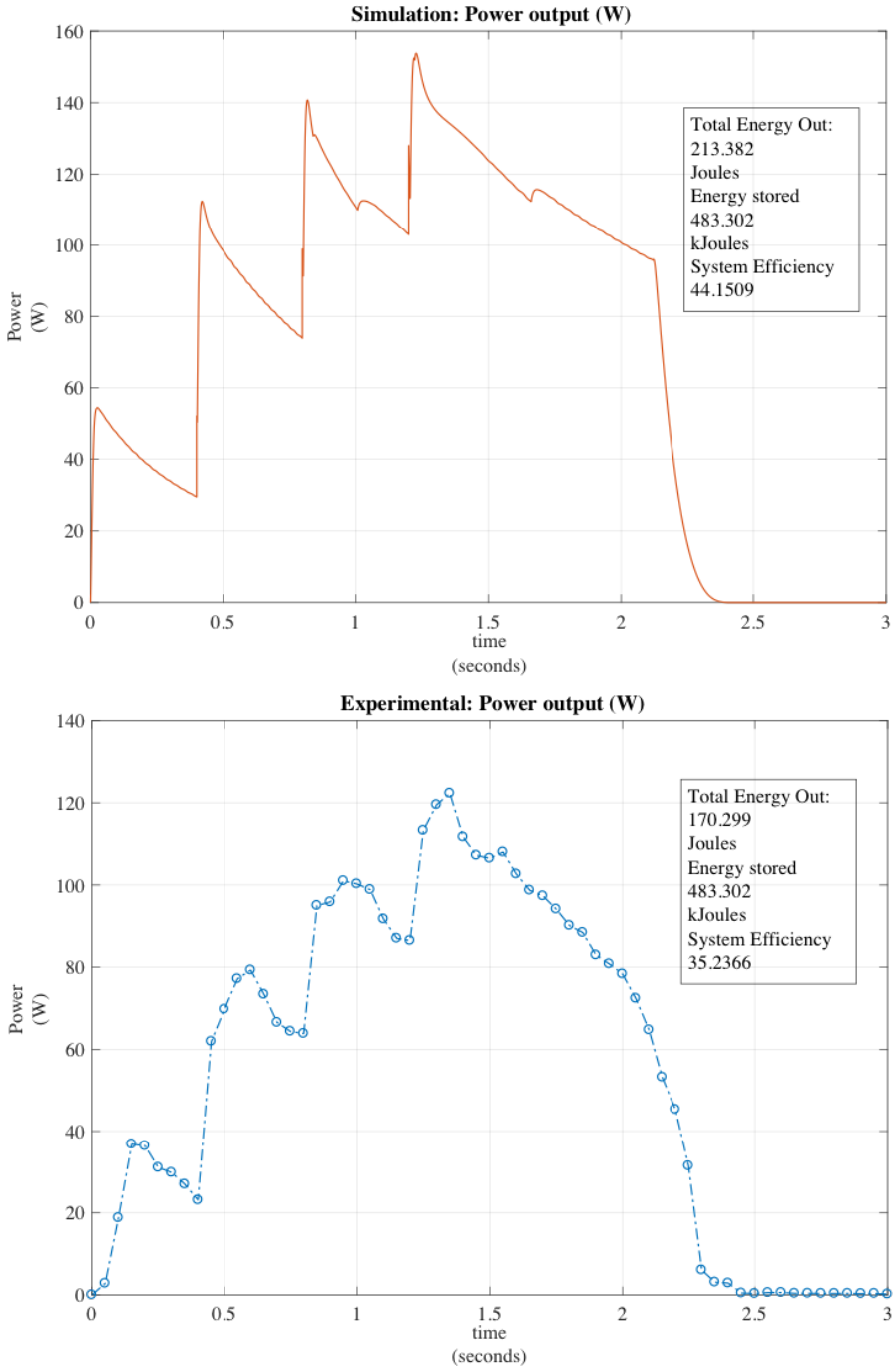

Figure 4.20: HPPFN model and testbed efficiencies

Chapter 5

Experimental Verification

5.1 Verification approach

This chapter focuses on the verification of model functionality as a HPPFN synthesis and design tool. The function of the model is evaluated through three series of tests. The first uses the model as a synthesis tool to design a viable pulse at a tuned operating condition. In order to properly conduct this evaluation, a metric is introduced to quantify pulse performance and used in conjunction with the evaluation methods discussed in Chapter 4. A second series of tests studies the performance of the model when used at operating points other than the tuned condition. Finally, an evaluation series investigates how well the model predicts timing excursions at the tuned operating condition. Each simulation-based evaluation compares to data from the testbed, with each test using the identical initial conditions and timing sequences for their respective test series condition. In this way, the ability to use the model-based simulation as a viable synthesis and design tool is evaluated.

5.2 Pulse quality metric

The pulse quality (ϕ_q) is the metric that will be applied to the model output during the pulse synthesis process. It is a measure of flatness of the output pulse top, for which a half cycle square wave is the theoretical limit and where the value of ϕ_q would be unity. The expression for ϕ_q is given as,

$$\phi_q = \left(\left(\sum_{0}^{n-1} \frac{P_{np}}{P_{nv}} \right) + \frac{P_{np}}{P_{knee}} \right) \cdot \frac{1}{n_{brnch}} \tag{5.1}$$

where P_{np} and P_{nv} are the pressure values at nth peak and valley, respectively, of the output, the parameter n_{brnch} is the number of branches discharged in the simulation, and P_{knee} is the pressure value of the curves knee during output final decent. This method can be applied to any of the three (pressure, flow, or power) multi-branch output curves of the system.

As simulation tests are conducted, an evaluation is made using the pulse performance metric in order to rank each case. The process is repeated until the simulation iteration with the 'best' acceptable pulse quality score is reached. This process is intended to yield the corresponding required HPPFN valve timing sequence for a particular set of initial conditions. Once the timing values and initial conditions are applied to the testbed, an experimental test is conducted and the output recorded. This output is then compared with the model's predicted output qualitatively based on the trend of the output and the feature amplitudes.

5.3 HPPFN synthesis procedure

During the course of familiarization with using the HPPFN model for pulse synthesis, it was discovered that pulse lengths could be considerably increased by following the procedure below:

1. Set charge pressure for the first accumulator in the discharge order to the manufacturer maximum allowed operating pressure.

2. Set initial charge pressure for remaining accumulators to approximately 60% the charge pressure set for the first accumulator. In contrast, the large majority of tests conducted had charge pressures that were the same for all accumulators.

3. Initially set discharge Δt's to be equivalent between each discharge. The initial value is fairly arbitrary but a good starting value for the time difference could be based on the single branch discharge pulse period for the first accumulator, if this has been previously characterized.

4. Run model simulation using the initial timing sequence.

5. Study output curve to estimate necessary change in first Δt to make second discharge peak amplitude similar to the first discharge and implement into simulation timing sequence.

6. Iterate steps 4 & 5 until the first and second peak amplitudes are within an acceptable margin, for example: $\pm 5\%$ was used in the following test series.

7. Repeat steps 4-6 for each branch thereafter until Δt's have been attained for all branches.

8. Apply pulse quality analysis. If pulse quality value is not satisfactory, repeat entire process until minimal allowed pulse quality value is reached, or value is as close to unity as manually possible.

This method was used as a guide for the pulse forming experiments conducted during this investigation, with the exception of the timing excursion series.

5.4 Model synthesis performance

5.4.1 Pulse synthesis results

Using the tuned multi-branch model and the procedure outlined in 5.3, a pulse was synthesized (Figure 5.1) that had a measured value of pulse quality of $\phi_q = 1.47$ for the pressure output, and a $\phi_q = 1.22$ for the flow output. Five tests were conducted using the derived timing on the testbed system. The results from these tests were averaged and prepared as one data set for the purpose of this comparison, see Appendix A.3 for tabular experimental data.

This first attempt at pulse synthesis using the model showed reasonable similarity to the experimental output with the initial conditions and derived timing. Another attempt to tune the model was made to determine if better results could be attained. This was done by breaking the resistances up for the manifold and exhaust and changing the values slightly until a better match was reached, as seen in Figure 5.2.

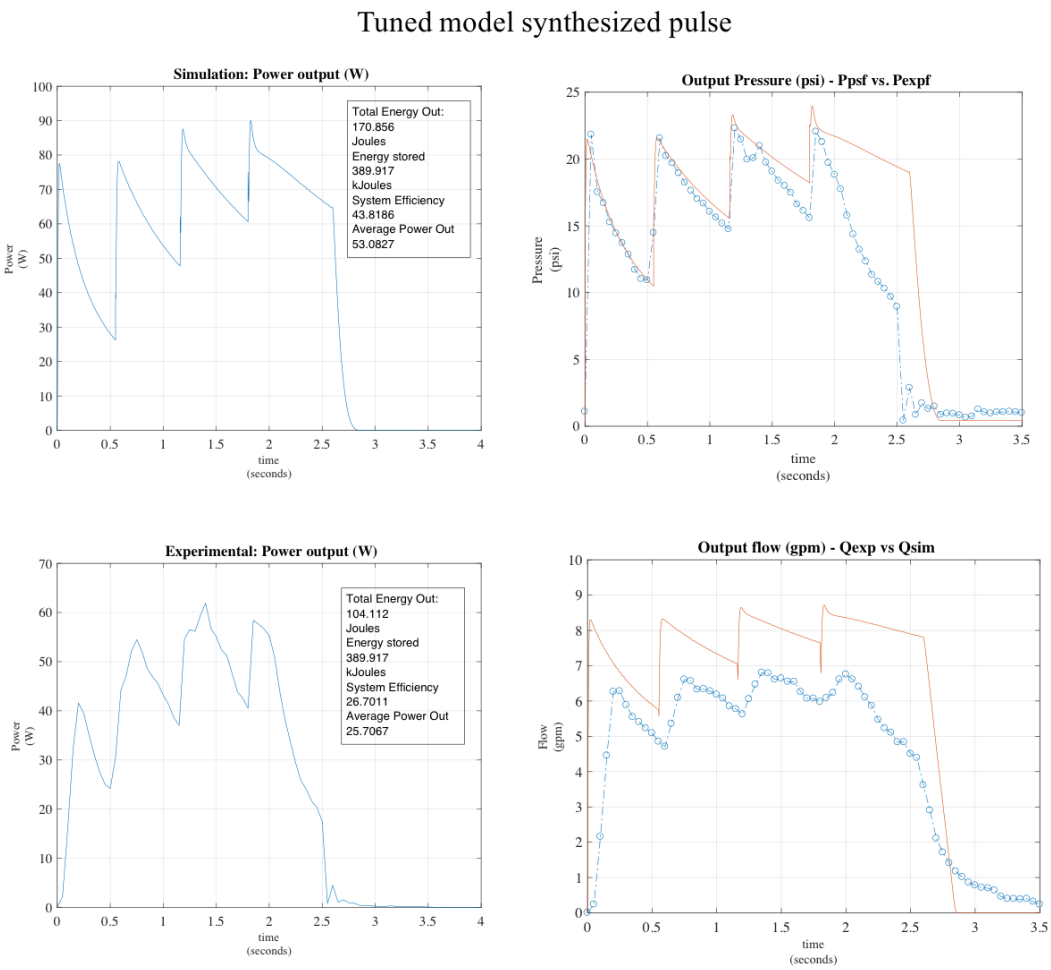

Figure 5.1: Tuned model synthesized pulse

The fine-tuned model gave a pulse performance value for the pressure output of $\phi_q = 1.43$ and for the flow output $\phi_q = 1.23$. Even though the pulse performance values for tuned and the fine-tuned systems were almost identical, it can be observed on the right hand side plots of Figure 5.2 that the fine-tuned model simulation had noticeably better agreement with the flow output. This

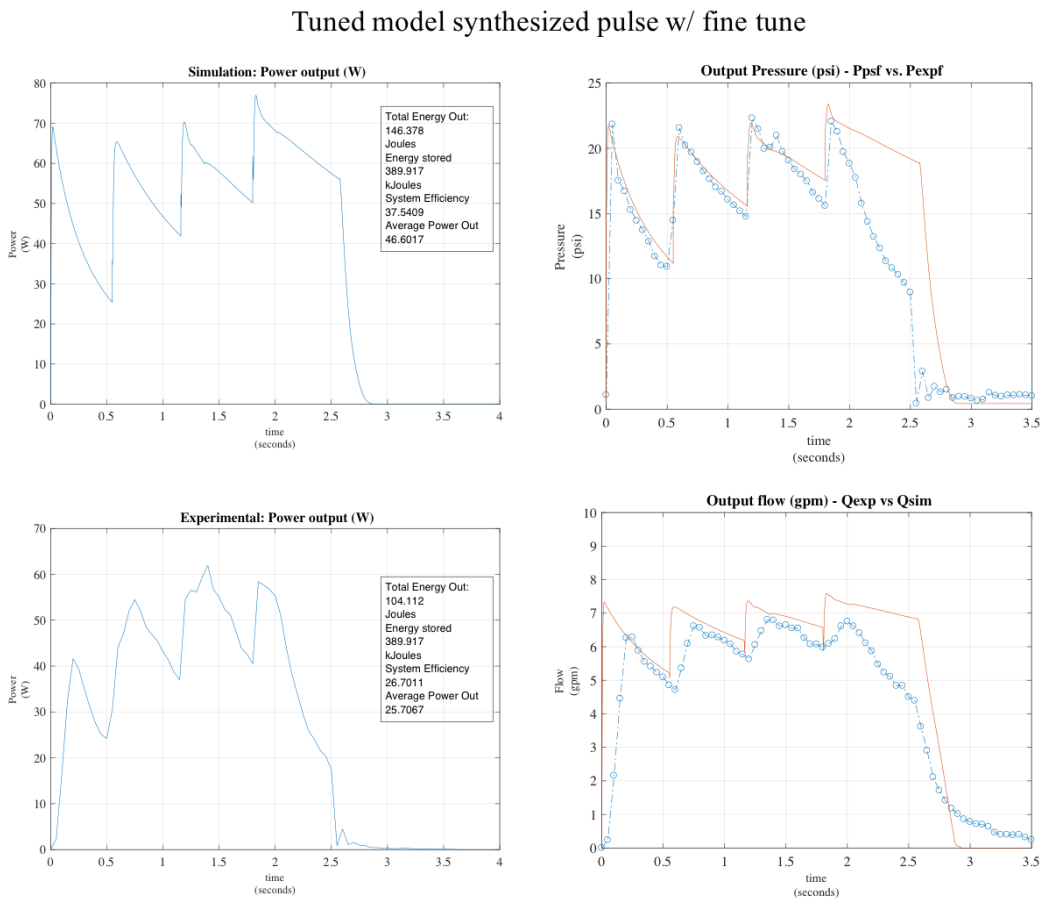

Figure 5.2: Re-tuned model synthesized pulse

indicates a more reliable agreement in the power output, which is evident in total energy discharged (see values on plots) as observed by comparing the left hand side plots of Figures 5.1 and 5.2.

Also observed is the difference between the outputs for the final pulse. The simulation's final pulse produced higher power for a longer duration than the experimental. This may be due to the preceding pulses having a more

persistent influence on the final pulse than in the experimental system. This output difference produced a slightly more than 10% difference in system efficiency between simulated system output with 37.5% and the testbed with 26.7%.

5.4.2 Excursions from tuned operating point

This series was comprised of tests conducted at six operating conditions. Three operating conditions were investigated with each roughly following the developed synthesis procedure to produce a reasonable output pulse. Since the charge pressure of the first discharged accumulator is greater than the rest when using the synthesis procedure, the test conditions were identified by the the first accumulator charge pressure. Each test condition is then further defined by two pre-charge pressures conditions. Table 5.1 summarizes the operating point excursion test conditions.

Condition	Charge P_{c0}	Charge $P_{c1,2,3}$	Pre-charge P_{pc}
OC 1a	80 psi	72 psi	30 psi
OC 1b	80 psi	72 psi	40 psi
OC 2a	70 psi	60 psi	30 psi
OC 2b	70 psi	60 psi	40 psi
OC 3a	60 psi	55 psi	30 psi
OC 3b	60 psi	55 psi	40 psi

Table 5.1: Operating condition excursion (OCE) test conditions

The results from the tests show that the model is less capable of predicting output at conditions further away from the tuned operating condition.

This trend goes as the capacity of the storage as seen in Figures 5.3, and 5.4. For instance as the depth of discharge (stroke) decreases in the physical system, differences in output between it and the simulation become larger. This can also be seen to a lesser extent in tracking the peak amplitudes of both the pressure and the flow as accumulator 'stroke' becomes smaller. Experimental data can be seen in tabular form in Appendix E.4.

A second major observation is that there currently may be a limitation of the model to capture discharge effectively when the Δt between discharges become larger than the characteristic discharge period for individual accumulators. This is evident in the breaks in the pressure pulse, and large drops in flow amplitude between accumulator discharges that are seen for the large Δt's given for the OCE conditions. This phenomena becomes less as the Δt's become smaller and the branch output flows impose more influence on the following discharges. This is reflected in the ability of the tuned condition to match reasonably well with experimental data.

Given these results, the model demonstrates degraded performance as operating initial conditions move away from the tuned. The model does however maintain the ability to reasonably track peak pressure and flow trends with the caveat of the inability of capturing the severe drops in both flow and pressure between discharges at Δt's greater than the characteristic time constant discussed.

5.5 Timing excursion

To evaluate the model's ability to predict non-ideal pulsed outputs, an excursion of timing was applied to the discharge sequence while maintaining the tuned initial conditions from the multi-branch model in Ch 4.6. There are three excursions that were investigated, one had a severe, but equidistant in time, discharge sequence, and the other two had irregular Δts between accumulators in the discharge sequence. See Table 5.2 below for the test conditions.

Condition	$\Delta t1$	$\Delta t2$	$\Delta t3$
TE 1	700 ms	700 ms	700 ms
TE 2	200 ms	400 ms	600 ms
TE 3	600 ms	400 ms	200 ms

Table 5.2: Time excursion (TE) test conditions

The results of this test series (see Appendix E.5 - E.7 for tabular data) showed reasonable similarity in output trends for both the flow and the pressure curves. The output of the simulation consistently demonstrated the following characteristics in comparison with equivalent experimental data:

1. Under predicted pressure by no more than 16%.
2. Over predicted flow by no more than 16%.
3. Over predicted initial pressure and flow pulse.

Consistent with the observations in the OCE tests, the model underestimated the drops in pressure between pulses as the discharge Δt's are increased. The results also demonstrate that the model underestimates the pressure as the Δt's becomes smaller, implying a similar trend with increasing accumulator capacity with the previous test series. The results of this test demonstrated that the model best operates when the discharge timings are closer together, but yet maintains the ability to reasonably track pressure and flows trends given large changes in Δt's.

5.6 Observed model limitations

Combining the results of the three test series two limitations can be noted based on the recurring modeling trends and experienced gained while operating both model and testbed. The first is that as the timing between discharges is increased such that any discharge pulse begins to fall outside of the characteristic period of discharge of the preceding pulse, the model's ability to track output for that pulse is degraded. The evidence for this is given by the output comparisons demonstrating the model's inability to track the large drops in flow and pressure between pulses at Δt's beyond this threshold. This may in fact not be a result of the model itself but rather the way the model's logic is implemented in Matlab, and may possibly be corrected with further code development. In specific it may be due to the fact that the accumulator bladders are not sequentially added into the system but rather are put in by the discussed model switching technique after the last accumulator fully

empties.

Secondly as observed the further away the operating conditions move from the tuned, the less reliable the model becomes. This is primarily due to the assumptions used for the resistive models implemented in the system. Implementing better models for this may increase fidelity at non-tuned conditions, but effort should be made, as resources permit, to characterize the components of the system under expected operational conditions.

Lastly a note about the coded model state of development which should be considered before use. The accumulator discharge sequence must always be in the order from furthest to nearest branch to outlet, otherwise coded sequencing will not be valid. This is purely a coding issue. The model should, however, function with any discharge order or timing Δt, so long as the coding that implements the series of model state equations has logic to support this. This is a topic for future model development and improvement.

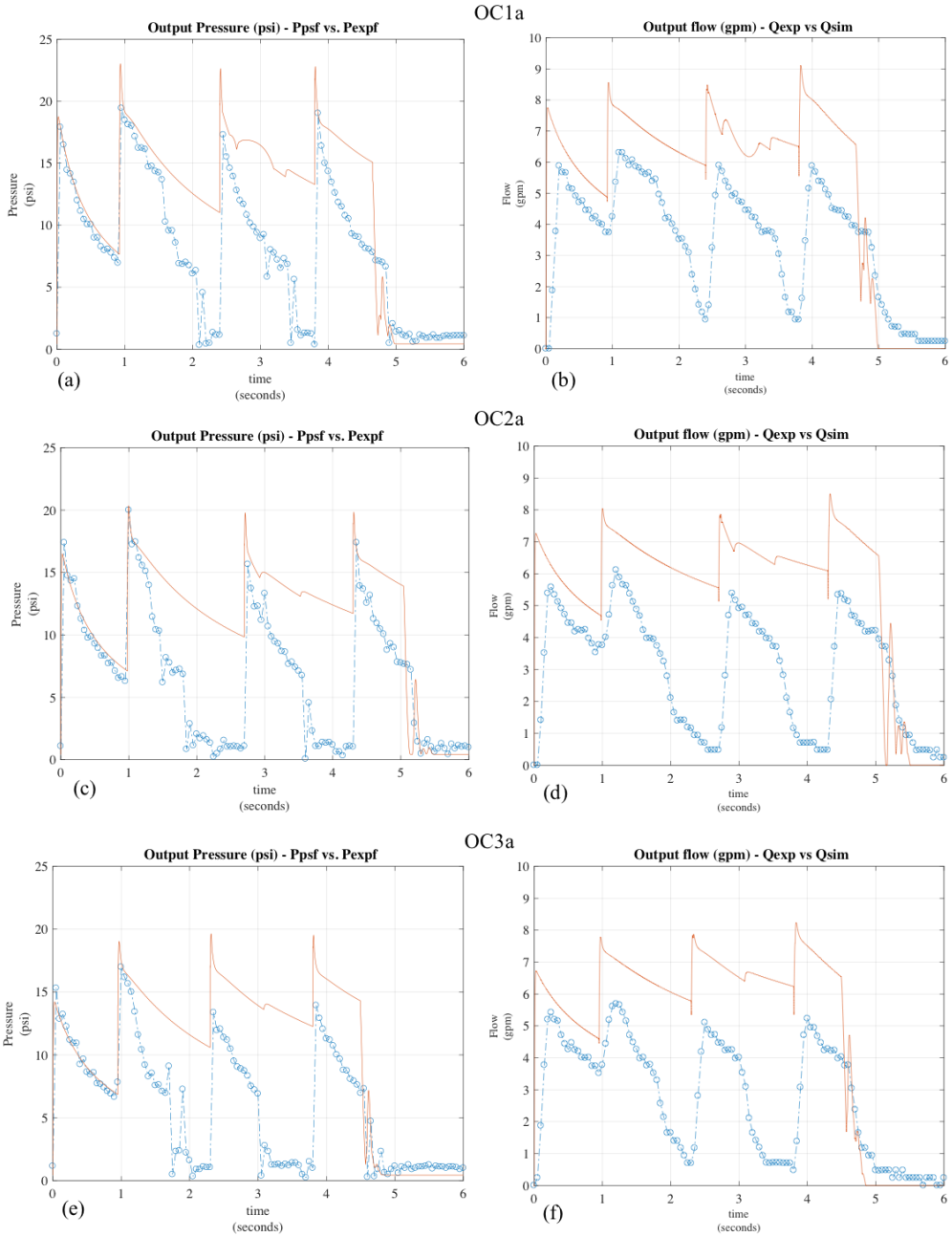

Figure 5.3: Operating condition excursion plots for OCa conditions presented on Table 5.1. Circle-dash trace is experimental, solid line is simulation.

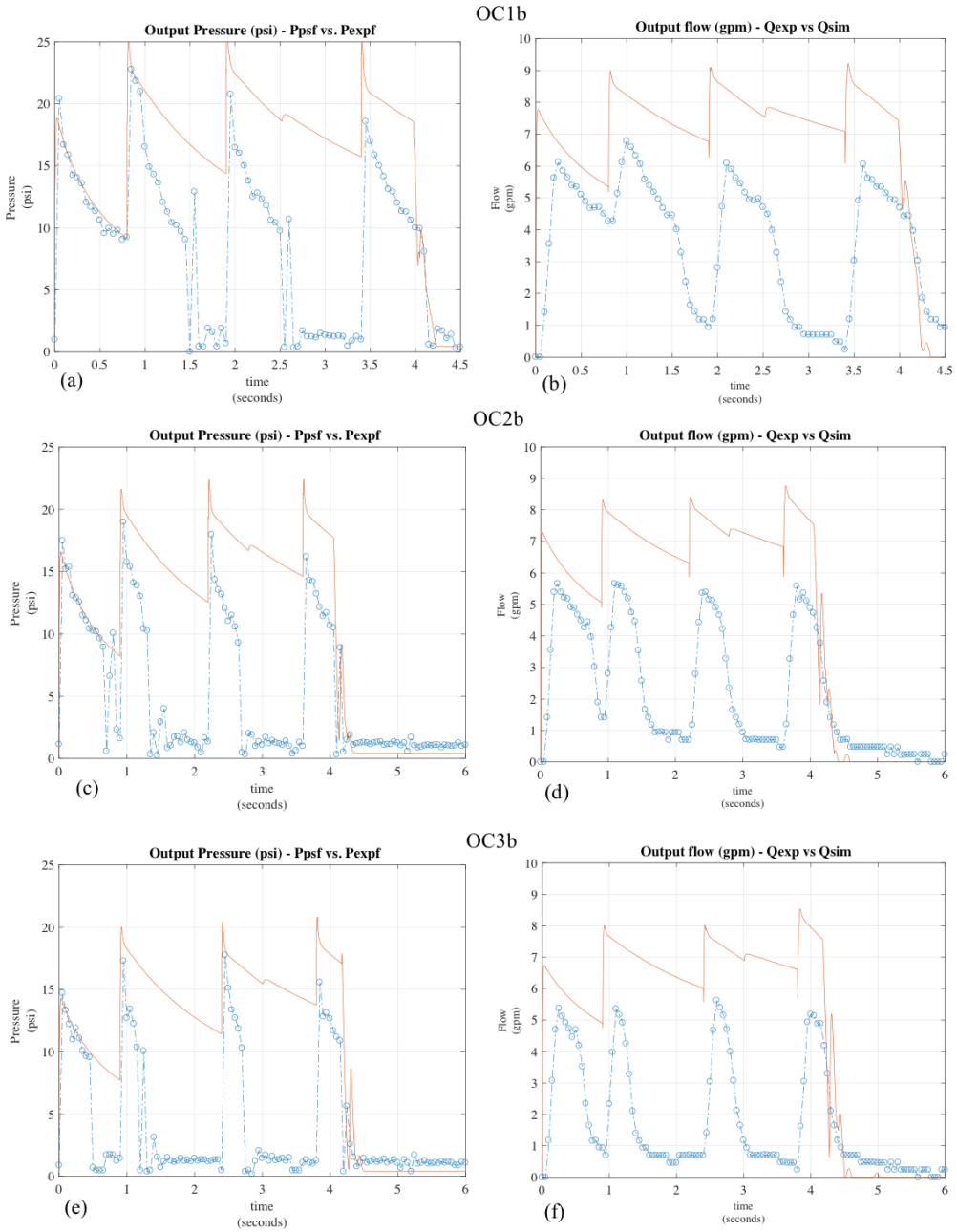

Figure 5.4: Operating condition excursion plots for OCb conditions presented on Table 5.1. Circle-dash trace is experimental, solid line is simulation.

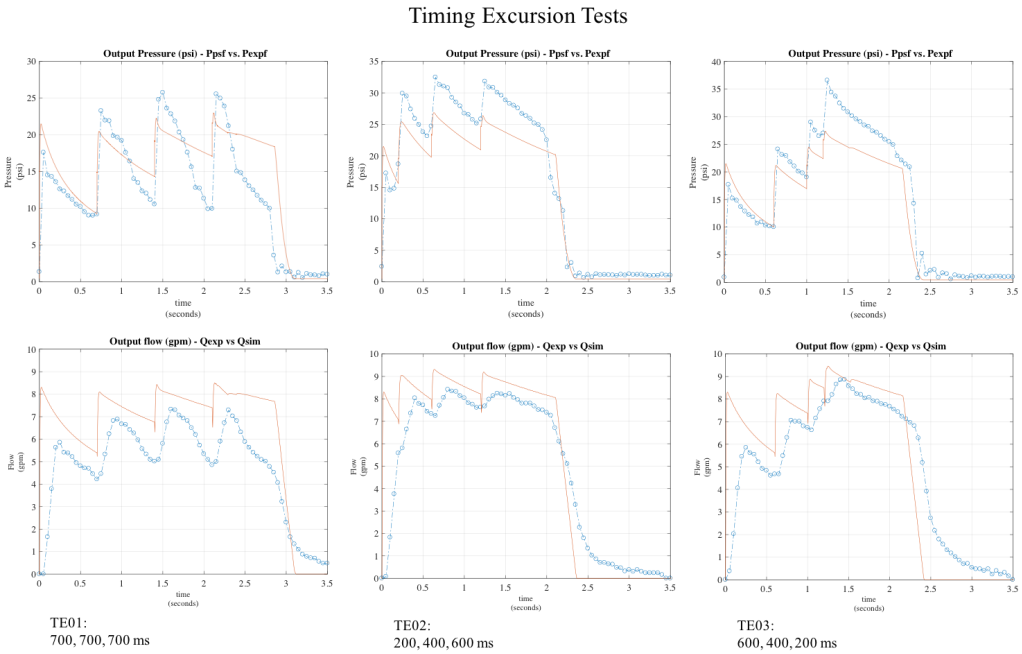

Figure 5.5: Time excursion plots; circle dash trace is experimental, solid line is simulation.

Chapter 6

Conclusions

6.1 HPPFN realization

It has been demonstrated herein that a physical system consisting of hydro-pneumatic energy storage elements, specifically bladder-type hydraulic accumulators, connected in fluid parallel can be constructed in conjunction with timed valving in such a manner as to form an operable sequentially-fired pulse forming network (SFPFN) [6, 7, 9, 19]. This concept was verified experimentally on a constructed bench-top, closed-loop system. The experimental system was shown to be capable of forming pulses synthesized in a manner similar to those demonstrated in SFPFN electromagnetic systems. Prior to formulation of an HPPFN system model, valve timing for pulse synthesis was determined by iterative experiments, until a timing was found that produced a pulse with the desired shape qualities. Once a system model was constructed and experimentally validated, it became possible to determine the valve timing for pulse synthesis by model-based, iterative simulation.

6.2 HPPFN Model

An experimentally-verified state space model was developed using bond graph modeling techniques that is capable of being used to synthesize an SF-PFN by iterative simulation. This model currently operates best when tuned for a specific set of initial conditions, about which it has been verified that reasonable agreement with experimental measurements can be achieved.

During the process of model tuning, certain system parameters were found to have significant influence on the output and these were singled out as key *tuning parameters*. These parameters were the *flow resistances* and the *compliance* of the accumulator bladders. Tuning of these parameters proved to be most effective in matching the simulated output shapes (pressure and flow) to the experimental data for given set of initial conditions.

Development of the validated system state space models required consideration of: a) nuances in how the fluid flows interact when discharged from sequentially discharged accumulators, b) difficulty in uncertain, and highly-variable flow resistance factors, and c) the unique characteristics of the bladder-type hydraulic accumulator, especially when pushed beyond its typical operational limits. The non-linear nature of the system was effectively handled by using a multi-mode model that can transition smoothly at the points of maximum non-linearity. Specifically, this was accomplished using an event-based simulation structure coupled with progressively staged components as specific accumulator branches become active. While there are likely other ways to implement this system model in simulation, this approach was used to explore its

potential utility in handling more complex systems. Such studies are proposed as future work.

As expected, it was found during experimental verification that the model's ability to predict output begins to diminish the further the operating condition moves from the tuned condition. Furthermore, it was observed that the model over-estimates the continuity of flow and pressure pulses for the system as the difference between discharge timing increases beyond the characteristic discharge time for the accumulator at the operating condition.

Given the stated range of the model's functional reliability, the recommended conditions for maximal model performance are:

1. Primary energy store must be a *bladder-type* accumulator
2. Output manifold must always be liquid-filled
3. Conditions do not approach cavitation
4. Fluid lines are considered non-compliant
5. System operates at tuned condition (charge and pre-charge pressures)
6. Operates at Δt's within the characteristic discharge time constant

6.3 Synthesis Technique

A synthesis technique was presented that will determine the accumulator discharge timings using the validated and tuned state space model de-

veloped herein. Pulse synthesis – i.e., the discharge timing specification – was accomplished by iterative simulation, in a manner similar to that for electromagnetic SFPFNs. The iterative simulation technique allows for a more efficient search for the HPPFN timing solutions, as opposed to time-intensive brute force iterative experiments conducted on the bench-top. Furthermore, excursions from the current bench-top operating point can be facilitated since operating parameters like charge pressure and pre-charge pressure do not need to be changed on a physical system. Finally, extended analytical development with the model form could be explored as a way to solve for the operating point in analytical form.

In conjunction with the synthesis technique, a metric of pulse flatness was proposed and applied. This metric along with efficiency allows for a more direct correlation of performance between pulse shapes, and allows the designer to determine suitable limits of performance with definitive values.

6.4 Future work

There are a number of improvements that can be made to the model that will allow for higher fidelity results and ultimately give more confidence as a reliable design tool. Furthermore, the underlying concept that gave genesis to this effort can be applied to systems outside the hydraulic domain. The following subsections describe some proposed improvements and investigations to extrapolate the concept outside of the current energy domain and application area.

6.4.1 Resistive models

It was shown that the model loses its ability to properly predict the output of the system for significant excursions away from proper design operating points, for example with observed differences in peak flow output of almost 40% and more than 50% for pulse valleys on the pressure output in the most extreme cases. While the model's ability to aid in the design of the pulse (flatness) was not affected, its ability to predict duration and amplitude of the pulse was degraded. This distinction can be attributed to resistive models used.

It was evident during the model tuning process that the resistance values in the system were the most sensitive tuning parameters of the system. This *empirical* discovery should be verified by conducting a more formal sensitivity study. In addition, an effort should be undertaken to determine if the resistive losses can be modeled such that excursions from design operating points will not degrade model performance. This could be done parameterizing resistive losses as a function of, flow rate, for example. This would entail moving away from constant resistance models to higher fidelity descriptions of key hydraulic components and their flow regime specific loss factors.

6.4.2 Valve model

The current control valve model does not include a typical valve finite-time opening characteristic, but rather is an ideal valve as discussed. This lends to the abrupt nature of the simulated output as compared to that seen

in experimental data. It is proposed that an experimentally-tuned valve model would allow for a more gradual pressure release to the system thereby reducing the peak pressure and flow values of the simulated output. This would have minimal effect on the design utility of the model but would have a reasonably positive effect on the model's ability to predict the amplitude, duration, and flatness of the pulse. Adding a tuned valve model will ultimately give more reliable efficiency numbers when sizing and designing systems.

6.4.3 Automated pulse synthesis tool

The system model in conjunction with the pulse flatness metric, any other proposed metrics, and the operating point efficiency values, provide a basis for an automated optimization tool. This tool could allow for automation of the iterative simulation technique presented here by being given goal values for pulse duration, power amplitude, pulse flatness, and optimal system efficiency. The optimization routine would then iteratively run simulations to find the discharge timing producing the optimal pulsed output for the given conditions. It is possible that such an automated process could be run in conjunction with this system, say as part of a networked system that allows valve timings to be re-configured based on observed system behavior.

6.5 Summary

In summary, this research effort introduced an entirely new class of system defined here as a hydro-pneumatic pulse forming network (HPPFN).

Furthermore, this preliminary research has identified foundational principles for how HPPFN systems can be modeled and synthesized so that useful systems can be designed and scaled for practical applications. It is hoped that with the foundational principles presented here, others will build upon the work to further the effectiveness and practical application of this new class of system.

Appendices

Appendix A

Simulink / SimHydraulics Models

A.1 Linear spring accumulator system

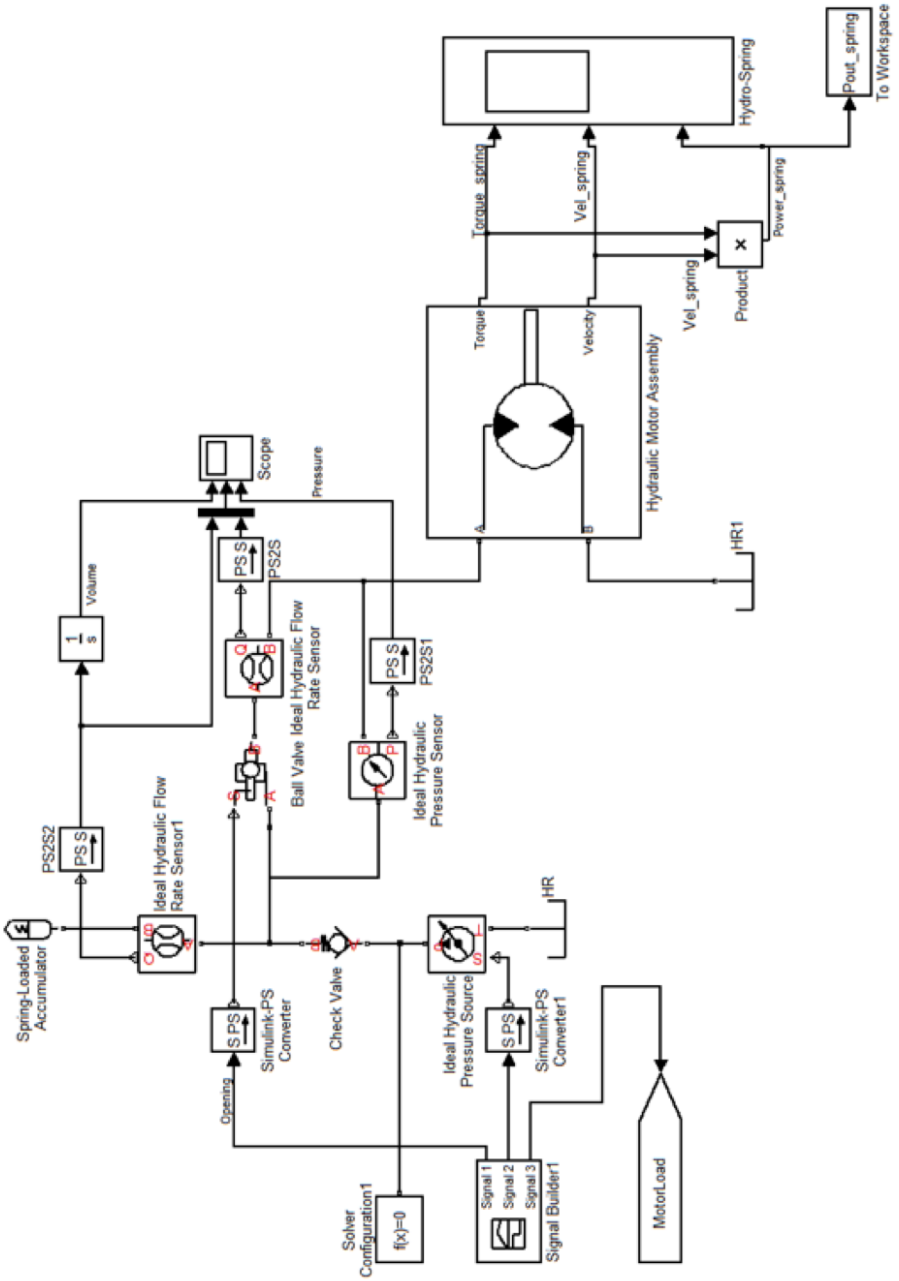

A.2 Gas charged accumulator system

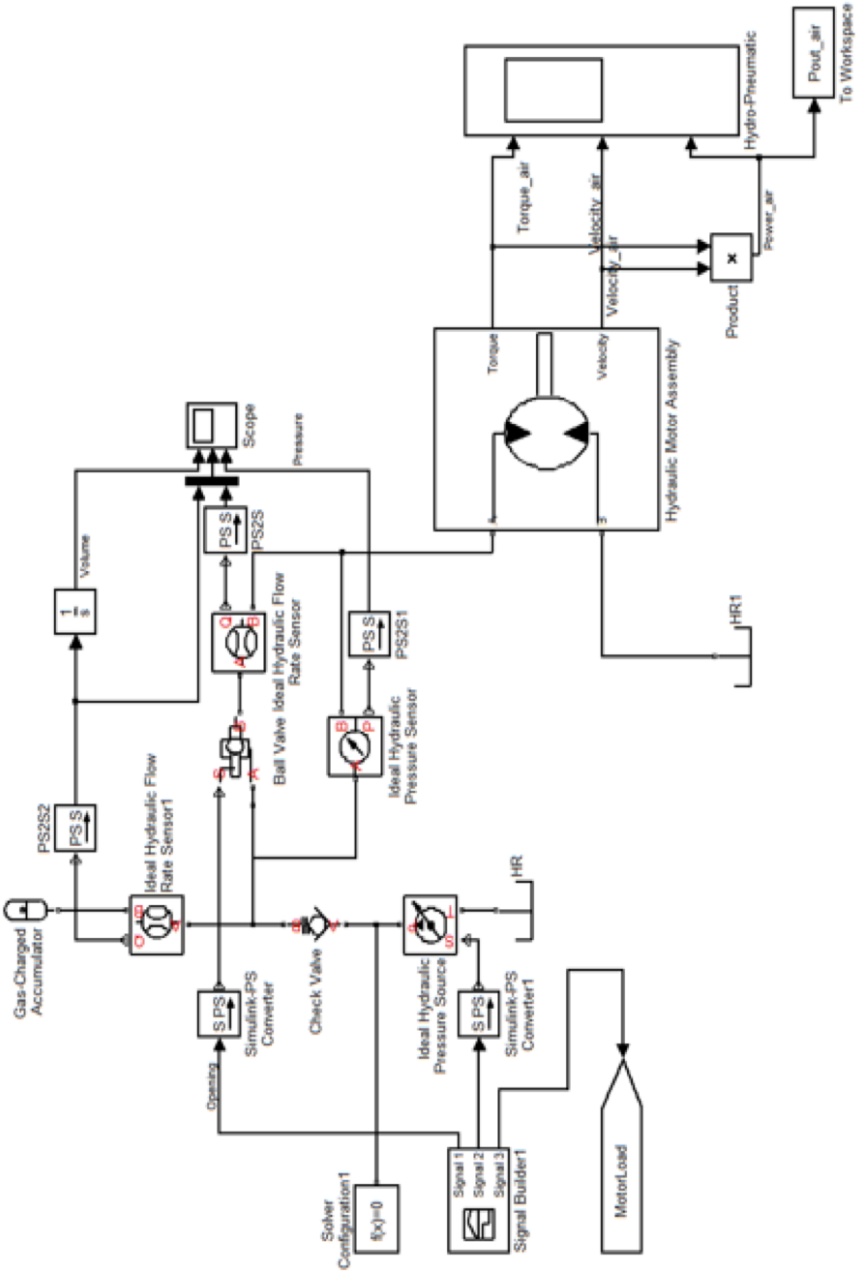

A.3 Gas charged accumulator SFPFN system

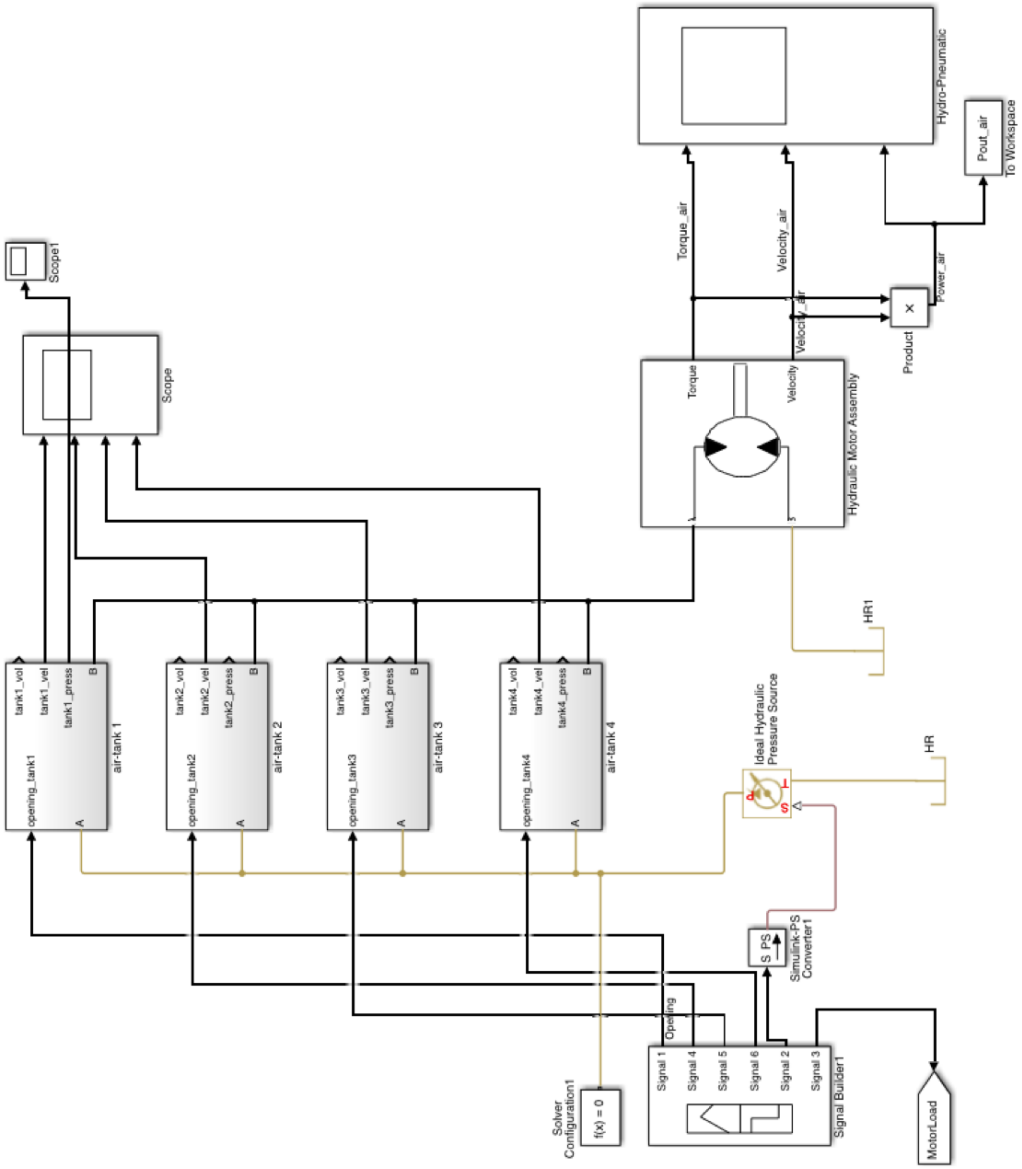

Appendix B

Experimental Hardware and Instrumentation

B.1 Accumulator

http://shurflo.com/

ACCUMULATOR TANK: Model 182
INSTALLATION MANUAL

The SHURflo Accumulator tank is a bladder type pressure storage vessel and/or pulsation-dampening device designed to hold water under pressure. The accumulator tank provides additional water storage to assist the pump in meeting the total demands of the system. It extends pressure switch-controlled pump life by reducing pump on-off pulsation.

NOTE: This product is not recommended for use with a 4900 or 5900 Series Smart Sensor Pump.

- See Product label and Specifications section on page 2 for factory pre-charge pressure. Do not exceed 40 psi [2.7 bar] pressure for long-term storage, shipping, or during system non-use.
- It is recommended the pre-charge be checked seasonally, or any time the accumulator does not appear to be functioning properly. Temperature extremes and changes in altitude can affect accumulator pressure and performance. Use a standard tire pressure gauge to check the pressure. The valve stem cap **MUST** be tight to prevent air leakage.
- The accumulator may be placed anywhere in the pressurized side of the plumbing. It should be installed after the pump and before any filters or check valves that can add backpressure to the pump or system. The ports are non-directional in flow and do not have to be plumbed in line (one side can be capped).
- The accumulator can be mounted in any position. However, for complete sanitizing/winterizing, the recommended mounting position is with pre-charge valve stem up. ***Do not*** freeze or mount near a high heat source.
- Threaded fittings (plastic/nylon only) should be torqued approximately 1/2 to 1 turn after ***hand-tightened***. ***Never*** exceed 6 ft/lbs [88 Nm] of torque on the ports. Plumb the system using high pressure (2x pump rating), braided, flexible tubing to minimize vibration/noise.

RV/MARINE APPLICATIONS WITH PRESSURE SWITCH-CONTROLLED PUMPS

The accumulator contributes to longer pump life, less noise, less amperage draw, and reduced water pulsation. The most efficient use of the accumulator occurs with the pre-charge set at the **SAME** pressure as the pump's pressure switch "turn on" setting. Typically, a 45 psi [3 bar] pump will turn on around 30 psi [2.07 bar]. Therefore, the pre-charge should also be 30 psi [2.07 bar]. The pre-charge **MUST** be set in a "**static**" condition (pump off and at least one water fixture opened).

Depending on pre-charge pressure to the accumulator, in relation to the pump turn on/off pressures, stored liquid is about 2 to 4 oz. [60-120 ml]. If accumulator tank pre-charge exceeds pump turn on pressure, the liquid volume is reduced.

WATER HAMMER APPLICATIONS

When used as a dampening device/water hammer or noise suppressor, the pre-charge should be set at the operating (dynamic) pressure. Place a gauge in the offending plumbing where the accumulator can be mounted. Adjust the valve so the noise is generated and read the pressure. Set the pre-charge to the observed pressure, remove the gauge, and install the accumulator. Refer to SHURflo Service Bulletin #1024 for more application information.

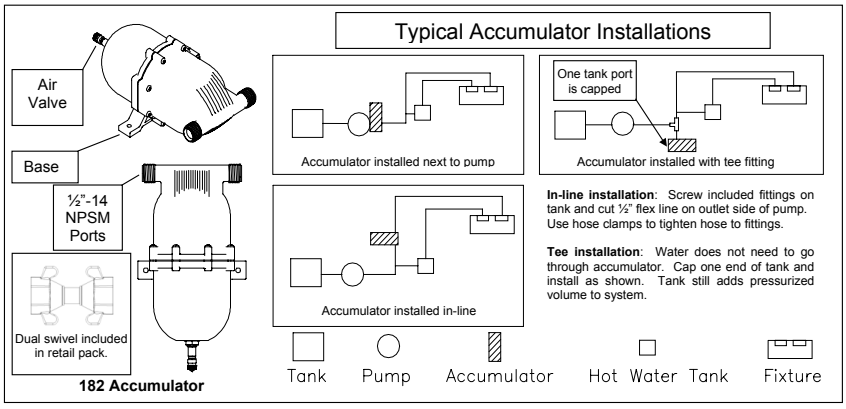

911-731-C 08/06 ECN 12681 Page 1 of 2

http://shurflo.com/

TROUBLESHOOTING

SYMPTOMS	POSSIBLE SOLUTIONS
Does not function; pump cycles rapidly	Check air pressure. Add or remove air as necessary.
Water leaks from valve	Diaphragm is torn or has a hole. Replace accumulator.
Does not hold air pressure	Screws loose, air valve, torn/hole in diaphragm. Replace accumulator.
Leaks from fittings or ports	Check fitting connection. Ports must seal on internal port taper, Ports should not be sealed on threads with NPT fittings

TESTING AIR PRESSURE

Check air pressure with pump off and one or more faucets open [no water pressure in the system]. Adjust pressure as needed. If unit leaks water from air valve or does not hold pressure, unit must be replaced.

NOTE: There are no replacement parts or kits for this accumulator. If it is not working, it must be removed or replaced.

WINTERIZING

To winterize, drain all water from the system. Blow system out with low-pressure air, or add potable water anti-freeze. **Never** use automotive anti-freeze. Death or severe injury can occur.

SPECIFICATIONS

Maximum Working Pressure:	125 psi [25 bar]
Pre-Charge Pressure:	Models 182-100 & 182-200: 30 psi [2.07 bar] Models 182-102 & 182-202: 20 psi [1.4 bar]
Total Volume: (gas/liquid):	21 oz. [620 ml]
Temperature Range:	34-120° F [1-49°C]
Diameter:	3 3/4" [95 mm]
Length:	8 3/4" [22 cm]
Listings:	CSA & NSF listed
Housing Material:	Nylon
Bladder Material:	Butyl
Ports:	1/2-14NPSM-Male
Mounting Bracket:	Two 7/32" [5.3 mm] ϕ holes at 4-1/16" [103 mm] centerline apart

LIMITED WARRANTY

SHURflo warrants the 182 series accumulator to be free from material and workmanship defects (under normal use and service) for a period of one (1) year from the date of manufacture or one (1) year use, with proof of purchase, not to exceed two (2) years in any event.

The limited warranty will not apply to accumulators that were improperly installed, misapplied, or are incompatible with components or liquid not manufactured by SHURflo. Failure due to foreign debris is not covered under the terms of this limited warranty. SHURflo will not warrant any accumulator, which is physically damaged or altered outside the SHURflo factory. SHURflo's obligation under this warranty policy is limited to the repair or replacement of the accumulator. SHURflo is not responsible nor will it reimburse for labor necessary to remove and reinstall an accumulator if found defective.

This limited warranty covers products distributed within the United States of America. Other world market areas should consult with their distributors for any deviation from this document.

★ISO Certified Facility

★★ISO Certified Facility

SHURflo reserves the right to update specifications, prices, or make substitutions.

SHURflo, LLC ★
5900A Katella Ave.
Cypress, CA 90630
(562) 795-5200
(800) 854-3218
FAX (562) 795-7564

SHURflo East
52748 Park Six Court
Elkhart, IN 46514-5427
(800) 762-8094
FAX (574) 264-2169

www.shurflo.com

SHURflo Ltd. ★★
Unit 5 Sterling Park
Gatwick Road, Crawley
West Sussex, RH10 2QT
United Kingdom
+44 1293 424000
FAX +44 1293 421880

B.2 Pump

http://www.aquatec.com

DEMAND/DELIVERY PUMPS
TRANSFER/DISPENSING PUMPS
5800/7800 SERIES

DIAPHRAGM PUMPS

These pumps are designed for intermittent duty, though most models can be run continuously for hours at a time. They are commonly used either to pressurize water from an atmospheric tank, to deliver purified water to a specific point of use, or simply to increase pressure when required.

These pumps can be controlled by either a pressure switch ("demand" mode) or an external power control device ("delivery" mode). When required, an integrated bypass can be incorporated to help regulate pressure levels.

TYPICAL APPLICATIONS

Water Treatment/RO
Beverage/Foodservice(*)
Distillation Equipment
Agricultural Spraying
General Industrial
Automotive

(*)See sample data sheet at right for model number 5852-7E12-B584, a basic demand/delivery pump

FULL RANGE CAPABILITIES FOR 5800/7800 MODELS ARE .2 GPM TO 2.0 GPM, 150 PSI MAXIMUM.

PERFORMANCE DATA

DISCHARGE PRESSURE	PUMPHEAD MODEL									
	58X0		58X1		58X2		58X3		58X4	
(PSI)	FLOW (GPM)	CURRENT (AMPS)	FLOW (GPM)	CURRENT (AMPS)	FLOW (GPM)	CURRENT (AMPS)	FLOW (GPM)	CURRENT (AMPS)	FLOW (GPM)	CURRENT (AMPS)
70	0.54	0.41	0.67	0.48	0.87	0.59	0.95	0.68	1.00	0.75
60	0.60	0.38	0.72	0.45	0.91	0.54	1.00	0.63	1.07	0.70
50	0.66	0.35	0.78	0.41	0.95	0.50	1.06	0.58	1.16	0.64
40	0.70	0.32	0.83	0.37	0.98	0.46	1.14	0.53	1.24	0.58
30	0.76	0.30	0.87	0.34	1.03	0.41	1.20	0.48	1.30	0.52
20	0.83	0.26	0.91	0.30	1.10	0.36	1.27	0.42	1.37	0.47
10	0.90	0.23	0.95	0.26	1.16	0.33	1.34	0.39	1.44	0.43
OPEN	0.97	0.21	0.99	0.22	1.22	0.30	1.40	0.36	1.50	0.40

COMPLETING THE PART NUMBER:

58XX-7X12-B584

- Steel Mounting Plate (Other Types Available)
- Desired Shut-off Pressure & Code
  A = 30PSI C = 45PSI E = 60PSI
  B = 40PSI D = 50PSI F = 70PSI
- 70 PSI Pressure Switch Limit (Maximum Flow Components)
- Select Pumphead Model From Performance Data Chart
- 3 = Open Ports for 3/8I Compression Fitting
  5 = Push-to-Connect Ports for 3/8I Tubing

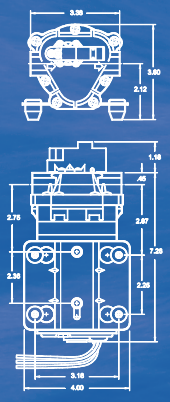

TECHNICAL SPECIFICATIONS:

POWER: Available motors from 12VDC to 230VAC, energy requirements between 25W-100W (depending on flow, pressure). Can be used with compatible transformers and/or DC power supplies, to be ordered separately. Standard terminations are 12", stripped end leadwires. Connectors and power cords are also available.

ENVELOPE DIMENSIONS: Approximately 3"x 4"x 7", weighing 6 lbs.

MOUNTING: All positions. Standard offering is a steel mounting base with four hollow rubber grommets.

CONTROL OPTIONS: Internal Bypass (20-200 psi), Pressure Switch (40-100 psi)

FITTINGS: 5800 Series options include built-in 3/8", 1/4", or 5/16" John Guest half cartridges. 7800 Series options include 3/8" or 1/2" hose barb, quick connect fittings. For additional information on fittings, please refer to page 21.

PRIMING CAPABILITIES:

	58X0	58X1	58X2	58X3	58X4
PRIME (FEET)	7	8	9	10	11

PHONE: **949-225-2200** • FAX: **949-225-2222** • WEBSITE: **www.aquatec.com**

B.3 Solenoid Valve

https://www.dultmeier.com/

SOLENOID VALVE
MODELS: 442P & 443P
INSTALLATION INSTRUCTIONS

1. **INSTALLATION:**
Model 442P has 1/4" NPT pipe connections and Model 443P has 3/8" NPT pipe connections. The valve may be mounted horizontally, on its side or in a vertical position. Connect piping to the valve so that the flow through the valve will follow the directional marking on the valve body. Apply pipe compound sparingly to the male fittings only. Note: If applied to the valve's threads, it may enter the valve and interfere with the valve operation. Avoid over tightening pipe to valve body and support and align pipe to eliminate pipe strain on valve body. **NOTE:** Wiring must comply with Local and National Electrical Codes.

2. **FLUIDS:**
Valves are intended for water, air, light oil, and other noncorrosive fluids. They should *not* be used for gasoline and other hazardous or explosive fluids. Maximum fluid temperature is 180° F (82°C). Ambient temperature shall not exceed 120°F (48.8°C).

WARNING: NOT FOR USE WITH HAZARDOUS OR CORROSIVE OR EXPLOSIVE FLUIDS.

3. **OPERATION:**
When the solenoid coil is energized the plunger is pulled up, thus opening the small "pilot port" in the center of the diaphragm plate. This releases the pressure on top of the diaphragm allowing incoming pressure to lift it off the larger center port. When the coil is de-energized the solenoid plunger is pushed down by the kick-off spring and closes the pilot port. Fluid passes through the small diaphragm bleed hole until pressure is equalized on both sides of the diaphragm to shut off the larger port.

4. **SPECIFICATIONS:**
Maximum operating pressure differential: 125 PSI
Safe working pressure: 150 PSI
Flow factor (C_v): 1.0
Maximum temperature: 180°F fluid temp.; 120° ambient temp.
Power: 10 Watts
Volt-Amp rating: Inrush - 16.0 VA
Holding - 11.5 VA

5. **TROUBLE SHOOTING:**
A) Failure to open or close:
   1. Coil burnout (over-voltage) or an open circuit to coil connections.
   2. No power or low voltage.
   3. Dirt, scale or sludge may prevent the plunger and diaphragm from operating.
   4. High differential pressure that exceeds the MOPD rating of valve (125 PSI Max.).
   5. Low differential pressure (3 PSI Min.)

B) Water Hammer:
   1. Quick acting valves may cause water hammer when operated. If this occurs, it may be minimized by the use of a standpipe or other commercially available shock absorber installed near the valve inlet.

CAUTION: WHEN SERVICING UNIT BE SURE THAT REPLACEMENT PARTS HAVE BEEN INSTALLED ACCORDING TO DRAWING.

RETURNS: NO MERCHANDISE MAY BE RETURNED FOR CREDIT WITHOUT DEMA'S WRITTEN PERMISSION. RETURN MERCHANDISE AUTHORIZATION NUMBER REQUIRED IN ADVANCE OF RETURN.

WARRANTY: DEMA products are warranted against defective material and workmanship under normal use and service for one year from the date of manufacture. This limited warranty does not apply to any products which have a normal life shorter than one year or failure and damage caused by chemicals, corrosion, improper voltage supply, physical abuse, or misapplication. Rubber and synthetic rubber parts such as "o"- rings, diaphragms, squeeze tubing and gaskets are considered expendable and are not covered under warranty. This warranty is extended only to the original buyer of DEMA products. If products are altered or repaired without prior approval of DEMA, this warranty will be void.

Defective units or parts should be returned to the factory with transportation prepaid. If inspection shows them to be defective, they will be repaired or replaced without charge, F.O.B. factory. DEMA assumes no liability for damages. Return merchandise authorization number, to return units for repair or replacement, must be granted in advance of return.

SOLENOID VALVE
MODELS: 442P & 443P
INSTALLATION INSTRUCTIONS

1. **INSTALLATION:**
Model 442P has 1/4" NPT pipe connections and Model 443P has 3/8" NPT pipe connections. The valve may be mounted horizontally, on its side or in a vertical position. Connect piping to the valve so that the flow through the valve will follow the directional marking on the valve body. Apply pipe compound sparingly to the male fittings only. Note: If applied to the valve's threads, it may enter the valve and interfere with the valve operation. Avoid over tightening pipe to valve body and support and align pipe to eliminate pipe strain on valve body. **NOTE:** Wiring must comply with Local and National Electrical Codes.

2. **FLUIDS:**
Valves are intended for water, air, light oil, and other noncorrosive fluids. They should *not* be used for gasoline and other hazardous or explosive fluids. Maximum fluid temperature is 180° F (82°C). Ambient temperature shall not exceed 120°F (48.8°C).

WARNING: NOT FOR USE WITH HAZARDOUS OR CORROSIVE OR EXPLOSIVE FLUIDS.

3. **OPERATION:**
When the solenoid coil is energized the plunger is pulled up, thus opening the small "pilot port" in the center of the diaphragm plate. This releases the pressure on top of the diaphragm allowing incoming pressure to lift it off the larger center port. When the coil is de-energized the solenoid plunger is pushed down by the kick-off spring and closes the pilot port. Fluid passes through the small diaphragm bleed hole until pressure is equalized on both sides of the diaphragm to shut off the larger port.

4. **SPECIFICATIONS:**
Maximum operating pressure differential: 125 PSI
Safe working pressure: 150 PSI
Flow factor (C_v): 1.0
Maximum temperature: 180°F fluid temp.; 120° ambient temp.
Power: 10 Watts
Volt-Amp rating: Inrush - 16.0 VA
Holding - 11.5 VA

5. **TROUBLE SHOOTING:**
A) Failure to open or close:
   1. Coil burnout (over-voltage) or an open circuit to coil connections.
   2. No power or low voltage.
   3. Dirt, scale or sludge may prevent the plunger and diaphragm from operating.
   4. High differential pressure that exceeds the MOPD rating of valve (125 PSI Max.).
   5. Low differential pressure (3 PSI Min.)

B) Water Hammer:
   1. Quick acting valves may cause water hammer when operated. If this occurs, it may be minimized by the use of a standpipe or other commercially available shock absorber installed near the valve inlet.

CAUTION: WHEN SERVICING UNIT BE SURE THAT REPLACEMENT PARTS HAVE BEEN INSTALLED ACCORDING TO DRAWING.

RETURNS: NO MERCHANDISE MAY BE RETURNED FOR CREDIT WITHOUT DEMA'S WRITTEN PERMISSION. RETURN MERCHANDISE AUTHORIZATION NUMBER REQUIRED IN ADVANCE OF RETURN.

WARRANTY: DEMA products are warranted against defective material and workmanship under normal use and service for one year from the date of manufacture. This limited warranty does not apply to any products which have a normal life shorter than one year or failure and damage caused by chemicals, corrosion, improper voltage supply, physical abuse, or misapplication. Rubber and synthetic rubber parts such as "o"- rings, diaphragms, squeeze tubing and gaskets are considered expendable and are not covered under warranty. This warranty is extended only to the original buyer of DEMA products. If products are altered or repaired without prior approval of DEMA, this warranty will be void.

Defective units or parts should be returned to the factory with transportation prepaid. If inspection shows them to be defective, they will be repaired or replaced without charge, F.O.B. factory. DEMA assumes no liability for damages. Return merchandise authorization number, to return units for repair or replacement, must be granted in advance of return.

B.4 Flow sensors

B.4.1 Electromagnetic Flow Sensor

http://www.omega.com/pptst/FMG90.html

ELECTROMAGNETIC FLOW METER

With PVDF and 316L Construction

FMG90 Series

1 YEAR WARRANTY CE

- **No Moving Parts or Obstructions**
- **Independent to Changes of Temperature, Pressure, Viscosity**
- **Lightweight and Compact Design**
- **PVDF and 316L Wetted Parts**
- **Fast Response (<100 ms)**

OMEGA's FMG90 Series electro-magnetic flow sensor for conductive liquid media was developed for OEM applications and does not contain any moving parts. FMG90 series is the most economic electromagnetic flow meter due to the cost optimized plastic construction. Its design is compact and lightweight. Six flow ranges are available. Changes in temperature, density, viscosity, concentration or electrical conductivity of the medium do not affect the output signal. The sensor is intended for continuous measurement of flow rates or for dosing/batching of liquids with a minimum conductivity of 20 µS/cm.

FMG94-PVDF shown actual size.

H

SPECIFICATIONS

Materials:
Electrodes and Grounding Rings: Stainless steel 316L
Measuring Pipe and Process Connections: PVDF
O-Rings: EPDM
Housing: ABS
Accuracy: 1% of reading
Repeatability: 1%
Minimum Conductivity of Medium: Water and other conductive liquids/ 20 µS/cm
Medium Temperature: -10 to 60ºC (14 to 140°F) (non-freezing)
Ambient Temperature: 5 to 60ºC (41 to 140°F)
Maximum Working Pressure:
145 psi at 20ºC (68°F)
116 psi at 40ºC (104°F)
87 psi at 60ºC (140°F)
Response Time: <100 ms
Indications: Red LED = power, green LED = flow
Signal Shape: Square wave frequency, can be connected as PNP or NPN open collector pulse duty ratio 50:50, maximum signal current 25 mA
Electrical Data:
Supply: 24 Vdc ±15%
Consumption: 0.6 W
Protection Measures: Short-circuit proof and polarity protection
Connection: 4 pin plug connector M12 x 1
Class: NEMA 4 (IP65) (with attached cable socket)

Model No.	FMG99-PVDF	FMG91-PVDF	FMG92-PVDF	FMG93-PVDF	FMG94-PVDF	FMG95-PVDF	FMG96-PVDF
Size	DN 3	DN 8	DN 8	DN 15	DN 20	DN 20	DN 25
Process Connection NPT	⅜–18	½–14	½–14	¾–14	1–11.5	1–11.5	1¼–11.5
Flow Range GPM	0.026 to 0.53	0.066 to 1.3	0.26 to 5.3	0.66 to 13.2	1.3 to 26.4	2.6 to 53	3.3 to 66
Signal Output Starts At GPM	0.013	0.02	0.07	0.27	0.52	1.05	1.3
Maximum Flow Rate GPM	0.55	1.6	6.6	15.8	31.7	63.4	79.3
Pulse Rate (pulse/gal)	30,000	15,000	3000	1500	750	380	300

H-1

http://www.omega.com/pptst/FMG90.html

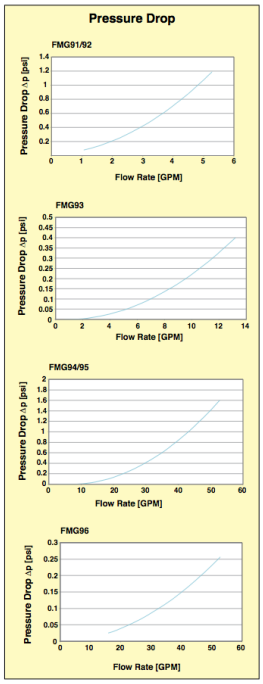

FMG99-PVDF thru FMG95-PVDF

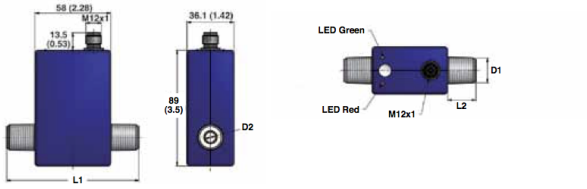

Model No.	L1	L2	D1	D2
FMG99-PVDF	3.68 ± 0.02	0.63 ± 0.01	⅜ - 18 NPT	Ø 0.118
FMG91-PVDF	4 ± 0.02	0.83 ± 0.01	½ - 14 NPT	Ø 0.31
FMG92-PVDF	4 ± 0.02	0.83 ± 0.01	½ - 14 NPT	Ø 0.31
FMG93-PVDF	4.02 ± 0.02	0.83 ± 0.01	¾ - 14 NPT	Ø 0.55
FMG94-PVDF	4.41 ± 0.02	0.98 ± 0.01	1 - 11.5 NPT	Ø 0.71
FMG95-PVDF	4.41 ± 0.02	0.98 ± 0.01	1 - 11.5 NPT	Ø 0.71

FMG96-PVDF

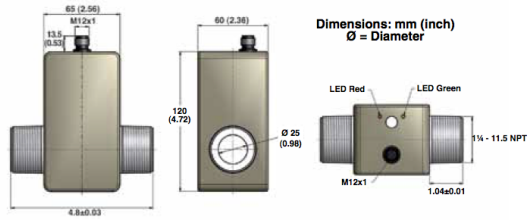

To Order

Model No.	Model No. with BSP	Description (cable sold separately)
FMG99-PVDF	**FMG99-PVDF-BSP**	Electromagnetic flow meter ⅜ NPT, 0.026 to 0.53 GPM
FMG91-PVDF	**FMG91-PVDF-BSP**	Electromagnetic flow meter ½ NPT, 0.07 to 1.3 GPM
FMG92-PVDF	**FMG92-PVDF-BSP**	Electromagnetic flow meter ½ NPT, 0.26 to 5.3 GPM
FMG93-PVDF	**FMG93-PVDF-BSP**	Electromagnetic flow meter ¾ NPT, 0.66 to 13.2 GPM
FMG94-PVDF	**FMG94-PVDF-BSP**	Electromagnetic flow meter 1 NPT, 1.3 to 26.4 GPM
FMG95-PVDF	**FMG95-PVDF-BSP**	Electromagnetic flow meter 1 NPT, 2.6 to 53 GPM
FMG96-PVDF	**FMG96-PVDF-BSP**	Electromagnetic flow meter 1¼ NPT, 3.3 to 66 GPM

Accessories

Model No.	Description
M12C-PVC-4-R-F-5	5 m (16.4') cable with right angle M12 x stripped leads
M12C-PVC-4-R-F-10	10 m (32.8') cable with right angle M12 x stripped leads
PSU-93	Unregulated power supply

Comes complete with operator's manual (cable sold separately).

Ordering Example: FMG91-PVDF, *electomagnetic flow meter with ½ NPT connections and 0.07 to 1.3 GPM range with* ***M12C-PVC-4-R-F-5*** *5 m (16.4') cable with right angle M12 connector.*

H-2

B.4.2 Paddle Wheel Flow Sensor

G1&2" Water Flow Sensor

SKU 314150005

- Compact, Easy to Install
- High Sealing Performance
- High-Quality Hall Effect Sensor

https://www.seeedstudio.com/water-flow-sensor-p-635.html

Description

Water flow sensor consists of a plastic valve body, a water rotor, and a hall-effect sensor. When water flows through the rotor, rotor rolls. Its speed changes with different rate of flow. The hall-effect sensor outputs the corresponding pulse signal. This one is suitable to detect flow in water dispenser or coffee machine. We have a comprehensive line of water flow sensors in different diameters. Check them out to find the one that meets your need most.

Features

- Compact, Easy to Install
- High Sealing Performance
- High Quality Hall Effect Sensor
- RoHS Compliant

Specifications

- Mini. Wokring Voltage: DC 4.5V
- Max. Working Current: 15mA (DC 5V)
- Working Voltage: DC 5V~24V
- Flow Rate Range: 1~30L/min
- Load Capacity: ≤10mA (DC 5V)
- Operating Temperature: ≤80°C
- Liquid Temperature: ≤120°C
- Operating Humidity: 35%~90%RH
- Water Pressure: ≤1.75MPa
- Storage Temperature: -25~+ 80°C
- Storage Humidity: 25%~95%RH

B.5 Pressure sensors

http://www.wika.us/a_10_en_us.WIKA

Electronic pressure measurement

Pressure transmitter
For general industrial applications
Model A-10

WIKA data sheet PE 81.60

Applications

- Machine building
- Ship building
- Measurement and control technology
- Hydraulics and pneumatics
- Pumps and compressors

Special features

- Measuring ranges from 0 … 15 to 0 … 10,000 psi (0 … 0.6 to 0 … 1,000 bar)
- Non-linearity: 0.25 % or 0.5 %
- Output: 4 ... 20 mA, DC 0 ... 10 V, DC 0 ... 5 V and others
- Electrical connection: Angular connector form A and C, circular connector M12 x 1, cable outlet 2 m
- Process connection G ¼ A DIN 3852-E, ¼ NPT and others

Pressure transmitter model A-10

Description

The model A-10 pressure transmitter for general industrial applications not only has a compact design, but it also offers excellent quality at an extremely competitive price.

The user can choose between a non-linearity of 0.25 % or 0.5 %. A free test certificate provides information on the measuring points recorded during the manufacturing process.

The model A-10 is set up for worldwide use through the international cULus and GOST-R certifications. The various pressure ranges and process connections required for particular operating conditions are available on short notice.

Data sheets showing similar products:
Pressure transmitter for general applications; model S-10; see data sheet PE 81.01

WIKA
Part of your business

Measuring ranges

Relative pressure									
bar	**Measuring range**	**0 ... 0.6**	**0 ... 1**	**0 ... 1.6**	**0 ... 2.5**	**0 ... 4**	**0 ... 6**	**0 ... 10** [1]	**0 ... 16** [1]
	Overpressure limit	1.2	2	3.2	5	8	12	20	32
	Measuring range	**0 ... 25** [1]	**0 ... 40**	**0 ... 60**	**0 ... 100**	**0 ... 160**	**0 ... 250**	**0 ... 400**	**0 ... 600**
	Overpressure limit	50	80	120	200	320	500	800	1,200
	Measuring range	**0 ... 1,000**							
	Overpressure limit	1,500							
psi	**Measuring range**	**0 ... 15**	**0 ... 25**	**0 ... 30**	**0 ... 50**	**0 ... 100**	**0 ... 160** [1]	**0 ... 200** [1]	**0 ... 300** [1]
	Overpressure limit	30	60	60	100	200	290	400	600
	Measuring range	**0 ... 500**	**0 ... 1,000**	**0 ... 1,500**	**0 ... 2,000**	**0 ... 3,000**	**0 ... 5,000**	**0 ... 10,000**	
	Overpressure limit	1,000	1,740	2,900	4,000	6,000	10,000	17,400	

Absolute pressure									
bar	**Measuring range**	**0 ... 1**	**0 ... 1.6**	**0 ... 2.5**	**0 ... 4**	**0 ... 6**	**0 ... 10**	**0 ... 16**	**0 ... 25**
	Overpressure limit	2	3.2	5	8	12	20	32	50
psi	**Measuring range**	**0 ... 15**	**0 ... 25**	**0 ... 30**	**0 ... 50**	**0 ... 100**	**0 ... 150**	**0 ... 200**	**0 ... 300**
	Overpressure limit	30	60	60	100	200	290	400	600

Vacuum and +/- measuring range						
bar	**Measuring range**	**-1 ... 0**	**-1 ... +0.6**	**-1 ... +1.5**	**-1 ... +3**	**-1 ... +5**
	Overpressure limit	2	3.2	5	8	12
	Measuring range	**-1 ... +9**	**-1 ... +15**	**-1 ... +24**		
	Overpressure limit	20	32	50		
psi	**Measuring range**	**-30 inHg ... 0**	**-30 inHg ... +15**	**-30 inHg ... +30**	**-30 inHg ... +60**	**-30 inHg ... +100**
	Overpressure limit	30	60	60	150	250
	Measuring range	**-30 inHg ... +160**	**-30 inHg ... +200**	**-30 inHg ... +300**		
	Overpressure limit	350	450	600		

1) If the medium water is measured, a higher overpressure limit is recommended.

The given measuring ranges are also available in kg/cm², MPa and kPa.
Other measuring ranges available on request

Vacuum resistance
Yes

Output signal

Signal type	Signal
Current (2-wire)	4 ... 20 mA
Voltage (3-wire)	DC 0 ... 10 V DC 0 ... 5 V DC 1 ... 5 V DC 0.5 ... 4.5 V
Ratiometric (3-wire)	DC 0.5 ... 4.5 V

Other output signals available on request

Depending on the signal type the following loads apply:

Current (2-wire): ≤ (power supply - 8 V) / 0.02 A
Voltage (3-wire): > maximum output signal / 1 mA
Ratiometric (3-wire): > 4.5k

Voltage supply

Power supply

Output signal	Power supply	
	Standard	Option
4 ... 20 mA	DC 8 ... 30 V	DC 8 ... 35 V [2]
DC 0 ... 10 V	DC 14 ... 30 V	DC 14 ... 35 V
DC 0 ... 5 V	DC 8 ... 30 V	DC 8 ... 35 V
DC 1 ... 5 V	DC 8 ... 30 V	DC 8 ... 35 V
DC 0.5 ... 4.5 V	DC 8 ... 30 V	DC 8 ... 35 V
DC 0.5 ... 4.5 V ratiometric	DC 5 V ± 10 %	-

2) Not possible with non-linearity 0.25 % BFSL

The power supply for the pressure transmitter must be made via an energy-limited electrical circuit in accordance with section 9.3 of UL/EN/IEC 61010-1, or an LPS to UL/EN/IEC 60950-1, or class 2 in accordance with UL1310/UL1585 (NEC or CEC). The power supply must be suitable for operation above 2,000 m should the pressure transmitter be used at this altitude.

Total current consumption

Current (2-wire): Signal current, max. 25 mA
Voltage (3-wire): 8 mA
Ratiometric (3-wire): 8 mA

Accuracy

Optionally the model A-10 is available with an improved non-linearity. Depending on the selected non-linearity the following values result:

	Standard	Option
Non-linearity per BFSL (IEC 61298-2)	≤ ±0.5 % of span	≤ ±0.25 % of span
Measuring deviation of the zero signal	Typical: ≤ ±0.5% of span Maximum: ≤ ±0.8 % of span	Typical: ≤ ±0.15% of span Maximum: ≤ ±0.4 % of span
Accuracy at room temperature [3]	≤ ±1 % of span	≤ ±0.5 % of span ≤ ±0.6 % of span (at DC 0 ... 5 V)

3) Including non-linearity, hysteresis, zero offset and end value deviation (corresponds to measured error per IEC 61298-2), calibrated in vertical mounting position with process connection facing downwards

Non-repeatability
≤ 0.1 % of span

Signal noise
≤ ±0.3 % of span

Temperature error at 32 ... 176 °F (0 ... 80 °C)
- Typical: 1 % of span
- Maximum: 2.5 % of span

Long-term drift
≤ ±0.1 % of span

Appendix C

Derivation of State Equations

C.1 Extended single branch model: Mode 1

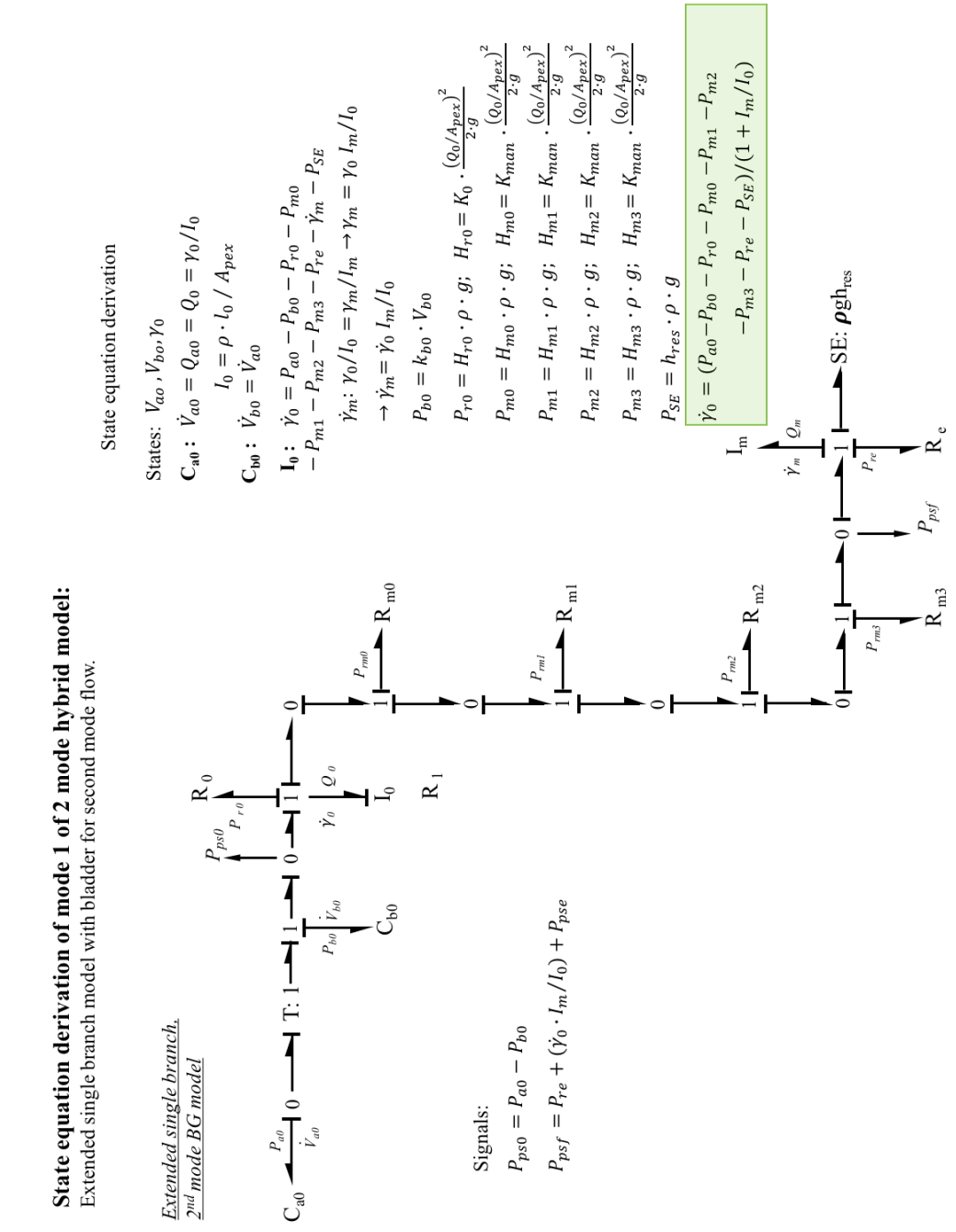

State equation derivation of mode 1 of 2 mode hybrid model:
Extended single branch model with bladder for second mode flow.

C.2 Extended single branch model: Mode 2

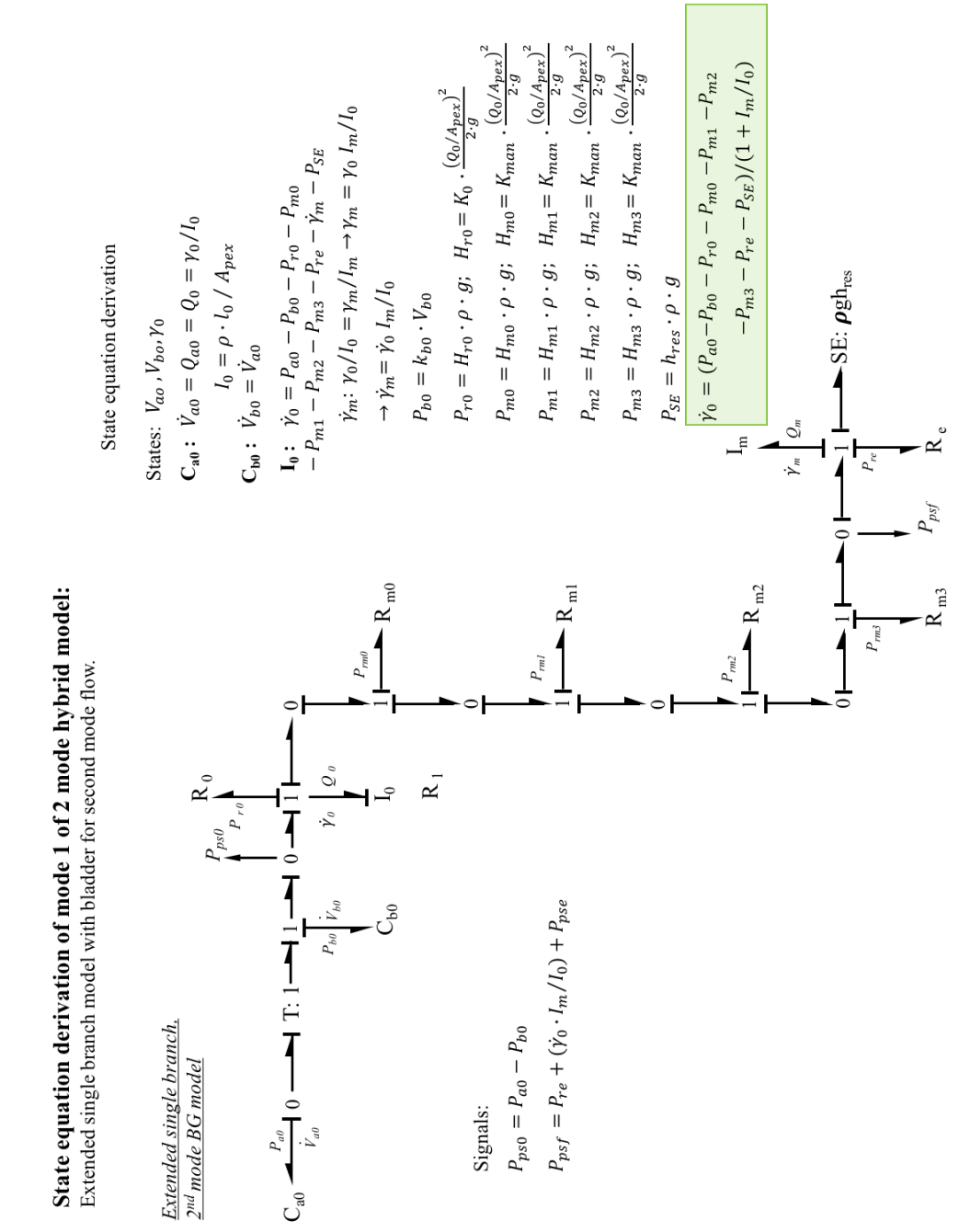

State equation derivation of mode 1 of 2 mode hybrid model:
Extended single branch model with bladder for second mode flow.

C.3 Multi-branch model: Mode 1

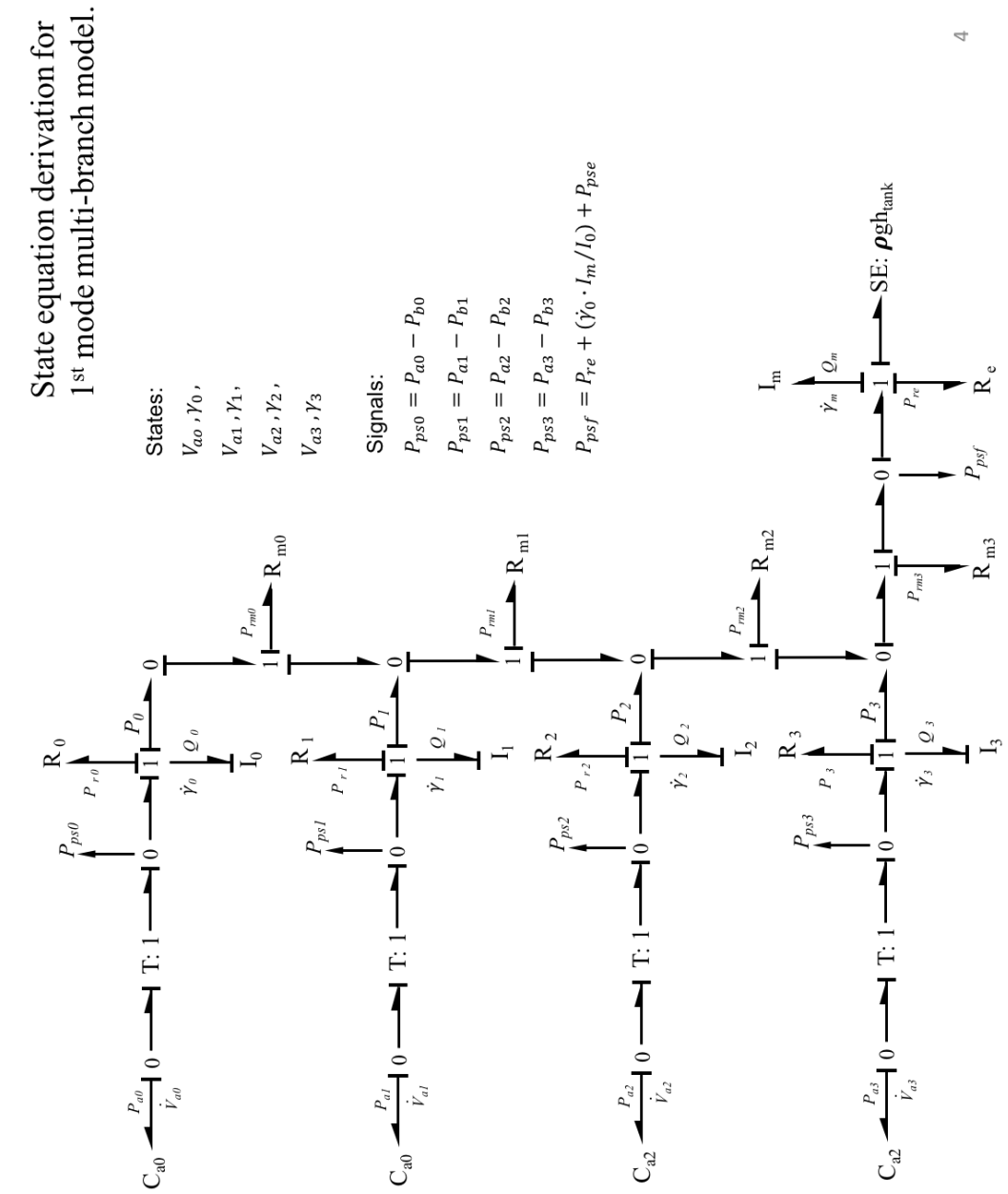

Derivation of the expression for coupled fluid inertia I_m:

$$\dot{\gamma}_0(1 + I_m/I_0) + \dot{\gamma}_1\, I_m/I_1 + \dot{\gamma}_2\, I_m/I_2 + \dot{\gamma}_3\, I_m/I_3 = P_{a0} - P_{r0} - P_{m0} - P_{m1} - P_{m2} - P_{m3} - P_{re} - P_{SE}$$

$$\dot{\gamma}_0\, I_m/I_0 + \dot{\gamma}_1\, (1 + I_m/I_1) + \dot{\gamma}_2\, I_m/I_2 + \dot{\gamma}_3\, I_m/I_3 = P_{a1} - P_{r1} - P_{m1} - P_{m2} - P_{m3} - P_{re} - P_{SE}$$

$$\dot{\gamma}_0\, I_m/I_0 + \dot{\gamma}_1\, I_m/I_1 + \dot{\gamma}_2\, I_m/I_2 + \dot{\gamma}_3(1 + I_m/I_3) = P_{a3} - P_{r3} - P_{m3} - P_{re} - P_{SE}$$

Giving us the matrix expression:

$$\begin{bmatrix} (1 + I_m/I_0) & I_m/I_1 & I_m/I_2 & I_m/I_3 \\ I_m/I_0 & (1 + I_m/I_1) & I_m/I_2 & I_m/I_3 \\ I_m/I_0 & I_m/I_1 & (1 + I_m/I_2) & I_m/I_3 \\ I_m/I_0 & I_m/I_1 & I_m/I_2 & (1 + I_m/I_3) \end{bmatrix} \begin{bmatrix} \dot{\gamma}_0 \\ \dot{\gamma}_1 \\ \dot{\gamma}_2 \\ \dot{\gamma}_3 \end{bmatrix} = \begin{bmatrix} P_{a0} - P_{r0} - P_{m0} - P_{m1} - P_{m2} - P_{m3} - P_{re} - P_{SE} \\ P_{a1} - P_{r1} - P_{m1} - P_{m2} - P_{m3} - P_{re} - P_{SE} \\ P_{a2} - P_{r2} - P_{m2} - P_{m3} - P_{re} - P_{SE} \\ P_{a3} - P_{r3} - P_{m3} - P_{re} - P_{SE} \end{bmatrix}$$

A $\quad \underline{\dot{\boldsymbol{\gamma}}}$ $\quad$ B

Thus we have the following matrix expression when solving for the derivative momentum vector $\underline{\dot{\boldsymbol{\gamma}}}$

$$\underline{\dot{\boldsymbol{\gamma}}} = inv\, A \cdot B$$

C.3.2 Multi-branch model, branch 0: Mode 1

State equation derivation for mode 1 branch 0 model of multibranch model:

$$\mathbf{C_{a0}}: \ \dot{V}_{a0} = Q_{a0} = Q_0 = \gamma_0 / I_0$$

$$I_0 = \rho \cdot l_0 \ / \ A_{pex}$$

$$\mathbf{I_0}: \ \dot{\gamma}_0 = P_{a0} - P_{r0} - P_0$$

$$\dot{\gamma}_m: \ (\gamma_0/I_0 + \gamma_1/I_1 + \gamma_2/I_2 + \gamma_3/I_3) = \gamma_m/I_m \ \rightarrow \ \gamma_m = (\gamma_0/I_0 + \gamma_1/I_1 + \gamma_2/I_2 + \gamma_3/I_3)I_m \rightarrow$$

$$\dot{\gamma}_m = \dot{\gamma}_0 \ I_m/I_0 + \dot{\gamma}_1 \ I_m/I_1 + \dot{\gamma}_2 \ I_m/I_2 + \dot{\gamma}_3 \ I_m/I_3$$

$$P_0 = P_{m0} - P_{m1} - P_{m2} - P_{m3} - P_{re} - \dot{\gamma}_m - P_{SE}$$

$$P_0 = P_{m0} - P_{m1} - P_{m2} - P_{m3} - P_{re} - (\dot{\gamma}_0 \ I_m/I_0 + \dot{\gamma}_1 \ I_m/I_1 + \dot{\gamma}_2 \ I_m/I_2 + \dot{\gamma}_3 \ I_m/I_3) - P_{SE}$$

$$P_{r0} = H_{r0} \cdot \rho \cdot g; \ \ H_{r0} = K_0 \cdot \frac{(Q_0/A_{pex})^2}{2 \cdot g}$$

$$P_{m0} = H_{m0} \cdot \rho \cdot g; \ \ H_{m0} = K_{man} \cdot \frac{(Q_0/A_{pex})^2}{2 \cdot g}$$

$$P_{m1} = H_{m1} \cdot \rho \cdot g; \ \ H_{m1} = K_{man} \cdot \frac{((Q_0+Q_1)/A_{pex})^2}{2 \cdot g}$$

$$P_{m2} = H_{m2} \cdot \rho \cdot g; \ \ H_{m2} = K_{man} \cdot \frac{((Q_0+Q_1+Q_2)/A_{pex})^2}{2 \cdot g}$$

$$P_{m3} = H_{m3} \cdot \rho \cdot g; \ \ H_{m3} = K_{man} \cdot \frac{((Q_0+Q_1+Q_2+Q_3)/A_{pex})^2}{2 \cdot g}$$

$$P_{re} = H_{re} \cdot \rho \cdot g; \ \ H_{re} = K_e \cdot \frac{((Q_0+Q_1+Q_2+Q_3)/A_{pex})^2}{2 \cdot g}$$

$$P_{SE} = h_{res} \cdot \rho \cdot g$$

$$\dot{\gamma}_0 = (P_{a0} - P_{r0} - P_{m0} - P_{m1} - P_{m2} - P_{m3} - P_{re} - (\dot{\gamma}_1 \ I_m/I_1 + \dot{\gamma}_2 \ I_m/I_2 + \dot{\gamma}_3 \ I_m/I_3) - P_{SE})/(1 + I_m/I_0)$$

C.3.3 Multi-branch model, branch 1: Mode 1

State equation derivation for mode 1 branch 1 model of multibranch model:

$$\mathbf{C_{a1}}: \ \dot{V}_{a1} = Q_{a1} = Q_1 = \gamma_1/I_1$$

$$I_1 = \rho \cdot l_1 \ / \ A_{pex}$$

$$\mathbf{I_1}: \ \dot{\gamma}_1 = P_{a1} - P_{r1} - P_1$$

$$\dot{\gamma}_m: \ (\gamma_0/I_0 + \gamma_1/I_1 + \gamma_2/I_2 + \gamma_3/I_3) = \gamma_m/I_m \ \rightarrow \ \gamma_m = \ (\gamma_0/I_0 + \gamma_1/I_1 + \gamma_2/I_2 + \gamma_3/I_3)I_m \ \rightarrow$$

$$\dot{\gamma}_m = \dot{\gamma}_0 \ I_m/I_0 + \dot{\gamma}_1 \ I_m/I_1 + \dot{\gamma}_2 \ I_m/I_2 + \dot{\gamma}_3 \ I_m/I_3$$

$$P_1 = P_{m1} - P_{m2} - P_{m3} - P_{re} - \dot{\gamma}_m - P_{SE}$$

$$P_1 = P_{m1} - P_{m2} - P_{m3} - P_{re} - (\dot{\gamma}_0 \ I_m/I_0 + \dot{\gamma}_1 \ I_m/I_1 + \dot{\gamma}_2 \ I_m/I_2 + \dot{\gamma}_3 \ I_m/I_3) - P_{SE}$$

$$P_{r1} = H_{r1} \cdot \rho \cdot g; \ \ H_{r1} = K_1 \cdot \frac{(Q_1/A_{pex})^2}{2 \cdot g}$$

$$P_{m1} = H_{m1} \cdot \rho \cdot g; \ \ H_{m1} = K_{man} \cdot \frac{((Q_0+Q1)/A_{pex})^2}{2 \cdot g}$$

$$P_{m2} = H_{m2} \cdot \rho \cdot g; \ \ H_{m2} = K_{man} \cdot \frac{((Q_0+Q1+Q2)/A_{pex})^2}{2 \cdot g}$$

$$P_{m3} = H_{m3} \cdot \rho \cdot g; \ \ H_{m3} = K_{man} \cdot \frac{((Q_0+Q1+Q2+Q3)/A_{pex})^2}{2 \cdot g}$$

$$P_{re} = H_{re} \cdot \rho \cdot g; \ \ H_{re} = K_e \cdot \frac{((Q_0+Q1+Q2+Q3)/A_{pex})^2}{2 \cdot g}$$

$$P_{SE} = h_{res} \cdot \rho \cdot g$$

$$\dot{\gamma}_1 = (P_{a1} - P_{r1} - P_{m1} \ - P_{m2} - P_{m3} - P_{re} - (\dot{\gamma}_0 \ I_m/I_0 + \dot{\gamma}_2 \ I_m/I_2 + \dot{\gamma}_3 \ I_m/I_3) - P_{SE})/(1 + I_m/I_1)$$

State equation derivation for mode 1 branch 2 model of multibranch model:

$\mathbf{C_{a2}}$: $\dot{V}_{a2} = Q_{a2} = Q_2 = \gamma_2/I_2$

$$I_2 = \rho \cdot l_2 \,/\, A_{pex}$$

$\mathbf{I_2}$: $\dot{\gamma}_2 = P_{a2} - P_{r2} - P_2$

$\dot{\gamma}_m$: $(\gamma_0/I_0 + \gamma_1/I_1 + \gamma_2/I_2 + \gamma_3/I_3) = \gamma_m/I_m \;\rightarrow\; \gamma_m = (\gamma_0/I_0 + \gamma_1/I_1 + \gamma_2/I_2 + \gamma_3/I_3)I_m \rightarrow$

$$\dot{\gamma}_m = \dot{\gamma}_0\, I_m/I_0 + \dot{\gamma}_1\, I_m/I_1 + \dot{\gamma}_2\, I_m/I_2 + \dot{\gamma}_3\, I_m/I_3$$

$$P_2 = P_{m1} + P_{m2} + P_{m3} + P_{re} + \dot{\gamma}_m + P_{SE}$$

$$P_2 = P_{m1} + P_{m2} + P_{m3} + P_{re} + (\dot{\gamma}_0\, I_m/I_0 + \dot{\gamma}_1\, I_m/I_1 + \dot{\gamma}_2\, I_m/I_2 + \dot{\gamma}_3\, I_m/I_3) + P_{SE}$$

$$P_{m2} = H_{m2} \cdot \rho \cdot g; \quad H_{m2} = K_{man} \cdot \frac{((Q_0+Q1+Q2)/A_{pex})^2}{2 \cdot g}$$

$$P_{m3} = H_{m3} \cdot \rho \cdot g; \quad H_{m3} = K_{man} \cdot \frac{((Q_0+Q1+Q2+Q3)/A_{pex})^2}{2 \cdot g}$$

$$P_{re} = H_{re} \cdot \rho \cdot g; \quad H_{re} = K_e \cdot \frac{((Q_0+Q1+Q2+Q3)/A_{pex})^2}{2 \cdot g}$$

$$P_{SE} = h_{res} \cdot \rho \cdot g$$

$$\dot{\gamma}_2 = (P_{a2} - P_{r2} - P_{m2} - P_{m3} - P_{re} - (\dot{\gamma}_0\, I_m/I_0 + \dot{\gamma}_1\, I_m/I_1 + \dot{\gamma}_3\, I_m/I_3) - P_{SE})/(1 + I_m/I_2)$$

State equation derivation for mode 1 branch 3 model of multibranch model:

$\mathbf{C_{a3}}$: $\dot{V}_{a3} = Q_{a3} = Q_3 = \gamma_3/I_3$

$$I_3 = \rho \cdot l_3 \,/\, A_{pex}$$

$\mathbf{I_3}$: $\dot{\gamma}_3 = P_{a3} - P_{r3} - P_3$

$\dot{\gamma}_m$: $(\gamma_0/I_0 + \gamma_1/I_1 + \gamma_2/I_2 + \gamma_3/I_3) = \gamma_m/I_m \;\rightarrow\; \gamma_m = (\gamma_0/I_0 + \gamma_1/I_1 + \gamma_2/I_2 + \gamma_3/I_3)I_m \rightarrow$

$$\dot{\gamma}_m = \dot{\gamma}_0\, I_m/I_0 + \dot{\gamma}_1\, I_m/I_1 + \dot{\gamma}_2\, I_m/I_2 + \dot{\gamma}_3\, I_m/I_3$$

$$P_3 = P_{m3} + P_{re} + \dot{\gamma}_m + P_{SE}$$

$$P_3 = P_{m3} + P_{re} + (\dot{\gamma}_0\, I_m/I_0 + \dot{\gamma}_1\, I_m/I_1 + \dot{\gamma}_2\, I_m/I_2 + \dot{\gamma}_3\, I_m/I_3) + P_{SE}$$

$$P_{m3} = H_{m3} \cdot \rho \cdot g; \quad H_{m3} = K_{man} \cdot \frac{\left((Q_0+Q1+Q2+Q3)/A_{pex}\right)^2}{2 \cdot g}$$

$$P_{re} = H_{re} \cdot \rho \cdot g; \quad H_{re} = K_e \cdot \frac{\left((Q_0+Q1+Q2+Q3)/A_{pex}\right)^2}{2 \cdot g}$$

$$P_{SE} = h_{res} \cdot \rho \cdot g$$

$$\dot{\gamma}_3 = (P_{a3} - P_{r3} - P_{m3} - P_{re} + (\dot{\gamma}_0\, I_m/I_0 + \dot{\gamma}_1\, I_m/I_1 + \dot{\gamma}_2\, I_m/I_2) + P_{SE})/(1 + I_m/I_3)$$

C.4 Multi-branch model: Mode 2

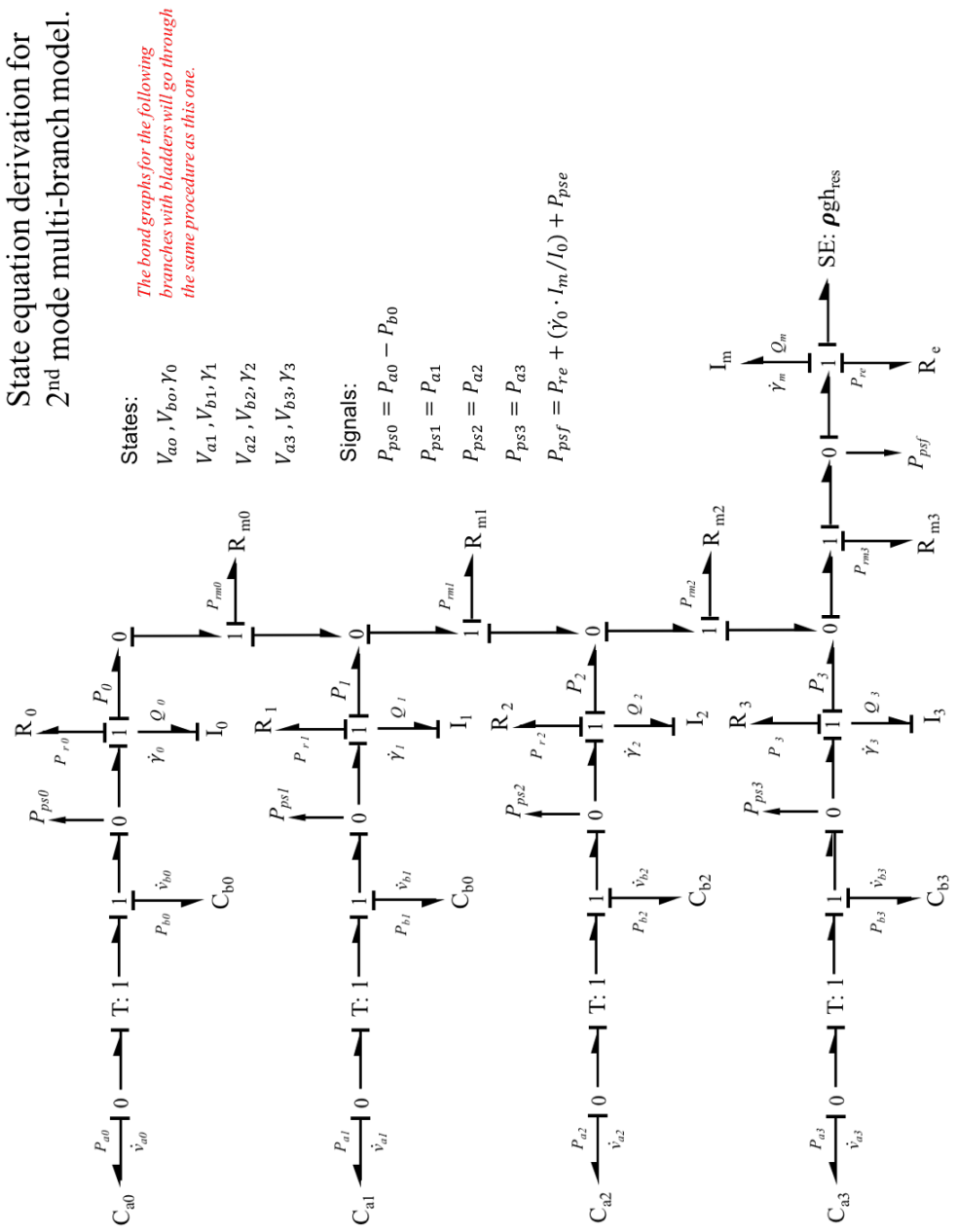

C.4.1 Multi-branch model, branch 0: Mode 2

State equation derivation for mode 2 branch 0 model of multibranch model:

$$\mathbf{C_{a0}}: \ \dot{V}_{a0} = Q_{a0} = Q_0 = \gamma_0 / l_0$$

$$l_0 = \rho \cdot l_0 / A_{pex}$$

$$\mathbf{C_{b0}}: \ \dot{V}_{b0} = \dot{V}_{a0}$$

$$\mathbf{I_0}: \ \dot{\gamma}_0 = P_{a0} - P_{b0} - P_{r0} - P_0$$

$$P_0 = P_{m0} + P_{m1} + P_{m2} + P_{m3} + P_{re} + \dot{\gamma}_m + P_{SE}$$

$$P_{r0} = H_{r0} \cdot \rho \cdot g; \ \ H_{r0} = K_0 \cdot \frac{(Q_0/A_{pex})^2}{2 \cdot g}$$

See derivation of gamma dot m vector

$$P_{m0} = H_{m0} \cdot \rho \cdot g; \ \ H_{m0} = K_{man} \cdot \frac{(Q_0/A_{pex})^2}{2 \cdot g}$$

$$P_{m1} = H_{m1} \cdot \rho \cdot g; \ \ H_{m1} = K_{man} \cdot \frac{((Q_0+Q1)/A_{pex})^2}{2 \cdot g}$$

$$P_{m2} = H_{m2} \cdot \rho \cdot g; \ \ H_{m2} = K_{man} \cdot \frac{((Q_0+Q1+Q2)/A_{pex})^2}{2 \cdot g}$$

$$P_{m3} = H_{m3} \cdot \rho \cdot g; \ \ H_{m3} = K_{man} \cdot \frac{((Q_0+Q1+Q2+Q3)/A_{pex})^2}{2 \cdot g}$$

$$P_{re} = H_{re} \cdot \rho \cdot g; \ \ H_{re} = K_e \cdot \frac{((Q_0+Q1+Q2+Q3)/A_{pex})^2}{2 \cdot g}$$

$$P_{SE} = h_{res} \cdot \rho \cdot g$$

$$P_{b0} = k_{b0} \cdot V_{b0}$$

$\dot{\gamma}_0$ ← See derivation of gamma dot m vector

C.4.2 Multi-branch model, branch 1: Mode 2

State equation derivation for mode 2 branch 1 model of multibranch model:

$\mathbf{C_{a1}}$: $\dot{V}_{a1} = Q_{a1} = Q_1 = \gamma_1 / I_1$

$$I_1 = \rho \cdot l_1 / A_{pex}$$

$\mathbf{C_{b1}}$: $\dot{V}_{b1} = \dot{V}_{a1}$

$\mathbf{I_1}$: $\dot{\gamma}_1 = P_{a1} - P_{b1} - P_{r1} - P_1$

$$P_1 = P_{m1} - P_{m2} - P_{m3} - P_{re} - \dot{\gamma}_m - P_{SE}$$

See derivation of gamma dot m vector

$$P_{r1} = H_{r1} \cdot \rho \cdot g; \quad H_{r1} = K_1 \cdot \frac{(Q_1/A_{pex})^2}{2 \cdot g}$$

$$P_{m1} = H_{m1} \cdot \rho \cdot g; \quad H_{m1} = K_{man} \cdot \frac{((Q_0+Q_1)/A_{pex})^2}{2 \cdot g}$$

$$P_{m2} = H_{m2} \cdot \rho \cdot g; \quad H_{m2} = K_{man} \cdot \frac{((Q_0+Q_1+Q_2)/A_{pex})^2}{2 \cdot g}$$

$$P_{m3} = H_{m3} \cdot \rho \cdot g; \quad H_{m3} = K_{man} \cdot \frac{((Q_0+Q_1+Q_2+Q_3)/A_{pex})^2}{2 \cdot g}$$

$$P_{re} = H_{re} \cdot \rho \cdot g; \quad H_{re} = K_e \cdot \frac{((Q_0+Q_1+Q_2+Q_3)/A_{pex})^2}{2 \cdot g}$$

$$P_{SE} = h_{res} \cdot \rho \cdot g$$

$$P_{b1} = k_{b1} \cdot V_{b1}; \; k_{b1} = 1/C_{b1}$$

$\dot{\boldsymbol{\gamma}}_{\mathbf{1}}$ ← See derivation of gamma dot m vector for coupled gamma dot

C.4.3 Multi-branch model, branch 2: Mode 2

State equation derivation for mode 2 branch 2 model of multibranch model:

$\mathbf{C_{a2}}$: $\dot{V}_{a2} = Q_{a2} = Q_2 = \gamma_2 / I_2$

$I_2 = \rho \cdot l_2 \,/\, A_{pex}$

$\mathbf{C_{b2}}$: $\dot{V}_{b2} = \dot{V}_{a2}$

$\mathbf{I_2}$: $\dot{\gamma}_2 = P_{a2} - P_{b2} - P_{r2} - P_2$

$P_2 = P_{m1} + P_{m2} + P_{m3} + P_{re} + \dot{\gamma}_m + P_{SE}$

$P_2 = P_{m1} + P_{m2} + P_{m3} + P_{re} + (\dot{\gamma}_0\, I_m/I_0 + \dot{\gamma}_1\, I_m/I_1 + \dot{\gamma}_2\, I_m/I_2 + \dot{\gamma}_3\, I_m/I_3) + P_{SE}$

$P_{m2} = H_{m2} \cdot \rho \cdot g;\;\; H_{m2} = K_{man} \cdot \frac{((Q_0+Q1+Q2)/A_{pex})^2}{2 \cdot g}$

$P_{m3} = H_{m3} \cdot \rho \cdot g;\;\; H_{m3} = K_{man} \cdot \frac{((Q_0+Q1+Q2+Q3)/A_{pex})^2}{2 \cdot g}$

$P_{re} = H_{re} \cdot \rho \cdot g;\;\; H_{re} = K_e \cdot \frac{((Q_0+Q1+Q2+Q3)/A_{pex})^2}{2 \cdot g}$

$P_{SE} = h_{res} \cdot \rho \cdot g$

$P_{b2} = k_{b2} \cdot V_{b2};\;\; k_{b2} = 1/\, C_{b2}$

$\dot{\gamma}_2$

See derivation of gamma dot m vector

See derivation of gamma dot m vector for coupled gamma dot

C.4.4 Multi-branch model, branch 3: Mode 2

State equation derivation for mode 2 branch 3 model of multibranch model:

$$\mathbf{C_{a3}}: \ \dot{V}_{a3} = Q_{a3} = Q_3 = \gamma_3 / l_3$$

$$l_3 = \rho \cdot l_3 \ / \ A_{pex}$$

$$\mathbf{C_{b3}}: \ \dot{V}_{b3} = \dot{V}_{a3}$$

$$\mathbf{I_3}: \ \dot{\gamma}_3 = P_{a3} - P_{b3} - P_{r3} - P_3$$

$$P_3 = P_{m3} + P_{re} + \dot{\gamma}_m + P_{SE}$$

$$P_3 = P_{m3} + P_{re} + (\dot{\gamma}_0 \ I_m / I_0 + \dot{\gamma}_1 \ I_m / I_1 + \dot{\gamma}_2 \ I_m / I_2 + \dot{\gamma}_3 \ I_m / I_3) + P_{SE}$$

$$P_{m3} = H_{m3} \cdot \rho \cdot g; \ \ H_{m3} = K_{man} \cdot \frac{((Q_0+Q1+Q2+Q3)/A_{pex})^2}{2 \cdot g}$$

$$P_{re} = H_{re} \cdot \rho \cdot g; \ \ H_{re} = K_e \cdot \frac{((Q_0+Q1+Q2+Q3)/A_{pex})^2}{2 \cdot g}$$

$$P_{SE} = h_{res} \cdot \rho \cdot g$$

$$P_{b3} = k_{b3} \cdot V_{b3}; \ k_{b3} = 1 / C_{b3}$$

$\dot{\gamma}_3$ ← See derivation of gamma dot m vector for coupled gamma dot

See derivation of gamma dot m vector

Appendix D

Matlab M-file code for HPPFN Models

D.1 Run file for extended single branch, *branch0_multi.m*

```
%%%% FILENAME: branch0_multi.m
% Extended single branch model, as modular piece of multi branch model.
% Branch 0 configuration see notes for multibranch 01
% Inertia Im full inertia of manifold.

% J. Campos
% 18 MAR 2017

clear all
%Ensure experimental data .mat files are loaded
load('t_exp0.mat')
load('Pa0_exp0.mat')
load('Pout_exp0.mat')

global g rho gamma
global K0 Km0 Km1 Km2 Km3 Ke kb0
global Aae Apex
global Vc0 Pc0 Vpc Pse I0 Im t_del

% Conversion factors
m32gal  = 264.172;        % m^3 to gallons
m3s2ls  = 1000;
m3s2gpm = 15852;          % (m^3)/s to gallons/min
Pa2PSI  = 0.145/1000;     % Pa to PSI
Psi2Pa  = 1/Pa2PSI;       % PSI to Pa

% Physical constants
gamma = 1.4;        % ideal gas ratio of the Cv and Cp heat capacity
g = 9.81;           % acceleration due to gravity [m/s^2]
rho = 1000;         % density of fluid (water) [kg/m^3]
mu = 1e-3;          % Dynamic viscousity of water [Pa-s]
nu = 9e-7;          % Kinematic viscosity of water [m^2/s]
Patm = 1.01e5;      % Atmospheric pressure (Pa)

% Geometric constants
Aacc  = pi() * .0381^2;% Accumulator crossectional area
Acc_r = .006;          % Inner radius of accumulator exit pipe
Aae = pi() * Acc_r^2;  % Hydraulic CS area of accumulator exit pipe
Pex_rad = .00635;      % Inner radius of PEX line [m]
Pex_t = 3.175e-4;      % Wall thickness of PEX line [m]
Pex_d = 2 * Pex_rad;
Apex = pi() * Pex_rad^2;% Hydraulic CS area of PEX tubing
Pex_l0 = .6016;        % Length of PEX line in branch [m] #### This
should probably be losses associated with 90 degree elbow.
Pex_lm0 = .500;        % Total length of PEX in manifold to psf
starting at junction with branch0. [m]
Pex_le = .615;         % Total length of PEX from psf to exhaust. [m]
Brass_rad = .0125;     % Inner radius of brass fittings [m]
Brass_t = .03175;      % Wall thickness of brass fitting [m]
Brass_l0 = .38;        % Length of brass fitting in branch [m]
Brass_lm0 = .127;      % Total length of brass fittings in manifold to
exhaust, starting at junction with branch0. [m]

% Hydraulic component friction flow factors
```

```
 52 Kpe  = 0.28;            % Flow factor for pipe entrance at accumulator
exit 0 - Ra0 (https://www.plumbingsupply.com/ed-frictionlosses.html)
 53 Kp0  = 0.54;            % Brass tee friction flow factor at pressure
sensor 0 (https://www.plumbingsupply.com/ed-frictionlosses.html)
 54 Kv0  = 1.00;            % Diaphragm valve value for control valve 0
(from product liturature DEMA eng)
 55 Kcv0 = 1.40;            % Brass check vavle for cv0 (https://www
plumbingsupply.com/ed-frictionlosses.html)
 56 Kfs0 = 1.00;            % Flow meter K estimated (see https://www.omega
com/Green/pdf/TURBINE_PADDLE_REF.pdf)
 57 Ke0  = 0.81;            % Brass 90 degree elbow (https://www
plumbingsupply.com/ed-frictionlosses.html)
 58 Ktm1 = Kp0;             % Brass tee fff at line one manifold connection.
 59 Ktm2 = Kp0;             % Brass tee fff at line two manifold connection.
 60 Ktm3 = Kp0;             % Brass tee fff at line three manifold
connection.
 61 Kpf  = Kp0;             % Brass tee fff at final pressure sensor.
 62 Kef  = Ke0;             % Brass 90 degree elbow (final)
 63 Kem  = 0.04;            % EM flow meter fff (ESTIMATED)
 64 Kff  = Kfs0;            % Flow meter K estimated (see https://www.omega
com/Green/pdf/TURBINE_PADDLE_REF.pdf)
 65 Kfe  = 1.00;            % Flow factor for pipe entrance at accumulator
exit into a much larger body of fluid (https://neutrium
net/fluid_flow/pressure-loss-from-pipe-entrances-and-exits/)
 66
 67 mrf = 6;
 68 K0   = 10 * (Kpe + Kp0 + Kv0 + Kcv0 + Kfs0);% Lumped parameter for R0
(before valve0)-1st stage
 69 Km0  = mrf * Ke0;    % Rm0 K value
 70 Km1  = mrf * Ktm1;   % Rm1 K value
 71 Km2  = mrf * Ktm2;   % Rm2 K value
 72 Km3  = mrf * Ktm3;   % Rm3 K value
 73 Ke   = 5 * (Kpf + Kef + Kem + Kff + Kfe);  % Lumped parameter for Re
(Psf to reservoir)
 74
 75 %System stiffnesses
 76 kb0  = 1.2e10;          % Assumption - spring constant for bladder
expansion (Pa / m^3), this is tunable
 77
 78 % Initial system component conditions
 79 Ppc = 35 * Psi2Pa;                   % accumulator pre-charge pressure
[Pa]
 80 Vpc = 7.1e-4;                         % accumulator pre-charge volume
(air) [m^3]
 81 Pc0 = 67 * Psi2Pa;                  % accumulator charge pressure [Pa]
 82 Vc0 = ((Ppc*Vpc^gamma)/Pc0)^(1/gamma); % accumulator charge volume (air)
[m^3]
 83 Vfluid0 = Vpc - Vc0;                  % volume of fluid in accumulator
at charge pressure [m^3]
 84 Pse = 2942;                           % back pressure from the resevoir
(10 in of water) [Pa]2942
 85
 86 t_del = .01;                       % valve opening delta
 87
```

```
 88 % System fluid inertia
 89 I0 = rho * 1 * ((Aacc / Vfluid0) + ((Pex_l0 + Brass_l0) / Apex)+((Pex_lm0
+ Brass_lm0) / Apex)+(Pex_le / Apex)); %%% Branch 0 fluid inertia
 90 Im = rho * 1 * (((Pex_lm0 + Brass_lm0) / Apex)+(Pex_le / Apex));%%%
Manifold fluid inertia
 91 %%%%%%%%%%%%%%%%%%%%%%%%%%%%%%%%%%%%%%%%%%%%%%%%%%%%%%%%%%%% FIRST STAGE OF BRANCH
DISCHARGE
 92 % Initial state conditions
 93 Va0_o  = Vc0;       % charged accumulator gas volume [m^3]
 94 G0_o  = 0;          % initial generalized momentum of fluid
 95
 96 % Integration variables
 97 tstart = 0;
 98 tfinal = 2;
 99 x0 = [Va0_o; G0_o];
100 refine = 4;
101 options = odeset('Events',@events_1,'OutputFcn',@odeplot,'OutputSel',
1,...
102                 'Refine',refine);
103
104 %%%%%%%%%%%%%%%%%%%%%%%%%%%%%%%% EVENT DRIVEN INTEGRATION FIRST STAGE
105 % Solve until accumulator empty is detected:
106    [t,x,te,xe,ie] = ode23(@f1,[tstart tfinal],x0,options);
107
108   % reset the initial conditions
109    nt = length(t);
110    x0(1) = x(nt,1);
111    x0(2) = x(nt,2);
112
113 t1 = t;
114
115 Va0_1  = x(:,1);
116 G0_1  = x(:,2);
117
118 for i=1:nt
119     y = zeros(1,5);
120     [xdot, y] = f1(t(i),x(i,:));
121     Pa0_1(i)   = y(1);
122     Qa0_1(i)   = y(2);
123     Pps0_1(i)  = y(3);
124     Ppsf_1(i)  = y(4);
125     G0_dot1(i) = y(5);
126 end
127
128
129 %%%%%%%%%%%%%%%%%%%%%%%%%%%%%%%%%%%%%%%%%%%%%%%%%%%%%%%%%%%% SECOND STAGE OF BRANCH
DISCHARGE
130 % Initial state conditions
131 Vb0_o  = 0;       % initial volume differential for bladder compliance
132 %x0 = [x0; Vb0_o];  % initial conditions for states from stage 01
133 x0(1) = x(nt,1);
134 x0(2) = x(nt,2);
135 x0(3) = Vb0_o;
136
```

```
% Integration variables
tstart = t(nt);
tfinal = 2;
refine = 4;
options = odeset('Events',@events_2,'OutputFcn',@odeplot,'OutputSel',↙
1,...
                 'Refine',refine);

%%%%%%%%%%%%%%%%%%%%%%%%%%%% EVENT DRIVEN INTEGRATION SECOND STAGE
   % Solve until an event is detected:
    [t,x,te,xe,ie] = ode23(@f2,[tstart tfinal],x0,options);

   % reset the initial conditions -> NOTE: this will only be used if↙
another
   % stage needs to be added as these will be the initial conditions fo
   % the next stage.
    nt    = length(t);
    x0(1) = x(nt,1);
    x0(2) = x(nt,2);
    x0(3) = x(nt,3);

    options = odeset(options,'InitialStep',t(nt)-t(nt-refine),...
       'MaxStep',t(nt)-t(1));

    t2 = t;

    for i=1:nt
     y = zeros(1,5);
     [xdot, y] = f2(t(i),x(i,:));
     Pa0_2(i)  = y(1);
     Qa0_2(i)  = y(2);
     Pps0_2(i) = y(3);
     Ppsf_2(i) = y(4);
     G0_dot2(i) = y(5);
   end

Va0_2  = x(:,1);
G0_2   = x(:,2);
Vb0    = x(:,3);


%%%%%%%%%%%%%%%%%%%%%%%%%%%% GATHER ALL TERMS AND COMBINE
t_sim0 = [t1 ; t2];

Pa0  = [Pa0_1 Pa0_2];
Qa0  = [Qa0_1 Qa0_2];
Pps0 = [Pps0_1 Pps0_2];
Ppsf = [Ppsf_1 Ppsf_2];
G0_dot = [G0_dot1 G0_dot2];

%%%%%%%%%%%%%%%%%%%%%%%%%%%% PLOT ; DISPLAY RESULTS
figure(1)
subplot(2,2,1), plot(t_sim0,Pa0 * Pa2PSI), title('Accumulator Pressure↙
(psi)')
```

```
188 subplot(2,2,2), plot(t_sim0,Qa0 * m3s2gpm), title('Accumulator flow
(gpm)')
189 subplot(2,2,3), plot(t_sim0,Pps0 * Pa2PSI), title('Pressure Sensor 0
(psi)')
190 subplot(2,2,4), plot(t_sim0,Ppsf * Pa2PSI), title('Output pressure
(psi)')
191
192 figure(2)
193 plot(t_exp0, Pa0_exp0, t_sim0, Pps0*Pa2PSI), title('Pps0 vs. Pexp0
(psi)')
194 lim = [0,1.2,0,80];
195 axis(lim)
196
197 figure(3)
198 plot(t_exp0, Pout_exp0, t_sim0, Ppsf*Pa2PSI), title('Ppsf vs. Pexpf
(psi)')
199 lim = [0,1.2,0,30];
200 axis(lim)
```

D.1.1 Mode 1 function for *branch0_multi.m*, *f1.m*

```
function [xdot,y] = f1(t,x)
%%%% FILENAME: f1.m
%%%% STAGE 1 FUNCTION OF branch0_multi.m
%%% VERSION 3.0
% J. Campos
% 18 MAR 2017

%%% See notes on multibranch 01

global g rho gamma
global K0 Km0 Km1 Km2 Km3 Ke kb0
global Aae Apex
global Vc0 Pc0 Vpc Pse I0 Im t_del

%% State Variables
Va0 = x(1); % differential volume change in stored air
G0  = x(2); % generalize momentum of fluid between bladder and valve 0


%% Flow / Line calculations

if t > t_del
   xv0 = 1;
else
    xv0 = .5 * (1 - cos(pi * t /t_del));
end

%%% Ca0 : Va0_dot --> Accumulator calculations
if G0 > 0
    Qf0 = G0 / I0; % Manifold fluid inertia for line 0 where L/D becomes
more significant.
else
    Qf0=0;
end

Qa0 = Qf0;

%%% If0 : Gf0_dot --> Branch fluid path pre-valve fluid inertia
Pa0 = Pc0 * (Vc0^gamma) / (Va0^gamma); % Assumed isothermal expansion
(for now)
Hr0 = K0 * (Qa0/Aae)^2 / (2 * g);% Combined headloss from accumulator to
manifold;
Pr0 = Hr0 * rho * g;
Hm0 = Km0 * (Qf0/Apex)^2 / (2 * g);% headloss for manifold section 0.
Pm0 = Hm0 * rho * g;
Hm1 = Km1 * (Qf0/Apex)^2 / (2 * g);% headloss for manifold section 1.
Pm1 = Hm1 * rho * g;
Hm2 = Km2 * (Qf0/Apex)^2 / (2 * g);% headloss for manifold section 2.
Pm2 = Hm2 * rho * g;
Hm3 = Km3 * (Qf0/Apex)^2 / (2 * g);% headloss for manifold section 3.
Pm3 = Hm3 * rho * g;
Hre = Ke * (Qf0/Apex)^2 / (2 * g);% Combined headloss exit section.
Pre = Hre * rho * g;

```

```
52
53 %% State Equations
54
55
56 Va0_dot  = xv0 * Qa0;
57
58 G0_dot  = (Pa0-Pr0-Pm0-Pm1-Pm2-Pm3-Pre-Pse)/(1 + (Im / I0));%%%<<<<<< It↙
seems as though this should be modulated with flow velocity input, if no flo↙w
no G0_dot.
59
60 %%% Pressure signals out
61 Pps0 = Pa0;
62 Ppsf = Pre + (G0_dot * (Im / I0)) + Pse;%%%%%% >>> WHY ON THIS STAGE↙
G0_dot term subtracts? Backpressure?
63
64 %% Output
65 xdot = [Va0_dot, G0_dot]';
66
67
68 %% Output variables
69 y(1) = Pa0;
70 y(2) = Qa0;
71 y(3) = Pps0;
72 y(4) = Ppsf;
73 y(5) = G0_dot;
74
75
```

D.1.2 Mode 2 function for *branch0_multi.m*, *f2.m*

```
function [xdot,y] = f2(t,x)
%%%% FILENAME: f2.m
%%%% STAGE 2 OF branch0_multi.m
%%% VERSION 4.0
% J. Campos
% 18 MAR 2017

%%% See notes on multibranch 01

global g rho gamma
global K0 Km0 Km1 Km2 Km3 Ke kb0
global Aae Apex
global Vc0 Pc0 Vpc Pse I0 Im

%% State Variables

Va0  = x(1); % differential volume change in stored air
G0  = x(2); % generalized momentum of fluid between valve and ps0
Vb0  = x(3); % differential change in volume attributed to bladder
expansion

%% Flow / Line calculations

%%% Ca0 : Va0_dot --> Accumulator calculations
Qf0 = G0 / I0; % Manifold fluid inertia for line 0 where L/D becomes more
significant.
Qa0 = Qf0;

%%% If0 : Gf0_dot --> Branch fluid path pre-valve fluid inertia
Pa0 = Pc0 * (Vc0^gamma) / (Va0^gamma); % Assumed isothermal expansion
(for now)
Pb0 = kb0 * Vb0;
Hr0 = K0 * (Qa0/Aae)^2 / (2 * g);% Combined headloss from accumulator to
manifold;
Pr0 = Hr0 * rho * g;
Hm0 = Km0 * (Qf0/Apex)^2 / (2 * g);% headloss for manifold section 0.
Pm0 = Hm0 * rho * g;
Hm1 = Km1 * (Qf0/Apex)^2 / (2 * g);% headloss for manifold section 1.
Pm1 = Hm1 * rho * g;
Hm2 = Km2 * (Qf0/Apex)^2 / (2 * g);% headloss for manifold section 2.
Pm2 = Hm2 * rho * g;
Hm3 = Km3 * (Qf0/Apex)^2 / (2 * g);% headloss for manifold section 3.
Pm3 = Hm3 * rho * g;
Hre = Ke * (Qf0/Apex)^2 / (2 * g);% Combined headloss exit section.
Pre = Hre * rho * g;

%%% Cb0 : Vb0_dot
Qb0 = Qf0;

%% State Equations

Va0_dot = Qa0;
G0_dot  = (Pa0 - Pb0 - Pr0 - Pm0 - Pm1 - Pm2 - Pm3 - Pre - Pse)/(1 + (Im/
I0));
```

```
50 Vb0_dot = Qb0;
51
52 %%% Pressure signals out
53 Pps0 = Pa0 - Pb0;
54 Ppsf = Pre + G0_dot * (Im / I0) + Pse;%%%%%% >>> WHY ON THIS STAGE G0_dot↙
term ADDS? Forward momentum?
55
56 %% Output
57 xdot = [Va0_dot, G0_dot, Vb0_dot]';
58
59
60 %% Output variables
61 y(1) = Pa0;
62 y(2) = Qa0;
63 y(3) = Pps0;
64 y(4) = Ppsf;
65 y(5) = G0_dot;
66
```

D.1.3 1st event function for *branch0_multi.m*, *events_1.m*

```
function [value,isterminal,direction] = events_1(t,x)
%%%% FILENAME: events_1.m
%%%% EVENT FUNCTION FOR STAGE 1 OF branch0_multi.m
%%% VERSION 1.0
% J. Campos
% 18 MAR 2017

% Locate the time when accumulator reaches empty
% and stop integration.
global Vpc
% value = [x(1)-Vpc; x(2)];   % detect accumulator empty
value = [x(1)-Vpc; x(2)];  % detect accumulator empty
isterminal = [1;0];        % stop the integration
direction = [0;0];         % negative direction

```

D.1.4 2nd event function for *branch0_multi.m*, *events_2.m*

```
function [value,isterminal,direction] = events_2(t,x)
%%%% FILENAME: events_2.m
%%%% EVENT FUNCTION FOR STAGE 2 OF branch0_multi.m
%%% VERSION 1.0
% J. Campos
% 18 MAR 2017

% Locate the time when bladder stops expanding
% and stop integration.
value = [x(1); x(2); x(3)];  % detect bladder expansion stop by reading fluid momentum
isterminal = [0;1;0];        % stop the integration
direction = [0;0;0];         % negative direction
```

D.2 Multi-branch model run file *Multibranch_full_tuned00.m*

```
%%%% FILENAME: Multibranch_full_tuned00.m
% Full multi-branch model tuned to orginal operating conditions.
% As left for synthesized pulse.
% See Ch5 for details on conditions.

% J. Campos
% 20 JUL 2017

clear all

%Ensure experimental data .mat files are loaded
load('Q_ex')
load('P_ex')
load('t_ex')

Q_exp = Q_ex;
P_exp = P_ex;
t_exp = t_ex;


global g rho gamma
global K0 K1 K2 K3 Km0 Km1 Km2 Km3 Ke
global kb0 kb1 kb2 kb3
global Aae Apex
global Vc0 Pc0 I0
global Vc1 Pc1 I1
global Vc2 Pc2 I2
global Vc3 Pc3 I3
global Im Pse
global tfire_1 tfire_2 tfire_3
global Vpc0 Vpc1 Vpc2 Vpc3

% Conversion factors
m32gal  = 264.172;        % m^3 to gallons
m3s2ls  = 1000;
m3s2gpm = 15852;          % (m^3)/s to gallons/min
Pa2PSI  = 0.145/1000;     % Pa to PSI
Psi2Pa  = 1/Pa2PSI;       % PSI to Pa

% Physical constants
gamma = 1.4;        % ideal gas ratio of the Cv and Cp heat capacity
g = 9.81;           % acceleration due to gravity [m/s^2]
rho = 1000;         % density of fluid (water) [kg/m^3]
mu = 1e-3;          % Dynamic viscousity of water [Pa-s]
nu = 9e-7;          % Kinematic viscosity of water [m^2/s]
Patm = 1.01e5;      % Atmospheric pressure (Pa)

% Geometric constants
Aacc  = pi() * .0381^2;% Accumulator crossectional area
Acc_r = .006;          % Inner radius of accumulator exit pipe
Aae = pi() * Acc_r^2;  % Hydraulic CS area of accumulator exit pipe
Pex_rad = .00635;      % Inner radius of PEX line [m]
Pex_t = 3.175e-4;      % Wall thickness of PEX line [m]
Pex_d = 2 * Pex_rad;
```

```
 55 Apex = pi() * Pex_rad^2;% Hydraulic CS area of PEX tubing
 56 Pex_l0 = .6016;         % Length of PEX line in branch 0 [m] #### This
should probably be losses associated with 90 degree elbow.
 57 Pex_l1 = .6016;         % Length of PEX line in branch 1 [m] #### This
should probably be losses associated with 90 degree elbow.
 58 Pex_l2 = .6016;         % Length of PEX line in branch 2 [m] #### This
should probably be losses associated with 90 degree elbow.
 59 Pex_l3 = .6016;         % Length of PEX line in branch 3 [m] #### This
should probably be losses associated with 90 degree elbow.
 60 Pex_lm0 = .125;         % Length of PEX in manifold section m0. [m]
 61 Pex_lm1 = .125;         % Length of PEX in manifold section m1. [m]
 62 Pex_lm2 = .125;         % Length of PEX in manifold section m2. [m]
 63 Pex_lm3 = .125;         % Length of PEX in manifold section m3. [m]
 64 Pex_le = .615;          % Total length of PEX from psf to exhaust. [m]
 65 Brass_rad = .0125;      % Inner radius of brass fittings [m]
 66 Brass_t = .03175;       % Wall thickness of brass fitting [m]
 67 Brass_l0 = .38;         % Length of brass fitting in branch 0 [m]
 68 Brass_l1 = Brass_l0;    % Length of brass fitting in branch 1 [m]
 69 Brass_l2 = Brass_l0;    % Length of brass fitting in branch 2 [m]
 70 Brass_l3 = Brass_l0;    % Length of brass fitting in branch 3 [m]
 71 Brass_lm0 = .127;       % Total length of brass fittings in manifold to
exhaust, starting at junction with branch0. [m]
 72
 73 % Hydraulic component friction flow factors
 74 Kpe  = 0.28;             % Flow factor for pipe entrance at accumulator
exit 0 - Ra0 (https://www.plumbingsupply.com/ed-frictionlosses.html)
 75 Kp0  = 0.54;             % Brass tee friction flow factor at pressure
sensor 0 (https://www.plumbingsupply.com/ed-frictionlosses.html)
 76 Kv0  = 1.00;             % Diaphragm valve value for control valve 0
(from product liturature DEMA eng)
 77 Kcv0 = 1.40;             % Brass check valve for cv0 (https://www
plumbingsupply.com/ed-frictionlosses.html)
 78 Kfs0 = 1.00;             % Flow meter K estimated (see https://www.omega
com/Green/pdf/TURBINE_PADDLE_REF.pdf)
 79 Ke0  = 0.81;             % Brass 90 degree elbow (https://www
plumbingsupply.com/ed-frictionlosses.html)
 80 Ktm1 = Kp0;              % Brass tee fff at line one manifold connection.
 81 Ktm2 = Kp0;              % Brass tee fff at line two manifold connection.
 82 Ktm3 = Kp0;              % Brass tee fff at line three manifold
connection.
 83 Kpf  = Kp0;              % Brass tee fff at final pressure sensor.
 84 Kef  = Ke0;              % Brass 90 degree elbow (final)
 85 Kem  = 0.04;             % EM flow meter fff (ESTIMATED)
 86 Kff  = Kfs0;             % Flow meter K estimated (see https://www.omega
com/Green/pdf/TURBINE_PADDLE_REF.pdf)
 87 Kfe  = 1.00;             % Flow factor for pipe entrance at accumulator
exit into a much larger body of fluid (https://neutrium
net/fluid_flow/pressure-loss-from-pipe-entrances-and-exits/)
 88
 89
 90 % Lumped parameter for R0 (before valve0)-1st stage
 91 K0   = 6.1 * (Kpe + Kp0 + Kv0 + Kcv0 + Kfs0);
 92 K1 = K0;
 93 K2 = K0;
```

```
 94 K3 = K0;
 95 % Lumped parameter for Rm (manifold sections)
 96 Km0  = 15 * Ke0;    % Rm0 K value
 97 Km1  = 7 * Ktm1;   % Rm1 K value
 98 Km2  = 3 * Ktm2;   % Rm2 K value
 99 Km3  = 8 * Ktm3;   % Rm3 K value
100 % Lumped parameter for Re (Psf to reservoir)
101 Ke   = 5 * (Kpf + Kef + Kem + Kff + Kfe);
102
103 %System stiffnesses
104 kb0  = 1.2e10;          % Assumption - spring constant for bladder↙
expansion (Pa / m^3), this is tunable
105 kb1 = kb0;
106 kb2 = kb0;
107 kb3 = kb0;
108 %%% Firing times
109 tfire_1 = .4;
110 tfire_2 = .8;
111 tfire_3 = 1.2;
112
113 %%% Initial conditions
114 % Accumulator 0
115 Ppc0 = 37 * Psi2Pa;                  % accumulator 0 pre-charge pressure↙
[Pa]
116 Vpc0 = 7.1e-4;                        % accumulator 0 pre-charge volume↙
(air) [m^3]
117 Pc0 = 72 * Psi2Pa;                   % accumulator 0 charge pressure↙
[Pa]
118 Vc0 = ((Ppc0*Vpc0^gamma)/Pc0)^(1/gamma); % accumulator 0 charge volume↙
(air)[m^3]
119 Vfluid0 = Vpc0 - Vc0;                  % volume of fluid in accumulator↙
0 at charge pressure [m^3]
120
121 % Accumulator 1
122 Ppc1 = 37 * Psi2Pa;                  % accumulator 1 pre-charge↙
pressure [Pa]
123 Vpc1 = 7.1e-4;                        % accumulator 1 pre-charge↙
volume (air) [m^3]
124 Pc1 = 72 * Psi2Pa;                   % accumulator 1 charge pressure↙
[Pa]
125 Vc1 = ((Ppc1*Vpc1^gamma)/Pc1)^(1/gamma);% accumulator 1 charge volume↙
(air)[m^3]
126 Vfluid1 = Vpc1 - Vc1;                  % volume of fluid in accumulator↙
1 at charge pressure [m^3]
127
128 % Accumulator 2
129 Ppc2 = 37 * Psi2Pa;                  % accumulator 2 pre-charge↙
pressure [Pa]
130 Vpc2 = 7.1e-4;                        % accumulator 2 pre-charge↙
volume (air) [m^3]
131 Pc2 = 72 * Psi2Pa;                   % accumulator 2 charge pressure↙
[Pa]
132 Vc2 = ((Ppc2*Vpc2^gamma)/Pc2)^(1/gamma);% accumulator 2 charge volume↙
(air)[m^3]
```

```
133 Vfluid2 = Vpc2 - Vc2;                    % volume of fluid in accumulator
2 at charge pressure [m^3]
134
135 % Accumulator 3
136 Ppc3 = 37 * Psi2Pa;                    % accumulator pre-charge pressure
[Pa]
137 Vpc3 = 7.1e-4;                          % accumulator pre-charge volume
(air) [m^3]
138 Pc3 = 72 * Psi2Pa;                     % accumulator 3 charge pressure
[Pa]
139 Vc3 = ((Ppc3*Vpc3^gamma)/Pc3)^(1/gamma);% accumulator 3 charge volume
(air)[m^3]
140 Vfluid3 = Vpc3 - Vc3;                    % volume of fluid in accumulator
3 at charge pressure [m^3]
141
142 % Resevoir
143 Pse = 2942;                             % back pressure from the resevoir
(10 in of water)[Pa]
144
145 % System fluid inertia
146 I0 = rho * 1 * ((Aacc / Vfluid0) + ((Pex_l0 + Brass_l0) / Apex));%%%
Branch 0 fluid inertia
147 I1 = rho * 1 * ((Aacc / Vfluid1) + ((Pex_l1 + Brass_l1) / Apex));%%%
Branch 1 fluid inertia
148 I2 = rho * 1 * ((Aacc / Vfluid2) + ((Pex_l2 + Brass_l2) / Apex));%%%
Branch 2 fluid inertia
149 I3 = rho * 1 * ((Aacc / Vfluid3) + ((Pex_l3 + Brass_l3) / Apex));%%%
Branch 3 fluid inertia
150 Im = rho * .5 * (((Pex_lm0 + Brass_lm0) / Apex)+(Pex_le / Apex)); %%%
Manifold fluid inertia
151
152
153 %%%%%%%%%%%%%%%%%%%%%%%%%%%%%%%%%%%%%%%%%%%%%%%% FIRST STAGE OF  DISCHARGE
154 % Initial state conditions
155 Va0_o  = Vc0;       % charged accumulator 0 gas volume [m^3]
156 Gamma0_o  = 0;      % initial generalized momentum of fluid
157
158 Va1_o  = Vc1;       % charged accumulator 1 gas volume [m^3]
159 Gamma1_o  = 0;      % initial generalized momentum of fluid
160
161 Va2_o  = Vc2;       % charged accumulator 2 gas volume [m^3]
162 Gamma2_o  = 0;      % initial generalized momentum of fluid
163
164 Va3_o  = Vc3;       % charged accumulator 3 gas volume [m^3]
165 Gamma3_o  = 0;      % initial generalized momentum of fluid
166
167 % Integration variables
168 tstart = 0;
169 tfinal = 3;
170 x0 = [Va0_o; Gamma0_o; Va1_o; Gamma1_o; Va2_o; Gamma2_o; Va3_o;
Gamma3_o];
171 refine = 4;
172 options = odeset('Events',@events_1,'OutputFcn',@odeplot,'OutputSel',
1,...
```

```
173                 'Refine',refine);
174
175 %%%%%%%%%%%%%%%%%%%%%%%%%%%% EVENT DRIVEN INTEGRATION FIRST STAGE
176 % Solve until accumulator empty is detected:
177    [t,x,te,xe,ie] = ode23(@f1,[tstart tfinal],x0,options);
178
179    % reset the initial conditions
180    nt = length(t);
181    x0(1) = x(nt,1);
182    x0(2) = x(nt,2);
183    x0(3) = x(nt,3);
184    x0(4) = x(nt,4);
185    x0(5) = x(nt,5);
186    x0(6) = x(nt,6);
187    x0(7) = x(nt,7);
188    x0(8) = x(nt,8);
189
190 t1 = t;
191
192
193 for i=1:nt
194     y = zeros(1,10);
195     [xdot, y] = f1(t(i),x(i,:));
196     Pps0_1(i)   = y(1);
197     Qa0_1(i)    = y(2);
198     Pps1_1(i)   = y(3);
199     Qa1_1(i)    = y(4);
200     Pps2_1(i)   = y(5);
201     Qa2_1(i)    = y(6);
202     Pps3_1(i)   = y(7);
203     Qa3_1(i)    = y(8);
204     Ppsf_1(i)   = y(9);
205     Gamma0_dot(i) =y(10);
206     Power_out01(i)=y(11);
207 end
208
209
210 %%%%%%%%%%%%%%%%%%%%%%%%%%%%%%%%%%%%%%%%%%%%%%%% SECOND STAGE OF BRANCH
DISCHARGE
211 % Initial state conditions
212 Vb0_o  = 0;       % initial volume differential for bladder compliance
213 Vb1_o  = 0;       % initial volume differential for bladder compliance
214 Vb2_o  = 0;       % initial volume differential for bladder compliance
215 Vb3_o  = 0;       % initial volume differential for bladder compliance
216 % Initial state conditions passed from stage 1, see line 182 plus add
217 % bladder for line 0 initial conditions
218 x0(9)  = Vb0_o;
219 x0(10) = Vb1_o;
220 x0(11) = Vb2_o;
221 x0(12) = Vb3_o;
222
223 % Integration variables
224 tstart = t(nt);
225 tfinal = 4;
```

```
refine = 4;
options = odeset('Events',@events_2,'OutputFcn',@odeplot,'OutputSel',1,...
                 'Refine',refine);

%%%%%%%%%%%%%%%%%%%%%%%%%%% EVENT DRIVEN INTEGRATION SECOND STAGE
   % Solve until an event is detected:
    [t,x,te,xe,ie] = ode23(@f2,[tstart tfinal],x0,options);

   % reset the initial conditions -> NOTE: this will only be used if another
   % stage needs to be added as these will be the initial conditions for
   % the next stage.
    nt    = length(t);
     x0(1) = x(nt,1);
     x0(2) = x(nt,2);
     x0(3) = x(nt,3);
     x0(4) = x(nt,4);
     x0(5) = x(nt,5);
     x0(6) = x(nt,6);
     x0(7) = x(nt,7);
     x0(8) = x(nt,8);
     x0(9) = x(nt,9);
     x0(10) = x(nt,10);
     x0(11) = x(nt,11);
     x0(12) = x(nt,12);


    t2 = t;

for i=1:nt
     y = zeros(1,17);
     [xdot, y] = f2(t(i),x(i,:));
     Pps0_2(i)   = y(1);
     Qa0_2(i)    = y(2);
     Pps1_2(i)   = y(3);
     Qa1_2(i)    = y(4);
     Pps2_2(i)   = y(5);
     Qa2_2(i)    = y(6);
     Pps3_2(i)   = y(7);
     Qa3_2(i)    = y(8);
     Ppsf_2(i)   = y(9);
     Vb0_2(i)    = y(10);
     Vb1_2(i)    = y(11);
     Vb2_2(i)    = y(12);
     Vb3_2(i)    = y(13);
     P0(i)       = y(14);
     P1(i)       = y(15);
     P2(i)       = y(16);
     P3(i)       = y(17);
     Va0(i)      = y(18);
     Power_out02(i) = y(19);
end

```

```
278
279
280
281 %%%%%%%%%%%%%%%%%%%%%%%%%%%% GATHER ALL TERMS AND COMBINE
282 t_sim0 = [t1 ; t2];
283 Pps0 = [Pps0_1 Pps0_2];
284 Qa0  = [Qa0_1 Qa0_2];
285 Pps1 = [Pps1_1 Pps1_2];
286 Qa1  = [Qa1_1 Qa1_2];
287 Pps2 = [Pps2_1 Pps2_2];
288 Qa2  = [Qa2_1 Qa2_2];
289 Pps3 = [Pps3_1 Pps3_2];
290 Qa3  = [Qa3_1 Qa3_2];
291 Ppsf = [Ppsf_1 Ppsf_2];
292 PPout_sim = [Power_out01 Power_out02];
293
294 %%%%%%%%%%%%%%%%%%%%%%%%%%%% Peformance metrics
295 %sim
296 Eout_sim  = trapz(t_sim0,PPout_sim);
297 E_stored = (101 + Ppc0) * Vpc0 * log(Pc0/Ppc0) + (101 + Ppc1) * Vpc1 *
log(Pc1/Ppc1) + (101 + Ppc2) * Vpc2 * log(Pc2/Ppc2) + (101 + Ppc3) * Vpc3 *
log(Pc3/Ppc3);
298 Eff_sim = (Eout_sim / E_stored) * 100;
299 PPavg_sim = mean(PPout_sim);
300 %exp
301 PPout_exp = times(P_exp * (Psi2Pa/1000), Q_exp);
302 Eout_exp = trapz(t_exp,PPout_exp);
303 Eff_exp = (Eout_exp / E_stored) * 100;
304 PPavg_exp = mean(PPout_exp);
305 %eval
306
307 % PP_delta = PPout_sim - PPout_exp;
308 %%%%%%%%%%%%%%%%%%%%%%%%%%%% PLOT ; DISPLAY RESULTS
309 set(0,'DefaultAxesFontName', 'Times New Roman')
310 set(0,'DefaultAxesFontSize', 12)
311
312 figure (1)
313 subplot(4,2,1), plot(t_sim0,Pps0 * Pa2PSI),
314 set(gca, 'xgrid', 'on'),
315 set(gca, 'ygrid', 'on'),
316 title('Accumulator 0 Pressure (psi)')
317 subplot(4,2,2), plot(t_sim0,Qa0 * m3s2gpm),
318 set(gca, 'xgrid', 'on'),
319 set(gca, 'ygrid', 'on'),
320 title('Accumulator 0 flow (gpm)')
321 subplot(4,2,3), plot(t_sim0,Pps1 * Pa2PSI),
322 set(gca, 'xgrid', 'on'),
323 set(gca, 'ygrid', 'on'),
324 title('Accumulator 1 Pressure (psi)')
325 subplot(4,2,4), plot(t_sim0,Qa1 * m3s2gpm),
326 set(gca, 'xgrid', 'on'),
327 set(gca, 'ygrid', 'on'),
328 title('Accumulator 1 flow (gpm)')
329 subplot(4,2,5), plot(t_sim0,Pps2 * Pa2PSI),
```

```
278
279
280
281 %%%%%%%%%%%%%%%%%%%%%%%%%%%% GATHER ALL TERMS AND COMBINE
282 t_sim0 = [t1 ; t2];
283 Pps0 = [Pps0_1 Pps0_2];
284 Qa0  = [Qa0_1 Qa0_2];
285 Pps1 = [Pps1_1 Pps1_2];
286 Qa1  = [Qa1_1 Qa1_2];
287 Pps2 = [Pps2_1 Pps2_2];
288 Qa2  = [Qa2_1 Qa2_2];
289 Pps3 = [Pps3_1 Pps3_2];
290 Qa3  = [Qa3_1 Qa3_2];
291 Ppsf = [Ppsf_1 Ppsf_2];
292 PPout_sim = [Power_out01 Power_out02];
293
294 %%%%%%%%%%%%%%%%%%%%%%%%%%%% Peformance metrics
295 %sim
296 Eout_sim  = trapz(t_sim0,PPout_sim);
297 E_stored = (101 + Ppc0) * Vpc0 * log(Pc0/Ppc0) + (101 + Ppc1) * Vpc1 *
log(Pc1/Ppc1) + (101 + Ppc2) * Vpc2 * log(Pc2/Ppc2) + (101 + Ppc3) * Vpc3 *
log(Pc3/Ppc3);
298 Eff_sim = (Eout_sim / E_stored) * 100;
299 PPavg_sim = mean(PPout_sim);
300 %exp
301 PPout_exp = times(P_exp * (Psi2Pa/1000), Q_exp);
302 Eout_exp = trapz(t_exp,PPout_exp);
303 Eff_exp = (Eout_exp / E_stored) * 100;
304 PPavg_exp = mean(PPout_exp);
305 %eval
306
307 % PP_delta = PPout_sim - PPout_exp;
308 %%%%%%%%%%%%%%%%%%%%%%%%%%%% PLOT ; DISPLAY RESULTS
309 set(0,'DefaultAxesFontName', 'Times New Roman')
310 set(0,'DefaultAxesFontSize', 12)
311
312 figure (1)
313 subplot(4,2,1), plot(t_sim0,Pps0 * Pa2PSI),
314 set(gca, 'xgrid', 'on'),
315 set(gca, 'ygrid', 'on'),
316 title('Accumulator 0 Pressure (psi)')
317 subplot(4,2,2), plot(t_sim0,Qa0 * m3s2gpm),
318 set(gca, 'xgrid', 'on'),
319 set(gca, 'ygrid', 'on'),
320 title('Accumulator 0 flow (gpm)')
321 subplot(4,2,3), plot(t_sim0,Pps1 * Pa2PSI),
322 set(gca, 'xgrid', 'on'),
323 set(gca, 'ygrid', 'on'),
324 title('Accumulator 1 Pressure (psi)')
325 subplot(4,2,4), plot(t_sim0,Qa1 * m3s2gpm),
326 set(gca, 'xgrid', 'on'),
327 set(gca, 'ygrid', 'on'),
328 title('Accumulator 1 flow (gpm)')
329 subplot(4,2,5), plot(t_sim0,Pps2 * Pa2PSI),
```

```
382 ylabel({'Flow', '(gpm)'}, 'Fontsize', 12)
383 lim = [0,3.5,0,14];
384 axis(lim)
385
386 figure(5)
387 subplot(2,1,1),plot(t_sim0, PPout_sim)
388 set(gca,'FontSize',14),
389 set(gca, 'xgrid', 'on'),
390 set(gca, 'ygrid', 'on'),
391 title('Simulation: Power output (W)')
392 xlabel({'time', '(seconds)'}, 'Fontsize', 12)
393 ylabel({'Power', '(W)'}, 'Fontsize', 12)
394 lim = [0,3.5,0,200];
395 dim = [0.7 0.6 0.3 0.3];
396 str = {'Total Energy Out:', Eout_sim 'Joules', 'Energy stored', E_stored↙
'kJoules', 'System Efficiency', Eff_sim, 'Average Power Out', PPavg_sim};
397 annotation('textbox',dim,'String',str,'FitBoxToText','on','Fontsize',↙
12);
398
399 subplot(2,1,2),plot(t_exp, PPout_exp)
400 set(gca,'FontSize',14),
401 set(gca, 'xgrid', 'on'),
402 set(gca, 'ygrid', 'on'),
403 title('Experimental: Power output (W)')
404 xlabel({'time', '(seconds)'}, 'Fontsize', 12)
405 ylabel({'Power', '(W)'}, 'Fontsize', 12)
406 lim = [0,3.5,0,200];
407 dim = [0.7 0.1 0.3 0.3];
408 str = {'Total Energy Out:', Eout_exp 'Joules', 'Energy stored', E_stored↙
'kJoules', 'System Efficiency', Eff_exp, 'Average Power Out', PPavg_exp};
409 annotation('textbox',dim,'String',str,'FitBoxToText','on','Fontsize',↙
12);
410
411 figure(6)
412 plot(t_exp, PPout_exp,'-.o', t_sim0, PPout_sim)
413 set(gca,'FontSize',16),
414 set(gca, 'xgrid', 'on'),
415 set(gca, 'ygrid', 'on'),
416 title('Power output (W): Model Vs. Experimental)
417 xlabel({'time', '(seconds)'}, 'Fontsize', 14)
418 ylabel({'Power', '(W)'}, 'Fontsize', 14)
419 lim = [0,3.5,0,200];
420
421
```

D.2.1 Mode 1 function, *f1.m* for multi-branch model

```
function [xdot,y] = f1(t,x)
%%%% FILENAME: f1.m
%%%% STAGE 1 FUNCTION OF Multibranch_full_tuned00.m
%%% VERSION 3.0
% J. Campos
% 20 MAR 2017

%%% See notes on multibranch 01c

global g rho gamma
global K0 K1 K2 K3 Km0 Km1 Km2 Km3 Ke
global kb0 kb1 kb2 kb3
global Aae Apex
global Vc0 Pc0 I0
global Vc1 Pc1 I1
global Vc2 Pc2 I2
global Vc3 Pc3 I3
global Im Pse
global tfire_1 tfire_2 tfire_3
global Vpc0 Vpc1 Vpc2 Vpc3

%% State Variables
Va0     = x(1); % differential volume change in stored air of accumulator
0
Gamma0  = x(2); % generalize momentum of fluid branch 0
Va1     = x(3); % differential volume change in stored air of accumulator
1
Gamma1  = x(4); % generalize momentum of fluid branch 1
Va2     = x(5); % differential volume change in stored air of accumulator
2
Gamma2  = x(6); % generalize momentum of fluid branch 2
Va3     = x(7); % differential volume change in stored air of accumulator
3
Gamma3  = x(8); % generalize momentum of fluid branch 3

%% Flow / Line calculations - effective action of checkvalve implimented

%%% Ca0 : Va0_dot --> Accumulator calculations
if Gamma0 > 0
    Q0 = Gamma0 / I0; % Manifold fluid inertia for line 0 where L/
becomes more significant.
else
    Q0 = 0;
end

Qa0 = Q0;

%%% Ca1 : Va1_dot --> Accumulator calculations
if Gamma1 > 0
    Q1 = Gamma1 / I1; % Manifold fluid inertia for line 0 where L/
becomes more significant.
else
    Q1 = 0;
end
```

```
 49
 50 Qa1 = Q1;
 51
 52 %%% Ca2 : Va2_dot --> Accumulator calculations
 53 if Gamma2 > 0
 54     Q2 = Gamma2 / I2;% Manifold fluid inertia for line 0 where L/↙
becomes more significant.
 55 else
 56     Q2 = 0;
 57 end
 58
 59 Qa2 = Q2;
 60
 61 %%% Ca3 : Va3_dot --> Accumulator calculations
 62 if Gamma3 > 0
 63     Q3 = Gamma3 / I3;% Manifold fluid inertia for line 0 where L/↙
becomes more significant.
 64 else
 65     Q3 = 0;
 66 end
 67
 68 Qa3 = Q3;
 69
 70
 71 %%% Rm0 --> Re
 72 Hm0 = Km0 * (Q0/Apex)^2 / (2 * g);% headloss for manifold section 0.
 73 Pm0 = Hm0 * rho * g;
 74 Hm1 = Km1 * ((Q0 + Q1)/Apex)^2 / (2 * g);% headloss for manifold section↙
1.
 75 Pm1 = Hm1 * rho * g;
 76 Hm2 = Km2 * ((Q0 + Q1 + Q2)/Apex)^2 / (2 * g);% headloss for manifold↙
section 2.
 77 Pm2 = Hm2 * rho * g;
 78 Hm3 = Km3 * ((Q0 + Q1 + Q2 + Q3)/Apex)^2 / (2 * g);% headloss for↙
manifold section 3.
 79 Pm3 = Hm3 * rho * g;
 80 Hre = Ke * ((Q0 + Q1 + Q2 + Q3)/Apex)^2 / (2 * g);% Combined headloss↙
exit section.
 81 Pre = Hre * rho * g;
 82
 83 %%% I0 : Gamma0_dot --> Branch 0 fluid inertia
 84 Pa0 = Pc0 * (Vc0^gamma) / (Va0^gamma); % Assumed isothermal expansion↙
(for now)
 85 Hr0 = K0 * (Qa0/Aae)^2 / (2 * g);% Combined headloss from accumulator to↙
manifold;
 86 Pr0 = Hr0 * rho * g;
 87
 88 %%% I1 : Gamma1_dot --> Branch 1 fluid inertia
 89 Pa1 = Pc1 * (Vc1^gamma) / (Va1^gamma); % Assumed isothermal expansion↙
(for now)
 90 Hr1 = K1 * (Qa1/Aae)^2 / (2 * g);% Combined headloss from accumulator to↙
manifold;
 91 Pr1 = Hr1 * rho * g;
 92
```

```
 93
 94 %%% I2 : Gamma2_dot --> Branch 2 fluid inertia
 95 Pa2 = Pc2 * (Vc2^gamma) / (Va2^gamma); % Assumed isothermal expansion
(for now)
 96 Hr2 = K2 * (Qa2/Aae)^2 / (2 * g);% Combined headloss from accumulator to
manifold;
 97 Pr2 = Hr2 * rho * g;
 98
 99
100 %%% I3 : Gamma3_dot --> Branch 3 fluid inertia
101 Pa3 = Pc3 * (Vc3^gamma) / (Va3^gamma); % Assumed isothermal expansion
(for now)
102 Hr3 = K3 * (Qa3/Aae)^2 / (2 * g);% Combined headloss from accumulator to
manifold;
103 Pr3 = Hr3 * rho * g;
104
105
106 P0 = Pr0+Pm0+Pm1+Pm2+Pm3+Pre+Pse;
107 P1 = Pr1+Pm1+Pm2+Pm3+Pre+Pse;
108 P2 = Pr2+Pm2+Pm3+Pre+Pse;
109 P3 = Pr3+Pm3+Pre+Pse;
110
111 %% State Equations
112
113 %%%%% Branch 0 flow
114 Va0_dot = Qa0;
115
116 %%%%% Branch 1 flow
117 if t >= tfire_1
118 % if t >= tfire_1 && Va1 <= Vc1
119     Va1_dot  = Qa1;
120 else
121     Va1_dot  = 0;
122 end
123
124 %%%%% Branch 2 flow
125 if t >= tfire_2
126 % if t >= tfire_2 && Va2 <= Vc2
127     Va2_dot  = Qa2;
128 else
129     Va2_dot  = 0;
130 end
131
132 %%%%% Branch 3 flow
133 if t >= tfire_3
134 % if t >= tfire_3 && Va3 <= Vc3
135     Va3_dot  = Qa3;
136 else
137     Va3_dot  = 0;
138 end
139
140 %%%%%% FINDING GAMMA DOTS
141 A=[(1+Im/I0),Im/I1,Im/I2,Im/I3; Im/I0,(1+Im/I1),Im/I2,Im/I3;Im/I0,Im/I1,
(1+Im/I2),Im/I3;Im/I0,Im/I1,Im/I2,(1+Im/I3)];
```

```
142
143 if t == 0
144     B=[0; 0; 0; 0];
145 end
146
147 if t > 0 && t < tfire_1
148     B=[Pa0-Pr0-Pm0-Pm1-Pm2-Pm3-Pre-Pse; 0; 0; 0];
149 end
150
151 if (tfire_1 <= t) && (t < tfire_2)
152     B=[Pa0-Pr0-Pm0-Pm1-Pm2-Pm3-Pre-Pse; Pa1-Pr1-Pm1-Pm2-Pm3-Pre-Pse; 0;
0];
153 end
154
155 if (tfire_2 <= t) && (t < tfire_3)
156     B=[Pa0-Pr0-Pm0-Pm1-Pm2-Pm3-Pre-Pse; Pa1-Pr1-Pm1-Pm2-Pm3-Pre-Pse; Pa2-
Pr2-Pm2-Pm3-Pre-Pse; 0];
157 end
158
159 if t >= tfire_3
160     B=[Pa0-Pr0-Pm0-Pm1-Pm2-Pm3-Pre-Pse; Pa1-Pr1-Pm1-Pm2-Pm3-Pre-Pse; Pa2-
Pr2-Pm2-Pm3-Pre-Pse; Pa3-Pr3-Pm3-Pre-Pse];
161 end
162
163 Gamma_dot = A\B;
164 Gamma0_dot = Gamma_dot(1);
165 Gamma1_dot = Gamma_dot(2);
166 Gamma2_dot = Gamma_dot(3);
167 Gamma3_dot = Gamma_dot(4);
168
169
170
171 %%% Pressure signals out
172 Pps0 = Pa0;
173 Pps1 = Pa1;
174 Pps2 = Pa2;
175 Pps3 = Pa3;
176 Ppsf = Pre + Im * ((Gamma0_dot / I0) + (Gamma1_dot / I1) + (Gamma2_dot /
I2) + (Gamma3_dot / I3)) + Pse;
177
178 %% Output
179 xdot = [Va0_dot, Gamma0_dot, Va1_dot, Gamma1_dot, Va2_dot, Gamma2_dot,
Va3_dot, Gamma3_dot]';
180
181 Power_out= Ppsf * (Va0_dot + Va1_dot + Va2_dot + Va3_dot);
182
183 %% Output variables
184 y(1)  = Pps0;
185 y(2)  = Va0_dot;
186 y(3)  = Pps1;
187 y(4)  = Va1_dot;
188 y(5)  = Pps2;
189 y(6)  = Va2_dot;
190 y(7)  = Pps3;
```

```
191 y(8)  = Va3_dot;
192 y(9) = Ppsf;
193 y(10)= Gamma0_dot;
194 y(11)= Power_out;
195
196
```

D.2.2 Mode 2 function, *f2.m* for multi-branch model

```
function [xdot,y] = f2(t,x)
%%%% FILENAME: f2.m
%%%% STAGE 2 FUNCTION OF Multibranch_full_tuned00.m
%%% VERSION 3.0
% J. Campos
% 20 MAR 2017
%%% See notes on multibranch 01c

global g rho gamma
global K0 K1 K2 K3 Km0 Km1 Km2 Km3 Ke
global kb0 kb1 kb2 kb3
global Aae Apex
global Vc0 Pc0 I0
global Vc1 Pc1 I1
global Vc2 Pc2 I2
global Vc3 Pc3 I3
global Im Pse
global tfire_1 tfire_2 tfire_3
global Vpc0 Vpc1 Vpc2 Vpc3

%% State Variables
Va0     = x(1); % differential volume change in stored air of accumulator
0
Gamma0  = x(2); % generalize momentum of fluid branch 0
Va1     = x(3); % differential volume change in stored air of accumulator
1
Gamma1  = x(4); % generalize momentum of fluid branch 1
Va2     = x(5); % differential volume change in stored air of accumulator
2
Gamma2  = x(6); % generalize momentum of fluid branch 2
Va3     = x(7); % differential volume change in stored air of accumulator
3
Gamma3  = x(8); % generalize momentum of fluid branch 3
Vb0     = x(9);
Vb1     = x(10);
Vb2     = x(11);
Vb3     = x(12);

%% Flow / Line calculations

%%% Ca0 : Va0_dot --> Accumulator calculations
if Gamma0 > 0
    Q0 = Gamma0 / I0; % Manifold fluid inertia for line 0 where L/A
becomes more significant.
else
    Q0 = 0;
end
Qa0 = Q0;

%%% Cb0 : Vb0_dot
Qb0 = Q0;


%%% Ca1 : Va1_dot --> Accumulator calculations
```

```
50 if Gamma1 > 0
51     Q1 = Gamma1 / I1;% Manifold fluid inertia for line 0 where L/
becomes more significant.
52 else
53     Q1 = 0;
54 end
55 Qa1 = Q1;
56
57 %%% Cb1 : Vb1_dot
58 Qb1 = Q1;
59
60 %%% Ca2 : Va2_dot --> Accumulator calculations
61 if Gamma2 > 0
62     Q2 = Gamma2 / I2;% Manifold fluid inertia for line 0 where L/
becomes more significant.
63 else
64     Q2 = 0;
65 end
66 Qa2 = Q2;
67
68 %%% Cb2 : Vb1_dot
69 Qb2 = Q2;
70
71 %%% Ca3 : Va3_dot --> Accumulator calculations
72 if Gamma3 > 0
73     Q3 = Gamma3 / I3;% Manifold fluid inertia for line 0 where L/
becomes more significant.
74 else
75     Q3 = 0;
76 end
77 Qa3 = Q3;
78
79 %%% Cb2 : Vb1_dot
80 Qb3 = Q3;
81
82 %%% Rm0 --> Re
83 Hm0 = Km0 * (Q0/Apex)^2 / (2 * g);% headloss for manifold section 0.
84 Pm0 = Hm0 * rho * g;
85 Hm1 = Km1 * ((Q0 + Q1)/Apex)^2 / (2 * g);% headloss for manifold section
1.
86 Pm1 = Hm1 * rho * g;
87 Hm2 = Km2 * ((Q0 + Q1 + Q2)/Apex)^2 / (2 * g);% headloss for manifold
section 2.
88 Pm2 = Hm2 * rho * g;
89 Hm3 = Km3 * ((Q0 + Q1 + Q2 + Q3)/Apex)^2 / (2 * g);% headloss for
manifold section 3.
90 Pm3 = Hm3 * rho * g;
91 Hre = Ke * ((Q0 + Q1 + Q2 + Q3)/Apex)^2 / (2 * g);% Combined headloss
exit section.
92 Pre = Hre * rho * g;
93
94 %%% I0 : Gamma0_dot --> Branch 0 fluid inertia
95 Pa0 = Pc0 * (Vc0^gamma) / (Va0^gamma); % Assumed isothermal expansion
(for now)
```

```
 96 Hr0 = K0 * (Qa0/Aae)^2 / (2 * g);% Combined headloss from accumulator to
manifold;
 97 Pr0 = Hr0 * rho * g;
 98 Pb0 = kb0 * Vb0;
 99
100 %%% I1 : Gamma1_dot --> Branch 1 fluid inertia
101 Pa1 = Pc1 * (Vc1^gamma) / (Va1^gamma); % Assumed isothermal expansion
(for now)
102 Hr1 = K1 * (Qa1/Aae)^2 / (2 * g);% Combined headloss from accumulator to
manifold;
103 Pr1 = Hr1 * rho * g;
104 Pb1 = kb1 * Vb1;
105
106 %%% I2 : Gamma2_dot --> Branch 2 fluid inertia
107 Pa2 = Pc2 * (Vc2^gamma) / (Va2^gamma); % Assumed isothermal expansion
(for now)
108 Hr2 = K2 * (Qa2/Aae)^2 / (2 * g);% Combined headloss from accumulator to
manifold;
109 Pr2 = Hr2 * rho * g;
110 Pb2 = kb2 * Vb2;
111
112 %%% I3 : Gamma3_dot --> Branch 3 fluid inertia
113 Pa3 = Pc3 * (Vc3^gamma) / (Va3^gamma); % Assumed isothermal expansion
(for now)
114 Hr3 = K3 * (Qa3/Aae)^2 / (2 * g);% Combined headloss from accumulator to
manifold;
115 Pr3 = Hr3 * rho * g;
116 Pb3 = kb3 * Vb3;
117
118
119 P0 = Pb0+Pr0+Pm0+Pm1+Pm2+Pm3+Pre+Pse;
120 P1 = Pb1+Pr1+Pm1+Pm2+Pm3+Pre+Pse;
121 P2 = Pb2+Pr2+Pm2+Pm3+Pre+Pse;
122 P3 = Pb3+Pr3+Pm3+Pre+Pse;
123
124 %% State Equations
125 %%%%% Branch 0 flow
126 Va0_dot = Qa0;
127 Vb0_dot = Qb0;
128
129 %%%%% Branch 1 flow
130 if t >= tfire_1
131     Va1_dot  = Qa1;
132 else
133     Va1_dot  = 0;
134 end
135 Vb1_dot = Qb1;
136
137 %%%%% Branch 2 flow
138 if t >= tfire_2
139     Va2_dot  = Qa2;
140 else
141     Va2_dot  = 0;
142 end
```

```
143 Vb2_dot = Qb2;
144
145 %%%%% Branch 3 flow
146 if t >= tfire_3
147     Va3_dot  = Qa3;
148 else
149     Va3_dot  = 0;
150 end
151 Vb3_dot = Qb3;
152
153 %%%%%% FINDING GAMMA DOTS
154 A=[(1+Im/I0),Im/I1,Im/I2,Im/I3; Im/I0,(1+Im/I1),Im/I2,Im/I3;Im/I0,Im/I1,
(1+Im/I2),Im/I3;Im/I0,Im/I1,Im/I2,(1+Im/I3)];
155
156 if t < tfire_1
157     B=[Pa0-Pb0-Pr0-Pm0-Pm1-Pm2-Pm3-Pre-Pse; 0; 0; 0];
158 end
159
160 if (tfire_1 <= t) && (t < tfire_2)
161     B=[Pa0-Pb0-Pr0-Pm0-Pm1-Pm2-Pm3-Pre-Pse; Pa1-Pb1-Pr1-Pm2-Pm3-Pre-Pse;
0; 0];
162 %     B=[Pa0-Pb0-Pr0-Pm0-Pm1-Pm2-Pm3-Pre-Pse; Pa1-Pb1-Pb0-Pr1-Pm2-Pm3-
Pre-Pse; 0; 0];
163 end
164
165 if (tfire_2 <= t) && (t < tfire_3)
166     B=[Pa0-Pb0-Pr0-Pm0-Pm1-Pm2-Pm3-Pre-Pse; Pa1-Pb1-Pr1-Pm2-Pm3-Pre-Pse;
Pa2-Pb2-Pr2-Pm2-Pm3-Pre-Pse; 0];
167 %     B=[Pa0-Pb0-Pr0-Pm0-Pm1-Pm2-Pm3-Pre-Pse; Pa1-Pb1-Pb0-Pr1-Pm2-Pm3-
Pre-Pse; Pa2-Pb2-Pb1-Pb0-Pr2-Pm2-Pm3-Pre-Pse; 0];
168 end
169
170
171 if t >= tfire_3
172     B=[Pa0-Pb0-Pr0-Pm0-Pm1-Pm2-Pm3-Pre-Pse; Pa1-Pb1-Pr1-Pm2-Pm3-Pre-Pse;
Pa2-Pb2-Pr2-Pm2-Pm3-Pre-Pse; Pa3-Pb3-Pr3-Pm3-Pre-Pse];
173 %     B=[Pa0-Pb0-Pr0-Pm0-Pm1-Pm2-Pm3-Pre-Pse; Pa1-Pb1-Pb0-Pr1-Pm2-Pm3-
Pre-Pse; Pa2-Pb2-Pb1-Pb0-Pr2-Pm2-Pm3-Pre-Pse; Pa3-Pb3-Pb2-Pb1-Pb0-Pr3-Pm3-
Pre-Pse];
174 end
175
176 Gamma_dot = A\B;
177 Gamma0_dot = Gamma_dot(1);
178 Gamma1_dot = Gamma_dot(2);
179 Gamma2_dot = Gamma_dot(3);
180 Gamma3_dot = Gamma_dot(4);
181
182 %%% Pressure signals out
183 Pps0 = Pa0;
184 Pps1 = Pa1;
185 Pps2 = Pa2;
186 Pps3 = Pa3;
187 % Ppsf = Pre + Im * ((Gamma0_dot / I0) + (Gamma1_dot / I1) + (Gamma2_dot
/ I2) + (Gamma3_dot / I3))+ Pse; %%%%%% >>> WHY ON THIS STAGE Gamma0_dot term
```

```
subtracts? Backpressure?
188 Ppsf = Pre + Im * 0 * ((Gamma0_dot / I0) + (Gamma1_dot / I1) +
(Gamma2_dot / I2) + (Gamma3_dot / I3))+ Pse;
189
190
191 %% Output
192 xdot = [Va0_dot, Gamma0_dot, Va1_dot, Gamma1_dot, Va2_dot, Gamma2_dot,
Va3_dot, Gamma3_dot, Vb0_dot, Vb1_dot, Vb2_dot, Vb3_dot]';
193
194 Power_out= Ppsf * (Va0_dot + Va1_dot + Va2_dot + Va3_dot);
195
196 %% Output variables
197 y(1)  = Pps0;
198 y(2)  = Va0_dot;
199 y(3)  = Pps1;
200 y(4)  = Va1_dot;
201 y(5)  = Pps2;
202 y(6)  = Va2_dot;
203 y(7)  = Pps3;
204 y(8)  = Va3_dot;
205 y(9)  = Ppsf;
206 y(10) = Vb0;
207 y(11) = Vb1;
208 y(12) = Vb2;
209 y(13) = Vb3;
210 y(14) = P0;
211 y(15) = P1;
212 y(16) = P2;
213 y(17) = P3;
214 y(18) = Va0;
215 y(19) = Power_out;
216
```

D.2.3 1st event function, *events_1.m* for multi-branch model

```
function [value,isterminal,direction] = events_1(t,x)
global Vpc0 Vpc1 Vpc2 Vpc3
%%%% FILENAME: events_1.m
%%%% EVENT FUNCTION FOR STAGE 1 OF Multibranch_full_tuned00.m
%%% VERSION 3.0
% J. Campos
% 20 MAR 2017

% Locate the time when accumulator reaches empty and stop integration.

% detect fluid in line 0 stops moving
value = [x(1); x(2); x(3); x(4); x(5); x(6); x(7)-Vpc3; x(8)];
% stop the integration when Accumulator 3 volume reaches Precharge
% volume (accumulator empty)
isterminal = [0;0;0;0;0;0;1;0];
% negative direction
direction  = [0;0;0;0;0;0;0;0];

```

D.2.4 2nd event function, *events_2.m* for multi-branch model

```
function [value,isterminal,direction] = events_2(t,x)
global Vpc0 Vpc1 Vpc2 Vpc3
%%%% FILENAME: events_2.m
%%%% EVENT FUNCTION FOR STAGE 2 OF Multibranch_full_tuned00.m
%%% VERSION 1.0
% J. Campos
% 18 MAR 2017

% Locate the time when accumulator reaches empty and stop integration.

% detect fluid in line 3 stops moving
value = [x(1); x(2); x(3);x(4); x(5); x(6); x(7); x(8); x(9)];
% stop the integration when Accumulator 1 volume reaches Precharge
% volume (accumulator empty)
isterminal = [0;0;0;0;0;0;0;0;0];
% negative direction
direction = [0;0;0;0;0;0;0;0;0];
```

Appendix E

Experimental Data

E.1 Single branch (branch 0) experimental data

t	P_828	Q_828	P_524	Q_524	P_340	Q_340	P_210	Q_210	Pavg	Qavg
seconds	(psi)	Liter	PSI	Liter	PSI	Liter	PSI	Liter	PSI	Liter
0	0.992	0	1.094	0	1.9	0	1.45	0	1.359	0
0.05	17.195	0	16.227	0	15.565	0	16.431	0.045	16.3545	0.01125
0.1	13.781	0.09	13.934	0.086	15.615	0.116	14.698	0.134	14.507	0.1065
0.15	14.596	0.209	13.679	0.2	14.138	0.231	13.475	0.248	13.972	0.222
0.2	13.221	0.327	12.813	0.314	12.915	0.347	12.405	0.327	12.8385	0.32875
0.25	12.507	0.342	12.151	0.353	12.456	0.348	11.59	0.355	12.176	0.3495
0.3	11.794	0.325	11.59	0.339	11.896	0.335	11.386	0.345	11.6665	0.336
0.35	11.233	0.31	10.826	0.329	11.284	0.322	11.386	0.322	11.18225	0.32075
0.4	10.622	0.31	10.418	0.306	10.724	0.306	10.52	0.31	10.571	0.308
0.45	9.552	0.312	10.062	0.308	9.96	0.308	9.96	0.295	9.8835	0.30575
0.5	9.705	0.297	9.348	0.291	9.705	0.307	9.501	0.294	9.56475	0.29725
0.55	9.093	0.293	9.195	0.275	9.042	0.295	9.297	0.277	9.15675	0.285
0.6	8.635	0.277	7.921	0.275	8.941	0.279	8.431	0.277	8.482	0.277
0.65	7.514	0.277	7.208	0.261	8.125	0.277	6.953	0.264	7.45	0.26975
0.7	4.813	0.264	0.584	0.263	6.953	0.275	0.278	0.262	3.157	0.266
0.75	0.431	0.248	1.094	0.217	0.431	0.261	1.705	0.231	0.91525	0.23925
0.8	4.151	0.217	0.839	0.189	2.215	0.234	0.482	0.188	1.92175	0.207
0.85	0.635	0.16	1.705	0.131	0.788	0.19	2.011	0.132	1.28475	0.15325
0.9	1.756	0.117	1.247	0.103	2.266	0.145	1.145	0.103	1.6035	0.117
0.95	1.297	0.089	1.603	0.087	1.145	0.102	1.654	0.087	1.42475	0.09125
1	1.297	0.073	1.705	0.073	1.501	0.073	1.501	0.073	1.501	0.073
1.05	1.501	0.074	1.196	0.073	1.552	0.074	1.501	0.072	1.4375	0.07325
1.1	1.399	0.059	1.501	0.059	1.654	0.073	1.45	0.058	1.501	0.06225
1.15	1.501	0.059	1.603	0.074	1.297	0.073	1.45	0.057	1.46275	0.06575
1.2	1.603	0.059	1.552	0.059	1.043	0.058	1.297	0.059	1.37375	0.05875
1.25	1.552	0.059	1.348	0.059	1.501	0.059	1.247	0.059	1.412	0.059
1.3	1.501	0.073	1.654	0.058	1.348	0.059	1.297	0.059	1.45	0.06225
1.35	1.45	0.059	1.348	0.059	1.297	0.059	1.196	0.058	1.32275	0.05875
1.4	0.38	0.058	0.329	0.059	1.705	0.058	0.482	0.058	0.724	0.05825
1.45	0.584	0.044	0.992	0.044	1.45	0.057	1.094	0.058	1.03	0.05075

E.1.1 Single branch (branch 0) experimental data cont.

t	P_828	Q_828	P_524	Q_524	P_340	Q_340	P_210	Q_210	Pavg	Qavg
seconds	(psi)	Liter	PSI	Liter	PSI	Liter	PSI	Liter	PSI	Liter
1.5	0.992	0.044	0.89	0.044	0.737	0.059	1.145	0.043	0.941	0.0475
1.55	1.043	0.044	1.094	0.044	0.584	0.044	0.635	0.044	0.839	0.044
1.6	0.89	0.044	1.094	0.044	0.533	0.046	1.552	0.043	1.01725	0.04425
1.65	1.094	0.044	0.38	0.044	1.094	0.043	1.043	0.029	0.90275	0.04
1.7	0.941	0.029	1.399	0.029	0.686	0.044	0.584	0.029	0.9025	0.03275
1.75	0.941	0.03	0.89	0.03	0.635	0.029	1.196	0.015	0.9155	0.026
1.8	0.941	0.015	0.992	0.015	0.788	0.029	0.941	0.031	0.9155	0.0225
1.85	0.992	0.03	0.89	0.03	0.839	0.029	1.094	0.016	0.95375	0.02625
1.9	1.043	0.015	0.941	0.015	0.635	0.029	1.094	0.031	0.92825	0.0225
1.95	1.094	0.029	1.094	0.029	0.941	0.029	1.145	0.015	1.0685	0.0255
2	1.043	0.014	1.043	0.014	0.635	0.014	0.992	0.029	0.92825	0.01775

E.2 Experimental comparison data for tuned model

t	P_exp	Q_exp
seconds	(psi)	Liter
0	0.89	0
0.05	18.52	0.022
0.1	15.157	0.18
0.15	14.953	0.357
0.2	14.036	0.376
0.25	12.813	0.352
0.3	12.303	0.352
0.35	11.794	0.332
0.4	10.826	0.31
0.45	26.723	0.336
0.5	25.348	0.399
0.55	24.329	0.46
0.6	23.615	0.487
0.65	22.596	0.471
0.7	21.73	0.444
0.75	21.119	0.442
0.8	20.711	0.447
0.85	30.749	0.448
0.9	29.577	0.47
0.95	29.067	0.504
1	27.641	0.526
1.05	27.895	0.514
1.1	26.978	0.493
1.15	25.908	0.487
1.2	25.959	0.483
1.25	33.653	0.488
1.3	32.328	0.536
1.35	31.666	0.56
1.4	30.494	0.531
1.45	30.545	0.509
1.5	29.984	0.515
1.55	29.169	0.537
1.6	28.965	0.514
1.65	28.405	0.504
1.7	27.895	0.506
1.75	27.742	0.492
1.8	26.622	0.491
1.85	26.061	0.492

Data continued

t	P_exp	Q_exp
seconds	(psi)	Liter
1.9	25.755	0.467
1.95	25.144	0.466
2	24.227	0.469
2.05	22.341	0.47
2.1	20.099	0.467
2.15	18.316	0.421
2.2	16.227	0.405
2.25	11.896	0.384
2.3	2.622	0.336
2.35	1.705	0.264
2.4	2.113	0.197
2.45	0.482	0.134
2.5	0.533	0.089
2.55	0.89	0.09
2.6	1.247	0.067
2.65	1.247	0.044
2.7	1.247	0.045
2.75	1.145	0.045
2.8	1.145	0.045
2.85	1.196	0.044
2.9	1.043	0.044
2.95	1.145	0.045
3	1.196	0.023
3.05	0.992	0.022
3.1	1.043	0.022
3.15	0.992	0.023
3.2	0.839	0.023
3.25	1.145	0.023
3.3	0.992	0.023
3.35	0.992	0
3.4	0.89	0.022
3.45	1.094	0.022
3.5	1.094	0
3.55	0.941	0.023
3.6	1.094	0.023
3.65	0.89	0
3.7	0.992	0
3.75	1.145	0

Data continued

t	P_exp	Q_exp
seconds	(psi)	Liter
3.8	0.839	0
3.85	0.89	0
3.9	1.094	0
3.95	1.043	0
4	1.043	0

E.3 Tuned condition synthesis (TCS) test data

	Test pair									
t	P_726	Q_726	P_157	Q_157	P_307	Q_307	P_avg	Q_avg
seconds	(psi)	Liter	PSI	Liter	PSI	Liter	PSI	Liter
0.05	1.196	0	1.094	0	0.992	0	1.094	0.000
0.1	21.22	0.015	21.22	0.029	23.055	0	21.832	0.015
0.15	18.061	0.131	16.176	0.16	18.316	0.118	17.518	0.136
0.2	16.584	0.281	16.533	0.295	16.991	0.266	16.703	0.281
0.25	14.647	0.384	15.208	0.399	15.972	0.402	15.276	0.395
0.3	13.883	0.401	13.985	0.386	15.463	0.402	14.444	0.396
0.35	12.558	0.37	15.055	0.372	13.526	0.372	13.713	0.371
0.4	12.456	0.353	12.915	0.355	13.17	0.342	12.847	0.350
0.45	12.049	0.338	11.03	0.34	12.049	0.344	11.709	0.341
0.5	10.928	0.323	11.335	0.337	10.826	0.331	11.030	0.330
0.55	11.896	0.327	10.265	0.31	10.622	0.327	10.928	0.321
0.6	16.889	0.296	16.074	0.31	10.469	0.311	14.477	0.306
0.65	21.271	0.297	21.373	0.298	22.036	0.295	21.560	0.297
0.7	19.743	0.34	19.998	0.344	20.915	0.329	20.219	0.338
0.75	19.743	0.388	19.59	0.388	19.743	0.376	19.692	0.384
0.8	18.52	0.417	18.673	0.419	19.641	0.416	18.945	0.417
0.85	17.857	0.401	18.622	0.413	18.214	0.429	18.231	0.414
0.9	17.552	0.399	17.297	0.401	18.061	0.398	17.637	0.399
0.95	16.787	0.401	16.991	0.398	17.246	0.401	17.008	0.400
1	16.584	0.402	16.482	0.402	16.94	0.383	16.669	0.396
1.05	15.768	0.389	16.227	0.384	16.176	0.397	16.057	0.390
1.1	15.412	0.384	15.717	0.382	15.768	0.383	15.632	0.383
1.15	14.749	0.369	15.514	0.367	15.259	0.372	15.174	0.369
1.2	14.444	0.367	15.004	0.367	14.8	0.359	14.749	0.364
1.25	21.424	0.354	22.596	0.354	22.902	0.357	22.307	0.355
1.3	21.271	0.381	21.475	0.382	21.628	0.384	21.458	0.382
1.35	20.252	0.398	18.214	0.411	21.424	0.414	19.963	0.408
1.4	19.845	0.428	19.743	0.425	20.609	0.433	20.066	0.429

E.3.1 Tuned condition synthesis (TCS) test data cont.

	Test pair								
t	P_726	Q_726	P_157	Q_157	P_307	Q_307	P_avg	Q_avg
seconds	(psi)	Liter	PSI	Liter	PSI	Liter	PSI	Liter
1.45	19.998	0.419	20.201	0.428	22.749	0.437	20.983	0.428
1.5	19.743	0.416	19.641	0.417	19.794	0.417	19.726	0.417
1.55	19.029	0.413	18.877	0.428	19.284	0.417	19.063	0.419
1.6	18.01	0.411	18.52	0.414	18.622	0.413	18.384	0.413
1.65	17.348	0.411	18.01	0.411	18.622	0.416	17.993	0.413
1.7	16.889	0.399	17.45	0.385	18.112	0.401	17.484	0.395
1.75	15.972	0.385	16.482	0.381	17.348	0.384	16.601	0.383
1.8	15.565	0.384	16.227	0.381	16.584	0.384	16.125	0.383
1.85	16.533	0.369	16.125	0.382	14.087	0.381	15.582	0.377
1.9	21.934	0.382	22.29	0.384	21.934	0.387	22.053	0.384
1.95	20.456	0.384	21.475	0.398	21.883	0.398	21.271	0.393
2	19.182	0.411	18.673	0.425	21.271	0.414	19.709	0.417
2.05	18.826	0.426	18.978	0.426	18.673	0.425	18.826	0.426
2.1	17.195	0.425	17.144	0.411	18.877	0.414	17.739	0.417
2.15	14.189	0.398	15.768	0.398	17.348	0.416	15.768	0.404
2.2	13.221	0.371	14.291	0.384	15.565	0.399	14.359	0.385
2.25	12.915	0.355	12.915	0.37	13.781	0.384	13.204	0.370
2.3	11.794	0.339	12.303	0.342	12.915	0.355	12.337	0.345
2.35	11.132	0.323	11.233	0.327	11.641	0.341	11.335	0.330
2.4	10.214	0.31	10.826	0.314	11.386	0.341	10.809	0.322
2.45	9.96	0.294	10.062	0.296	10.877	0.325	10.300	0.305
2.5	9.96	0.293	9.348	0.298	9.756	0.323	9.688	0.305
2.55	8.839	0.279	8.584	0.281	9.399	0.293	8.941	0.284
2.6	0.584	0.266	0.227	0.268	0.482	0.296	0.431	0.277
2.65	3.336	0.208	4.253	0.208	1.043	0.267	2.877	0.228
2.7	1.654	0.148	0.584	0.164	0.329	0.237	0.856	0.183
2.75	1.094	0.104	1.348	0.118	2.724	0.178	1.722	0.133
2.8	1.145	0.088	1.96	0.104	0.788	0.132	1.298	0.108

E.3.2 Tuned condition synthesis (TCS) test data cont.

Test pair									
t	P_726	Q_726	P_157	Q_157	P_307	Q_307	P_avg	Q_avg
seconds	(psi)	Liter	PSI	Liter	PSI	Liter	PSI	Liter
2.85	1.45	0.089	1.501	0.074	1.501	0.103	1.484	0.089
2.9	0.533	0.074	1.247	0.074	0.788	0.073	0.856	0.074
2.95	1.196	0.059	0.533	0.059	1.145	0.074	0.958	0.064
3	0.278	0.044	1.247	0.059	1.297	0.059	0.941	0.054
3.05	1.196	0.044	0.38	0.044	0.89	0.059	0.822	0.049
3.1	0.38	0.044	0.89	0.045	0.686	0.045	0.652	0.045
3.15	1.043	0.044	0.584	0.044	0.584	0.044	0.737	0.044
3.2	1.094	0.029	0.992	0.045	1.705	0.045	1.264	0.040
3.25	1.094	0.029	0.992	0.03	1.043	0.029	1.043	0.029
3.3	0.941	0.015	1.043	0.03	0.89	0.029	0.958	0.025
3.35	0.992	0.029	1.145	0.03	1.043	0.015	1.060	0.025
3.4	0.992	0.014	1.094	0.03	1.094	0.029	1.060	0.024
3.45	1.247	0.029	0.992	0.03	1.043	0.015	1.094	0.025
3.5	1.145	0.015	0.941	0.015	1.094	0.029	1.060	0.020
3.55	0.992	0.03	1.094	0	0.941	0.015	1.009	0.015
3.6	0.992	0	1.094	0	1.094	0.029	1.060	0.010
3.65	1.043	0	1.043	0	0.89	0.014	0.992	0.005
3.7	1.043	0	1.094	0	0.89	0	1.009	0.000
3.75	1.094	0	1.043	0	0.89	0	1.009	0.000
3.8	0.839	0	1.094	0	1.043	0	0.992	0.000
3.85	0.992	0	1.094	0	1.043	0	1.043	0.000
3.9	1.094	0	1.145	0	1.145	0	1.128	0.000
3.95	0.992	0	0.941	0	1.094	0	1.009	0.000
4	0.89	0	1.094	0	0.941	0	0.975	0.000
4.05	0.941	0	0.89	0	1.043	0	0.958	0.000

E.4 Operating condition excursion (OCE) test data

	OC1a		OC1b		OC2a		OC2b		OC3a		OC3b	
t	P	Q	P	Q	P	Q	P	Q	P	Q	P	Q
seconds	(psi)	Liter	PSI	Liter	PSI	Liter	PSI	Liter	PSI	Liter	PSI	Liter
0	1.247	0	0.992	0	1.094	0	1.145	0	1.145	0	0.89	0
0.05	17.908	0	20.405	0	17.399	0	17.501	0	15.31	0.015	14.698	0
0.1	16.482	0.118	16.686	0.089	14.749	0.089	15.208	0.089	12.864	0.118	13.323	0.074
0.15	14.444	0.238	15.87	0.224	14.342	0.222	15.361	0.224	13.221	0.238	12.202	0.194
0.2	14.138	0.371	14.24	0.355	14.495	0.34	13.068	0.34	12.253	0.328	10.979	0.296
0.25	13.475	0.358	14.036	0.386	12.303	0.352	12.915	0.357	11.183	0.342	11.896	0.339
0.3	11.998	0.357	13.577	0.369	11.284	0.337	12.558	0.34	10.928	0.328	11.081	0.323
0.35	11.132	0.326	12.049	0.356	10.367	0.323	11.488	0.329	10.928	0.325	10.062	0.31
0.4	10.469	0.324	11.692	0.34	9.756	0.31	11.081	0.327	9.246	0.297	9.654	0.298
0.45	10.062	0.31	11.335	0.337	9.858	0.298	10.418	0.31	9.654	0.28	9.552	0.281
0.5	10.062	0.297	10.622	0.322	9.297	0.281	10.265	0.308	8.635	0.269	0.686	0.296
0.55	8.992	0.3	9.552	0.308	8.941	0.281	10.163	0.295	8.431	0.282	0.482	0.264
0.6	8.992	0.281	9.96	0.295	8.329	0.264	9.654	0.283	8.584	0.268	0.482	0.222
0.65	8.278	0.281	9.501	0.296	8.329	0.268	8.941	0.269	7.718	0.265	0.482	0.148
0.7	7.972	0.264	9.807	0.297	7.718	0.266	0.584	0.28	7.667	0.253	1.705	0.104
0.75	8.074	0.268	9.042	0.284	7.769	0.268	6.597	0.25	7.412	0.252	1.756	0.073
0.8	7.769	0.255	9.246	0.269	7.106	0.251	10.062	0.19	7.106	0.253	1.705	0.074
0.85	7.361	0.252	22.749	0.269	6.546	0.24	2.317	0.119	6.902	0.236	1.247	0.06
0.9	6.953	0.236	21.832	0.324	6.648	0.223	1.603	0.089	6.648	0.236	1.45	0.059
0.95	19.437	0.236	20.966	0.386	6.291	0.238	18.978	0.089	7.82	0.222	17.297	0.044
1	18.469	0.268	16.533	0.428	19.998	0.237	15.768	0.177	16.991	0.238	12.711	0.147
1.05	18.112	0.338	14.902	0.416	17.246	0.253	15.412	0.269	16.176	0.28	13.424	0.251
1.1	18.01	0.398	14.291	0.399	17.45	0.297	14.087	0.357	15.666	0.327	12.253	0.338
1.15	17.144	0.398	13.628	0.382	16.176	0.355	13.883	0.354	15.004	0.354	10.367	0.326
1.2	16.227	0.386	12.049	0.352	15.565	0.386	13.017	0.352	13.424	0.359	0.482	0.31
1.25	16.227	0.372	11.284	0.34	15.106	0.371	10.418	0.34	11.59	0.357	10.062	0.268
1.3	16.125	0.383	10.418	0.327	13.985	0.357	10.265	0.327	10.418	0.342	0.38	0.207
1.35	14.698	0.37	10.214	0.313	11.437	0.355	0.329	0.299	9.195	0.325	0.482	0.133
1.4	14.749	0.367	9.705	0.295	10.418	0.339	2.062	0.281	8.278	0.297	3.132	0.088
1.45	14.342	0.358	9.042	0.281	10.316	0.323	0.227	0.223	8.533	0.283	1.552	0.073
1.5	14.24	0.354	0	0.281	6.189	0.308	2.928	0.162	7.565	0.269	0.737	0.059
1.55	13.679	0.357	12.915	0.253	8.176	0.295	3.998	0.105	7.616	0.251	1.196	0.059
1.6	10.265	0.34	0.431	0.207	7.769	0.267	0.839	0.089	7.106	0.253	1.501	0.044
1.65	9.552	0.344	0.431	0.149	6.953	0.251	1.043	0.074	6.953	0.237	1.247	0.044
1.7	9.552	0.313	1.909	0.103	7.157	0.251	1.705	0.059	9.093	0.239	1.145	0.044
1.75	8.584	0.296	1.603	0.09	7.259	0.249	1.756	0.06	0.482	0.222	1.247	0.044
1.8	6.902	0.264	0.431	0.074	6.851	0.236	1.297	0.06	2.317	0.208	1.45	0.044
1.85	6.851	0.266	1.909	0.074	0.839	0.22	2.062	0.059	2.368	0.162	1.247	0.044
1.9	7.004	0.253	0.686	0.059	2.877	0.205	1.501	0.044	7.259	0.135	1.297	0.029
1.95	6.75	0.239	20.762	0.075	1.145	0.176	1.297	0.059	2.215	0.104	1.196	0.029
2	6.087	0.222	16.482	0.177	2.062	0.133	1.247	0.059	1.603	0.104	1.45	0.029
2.05	6.342	0.223	16.023	0.298	1.705	0.104	0.89	0.059	0.329	0.088	1.247	0.044
2.1	0.329	0.207	15.004	0.384	1.909	0.088	0.482	0.044	0.89	0.088	1.348	0.044
2.15	4.559	0.195	13.781	0.372	1.603	0.089	1.654	0.044	0.89	0.074	1.348	0.044
2.2	0.431	0.15	12.507	0.355	1.348	0.089	1.348	0.044	1.094	0.059	1.196	0.045
2.25	0.482	0.12	12.813	0.344	0.227	0.075	17.959	0.074	1.043	0.044	1.247	0.044

E.4.1 Operating condition excursion (OCE) test data cont.

	OC1a		OC1b		OC2a		OC2b		OC3a		OC3b	
t	P	Q	P	Q	P	Q	P	Q	P	Q	P	Q
seconds	(psi)	Liter	PSI	Liter	PSI	Liter	PSI	Liter	PSI	Liter	PSI	Liter
2.3	1.348	0.089	12.303	0.326	0.482	0.073	14.342	0.176	1.043	0.044	1.348	0.044
2.35	1.145	0.074	11.794	0.312	0.839	0.059	13.526	0.279	13.374	0.074	1.348	0.044
2.4	1.145	0.059	10.622	0.31	1.552	0.059	13.17	0.338	11.947	0.177	0.482	0.044
2.45	17.297	0.088	10.418	0.314	1.043	0.045	12.049	0.34	12.049	0.264	17.756	0.089
2.5	15.514	0.205	9.756	0.297	1.043	0.044	11.03	0.325	11.386	0.322	15.106	0.192
2.55	14.596	0.311	0.38	0.283	1.094	0.03	11.488	0.323	11.183	0.308	13.374	0.295
2.6	13.934	0.372	10.673	0.251	1.043	0.03	10.571	0.309	10.469	0.297	12.711	0.355
2.65	12.813	0.36	0.329	0.207	0.89	0.03	9.297	0.294	9.501	0.298	11.845	0.341
2.7	11.998	0.34	0.431	0.149	1.094	0.03	0.482	0.266	9.042	0.282	10.316	0.325
2.75	11.692	0.327	1.705	0.09	15.666	0.074	0.329	0.207	8.89	0.281	0.38	0.297
2.8	10.826	0.31	1.247	0.074	13.73	0.177	2.011	0.148	8.737	0.267	0.482	0.252
2.85	10.163	0.314	1.247	0.059	12.253	0.296	1.909	0.104	8.329	0.268	0.176	0.194
2.9	9.858	0.299	1.145	0.059	12.303	0.34	0.992	0.089	7.514	0.268	1.247	0.134
2.95	9.399	0.297	1.501	0.045	11.183	0.326	1.348	0.075	7.208	0.251	2.062	0.104
3	8.941	0.281	1.348	0.044	13.323	0.31	1.094	0.059	6.902	0.253	1.45	0.074
3.05	9.246	0.281	1.297	0.044	10.673	0.312	1.705	0.045	0.38	0.223	1.705	0.059
3.1	5.832	0.267	1.247	0.044	9.858	0.296	1.196	0.044	2.775	0.195	1.247	0.045
3.15	8.023	0.266	1.297	0.044	9.45	0.297	1.45	0.045	2.317	0.133	1.603	0.044
3.2	7.769	0.249	1.247	0.044	9.297	0.28	1.247	0.045	1.247	0.104	1.297	0.044
3.25	7.208	0.236	0.482	0.044	8.686	0.279	1.196	0.044	1.247	0.089	1.348	0.044
3.3	6.546	0.238	0.89	0.03	8.635	0.264	1.094	0.044	1.297	0.075	1.45	0.045
3.35	7.31	0.239	1.247	0.03	7.667	0.264	1.399	0.044	1.145	0.059	1.247	0.045
3.4	6.851	0.236	0.992	0.015	7.82	0.251	0.992	0.044	1.297	0.045	1.501	0.044
3.45	0.482	0.223	18.571	0.075	7.412	0.25	0.38	0.044	1.196	0.044	0.482	0.045
3.5	5.629	0.192	16.991	0.191	7.106	0.235	0.635	0.044	1.399	0.045	0.482	0.044
3.55	1.552	0.15	15.87	0.31	6.75	0.234	1.297	0.029	1.399	0.045	0.482	0.03
3.6	1.094	0.104	15.004	0.382	0.075	0.206	0.992	0.03	1.196	0.045	1.094	0.03
3.65	1.297	0.074	14.138	0.354	4.559	0.178	16.176	0.075	0.482	0.044	1.348	0.029
3.7	1.297	0.074	13.119	0.351	2.317	0.133	14.291	0.206	0.227	0.044	1.094	0.029
3.75	1.247	0.059	12.915	0.337	1.094	0.104	14.189	0.294	1.501	0.044	1.043	0.029
3.8	0.38	0.059	11.998	0.337	1.094	0.073	13.221	0.352	0.992	0.03	1.247	0.015
3.85	19.029	0.102	11.335	0.325	1.399	0.059	12.151	0.325	13.934	0.087	15.565	0.102
3.9	16.38	0.219	11.284	0.312	1.348	0.044	11.437	0.338	12.915	0.194	12.813	0.192
3.95	15.004	0.325	10.622	0.311	1.399	0.044	11.692	0.322	12.049	0.297	13.119	0.311
4	14.342	0.371	10.011	0.296	1.196	0.044	10.673	0.308	11.284	0.33	12.66	0.327
4.05	13.475	0.359	9.96	0.279	0.635	0.044	10.52	0.298	11.183	0.312	11.692	0.324
4.1	12.609	0.34	8.074	0.28	0.635	0.045	0.329	0.268	10.724	0.312	11.183	0.308
4.15	11.845	0.339	0.584	0.25	0.329	0.03	8.89	0.238	10.011	0.295	10.877	0.308
4.2	11.488	0.323	0.482	0.191	1.043	0.03	0.533	0.162	9.654	0.282	0.38	0.264
4.25	10.775	0.312	1.858	0.117	1.094	0.03	1.501	0.119	8.788	0.267	5.629	0.208
4.3	10.52	0.285	1.705	0.089	1.043	0.03	1.909	0.089	8.737	0.27	2.571	0.133
4.35	9.297	0.282	1.094	0.074	17.399	0.13	1.094	0.074	8.074	0.266	1.552	0.104
4.4	9.093	0.28	1.399	0.074	13.934	0.234	1.196	0.059	7.921	0.267	0.788	0.074
4.45	9.042	0.28	0.329	0.059	13.679	0.337	1.247	0.044	7.616	0.251	1.094	0.06
4.5	8.431	0.268	0.38	0.059	12.558	0.339	1.297	0.044	6.953	0.254	1.45	0.045
4.55	8.125	0.267	0.992	0.044	13.17	0.327	1.247	0.045	7.31	0.237	1.094	0.044

E.4.2 Operating condition excursion (OCE) test data cont.

	OC1a		OC1b		OC2a		OC2b		OC3a		OC3b	
t	P	Q	P	Q	P	Q	P	Q	P	Q	P	Q
seconds	(psi)	Liter	PSI	Liter	PSI	Liter	PSI	Liter	PSI	Liter	PSI	Liter
4.6	8.074	0.25	1.094	0.03	11.284	0.324	1.145	0.03	0.278	0.238	1.196	0.044
4.65	7.82	0.249	0.992	0.03	10.928	0.296	1.247	0.03	4.711	0.192	1.348	0.044
4.7	7.157	0.236	0.992	0.029	10.469	0.294	1.297	0.03	0.329	0.15	1.145	0.044
4.75	7.106	0.238	0.992	0.029	10.062	0.281	1.348	0.03	0.89	0.104	1.247	0.03
4.8	7.004	0.236	1.247	0.03	8.788	0.279	1.094	0.03	2.317	0.074	1.399	0.03
4.85	6.648	0.236	0.992	0.015	9.297	0.264	1.145	0.03	0.635	0.074	1.094	0.03
4.9	0.482	0.205	0.992	0.03	8.992	0.264	1.145	0.03	0.482	0.059	1.247	0.03
4.95	2.062	0.148	0.992	0.015	7.82	0.266	1.348	0.03	0.89	0.059	1.348	0.03
5	1.399	0.104	1.145	0.029	7.769	0.266	1.247	0.03	1.145	0.03	1.094	0.029
5.05	1.501	0.089	1.145	0.015	7.667	0.249	1.043	0.03	0.584	0.029	0.686	0.029
5.1	1.145	0.073	0.992	0.015	7.616	0.235	1.247	0.03	1.094	0.03	1.348	0.029
5.15	1.043	0.059	1.043	0.015	7.208	0.234	0.584	0.015	0.992	0.03	1.094	0.015
5.2	1.196	0.045	0.941	0.015	2.928	0.207	1.705	0.03	1.247	0.03	0.38	0.03
5.25	0.584	0.044	0.992	0.015	1.45	0.176	1.043	0.015	0.89	0.015	1.705	0.015
5.3	0.635	0.044	0.992	0	0.482	0.118	0.89	0.029	0.992	0.03	0.992	0.03
5.35	1.145	0.029	1.043	0.015	1.297	0.088	0.941	0.014	1.094	0.015	1.094	0.015
5.4	1.043	0.03	0.992	0.015	1.603	0.074	1.043	0.014	1.094	0.03	1.247	0.015
5.45	0.89	0.029	0.941	0.015	1.043	0.059	1.094	0.015	1.145	0.015	1.043	0.015
5.5	0.941	0.029	1.043	0	0.635	0.059	1.043	0.015	1.247	0.015	1.043	0.015
5.55	1.145	0.029	1.094	0	0.89	0.044	1.094	0.015	0.941	0.015	1.094	0.015
5.6	0.89	0.015	0.992	0.015	1.297	0.029	1.094	0	1.145	0.015	1.043	0
5.65	0.89	0.015	1.145	0.015	0.89	0.03	0.89	0.015	1.094	0.015	1.196	0.015
5.7	1.043	0.015	1.297	0.015	0.431	0.03	1.094	0.015	1.094	0	1.094	0.015
5.75	1.094	0.015	0.89	0	1.247	0.03	1.043	0.015	0.992	0.015	1.145	0.015
5.8	1.043	0.015	0.89	0	0.89	0.029	0.992	0	1.094	0.015	1.094	0
5.85	1.094	0.015	0.89	0	1.145	0.015	1.043	0	1.094	0.015	0.89	0
5.9	1.094	0.015	0.89	0	1.043	0.03	1.247	0	1.043	0	0.89	0
5.95	1.094	0.015	1.247	0	1.094	0.015	0.992	0	0.89	0	1.145	0.015
6	1.094	0.015	1.094	0	0.992	0.015	1.094	0.015	0.992	0.015	1.094	0.015
6.05	1.145	0.015	0.992	0	1.043	0.015	1.094	0.015	0.992	0.015	1.247	0.015
6.1	0.89	0.015	1.043	0	0.89	0.015	1.145	0.015	1.094	0.015	0.89	0
6.15	1.043	0	0.89	0	0.941	0.015	1.145	0	0.89	0	1.094	0
6.2	1.043	0	1.145	0	0.992	0.014	0.89	0	1.094	0	1.145	0
6.25	0.89	0	0.992	0	1.145	0.014	1.247	0	1.043	0	1.043	0
6.3	1.043	0.015	1.145	0	0.839	0.014	1.043	0	1.043	0	0.992	0
6.35	1.145	0.015	0.89	0	1.145	0	0.941	0	1.043	0	1.145	0
6.4	0.89	0.015	1.094	0	0.992	0	1.094	0	0.89	0	1.247	0
6.45	1.043	0	1.043	0	0.992	0.014	1.196	0	1.094	0	1.145	0
6.5	1.043	0	0.89	0	1.043	0.014	1.247	0	0.992	0	1.043	0

E.5 Discharge timing excursion (TE) tests: TE01 cond.

Test pair

t	P_602	Q_602	P_742	Q_742	P_621	Q_621	Pavg	Q_avg
seconds	(psi)	Liter	PSI	Liter	PSI	Liter	PSI	Liter
0	0.89	0	2.062	0	1.094	0	1.349	0.000
0.05	17.144	0	17.552	0	18.112	0	17.603	0.000
0.1	15.157	0.1	14.698	0.105	13.679	0.106	14.511	0.104
0.15	14.036	0.243	15.004	0.236	13.883	0.238	14.308	0.239
0.2	13.934	0.351	13.119	0.354	13.73	0.359	13.594	0.355
0.25	12.507	0.382	12.405	0.367	12.915	0.359	12.609	0.369
0.3	12.253	0.342	12.303	0.34	12.405	0.34	12.320	0.341
0.35	11.692	0.353	11.692	0.338	11.692	0.325	11.692	0.339
0.4	11.335	0.325	10.928	0.325	11.284	0.338	11.182	0.329
0.45	10.826	0.312	10.367	0.31	10.367	0.314	10.520	0.312
0.5	10.265	0.297	10.265	0.298	10.112	0.314	10.214	0.303
0.55	9.909	0.297	9.348	0.298	9.246	0.297	9.501	0.297
0.6	8.584	0.296	9.297	0.296	9.195	0.296	9.025	0.296
0.65	8.788	0.281	9.246	0.281	8.992	0.28	9.009	0.281
0.7	8.839	0.266	9.858	0.264	8.839	0.267	9.179	0.266
0.75	23.666	0.28	23.055	0.283	23.106	0.281	23.276	0.281
0.8	21.883	0.34	22.239	0.329	21.781	0.338	21.968	0.336
0.85	22.087	0.398	22.239	0.385	21.373	0.396	21.900	0.393
0.9	20.303	0.431	19.233	0.43	19.998	0.428	19.845	0.430
0.95	20.048	0.427	19.488	0.444	19.386	0.431	19.641	0.434
1	19.539	0.414	18.673	0.434	19.437	0.414	19.216	0.421
1.05	18.775	0.426	16.787	0.414	17.195	0.416	17.586	0.419
1.1	15.463	0.414	15.768	0.401	17.959	0.399	16.397	0.405
1.15	14.444	0.397	13.323	0.384	14.24	0.404	14.002	0.395
1.2	13.374	0.369	13.323	0.374	13.73	0.385	13.476	0.376
1.25	12.303	0.355	12.405	0.342	12.303	0.357	12.337	0.351
1.3	11.896	0.344	11.947	0.34	12.253	0.325	12.032	0.336
1.35	11.641	0.327	10.928	0.323	10.877	0.314	11.149	0.321

E.5.1 TE test data: TE01 condition cont.

	Test pair								
t	**P_602**	**Q_602**	**P_742**	**Q_742**	**P_621**	**Q_621**	**Pavg**	**Q_avg**
seconds	**(psi)**	**Liter**	**PSI**	**Liter**	**PSI**	**Liter**	**PSI**	**Liter**
1.4	10.826	0.31	10.265	0.325	10.571	0.312	10.554	0.316
1.45	25.755	0.323	23.462	0.312	25.195	0.327	24.804	0.321
1.5	27.437	0.37	25.348	0.359	24.481	0.368	25.755	0.366
1.55	23.87	0.432	22.953	0.413	23.972	0.432	23.598	0.426
1.6	23.411	0.464	21.73	0.461	23.36	0.462	22.834	0.462
1.65	21.526	0.459	20.864	0.457	23.157	0.465	21.849	0.460
1.7	20.201	0.443	18.978	0.449	21.883	0.442	20.354	0.445
1.75	19.386	0.44	17.552	0.429	21.017	0.443	19.318	0.437
1.8	18.826	0.431	15.412	0.417	18.571	0.441	17.603	0.430
1.85	17.348	0.414	14.495	0.386	15.004	0.429	15.616	0.410
1.9	13.985	0.386	13.73	0.376	10.673	0.411	12.796	0.391
1.95	13.424	0.371	13.424	0.344	11.284	0.369	12.711	0.361
2	12.405	0.346	10.928	0.34	10.673	0.325	11.335	0.337
2.05	10.367	0.344	10.52	0.322	8.839	0.297	9.909	0.321
2.1	10.265	0.312	9.858	0.325	9.705	0.282	9.943	0.306
2.15	25.551	0.325	25.144	0.312	25.959	0.309	25.551	0.315
2.2	24.685	0.372	24.94	0.375	25.297	0.369	24.974	0.372
2.25	24.431	0.432	23.157	0.414	24.074	0.426	23.887	0.424
2.3	22.902	0.461	17.807	0.46	22.902	0.46	21.204	0.460
2.35	15.819	0.44	16.329	0.443	21.883	0.447	18.010	0.443
2.4	15.004	0.428	15.259	0.416	14.8	0.445	15.021	0.430
2.45	15.31	0.398	14.342	0.382	14.8	0.414	14.817	0.398
2.5	14.291	0.375	13.781	0.355	13.475	0.382	13.849	0.371
2.55	13.17	0.355	13.679	0.355	12.253	0.354	13.034	0.355
2.6	12.915	0.342	12.813	0.344	11.692	0.338	12.473	0.341
2.65	12.253	0.326	11.692	0.342	11.233	0.323	11.726	0.330
2.7	11.335	0.33	11.284	0.325	10.571	0.309	11.063	0.321
2.75	11.335	0.314	10.062	0.323	10.418	0.31	10.605	0.316

E.5.2 TE test data: TE01 condition cont.

t	Test pair								
	P_602	Q_602	P_742	Q_742	P_621	Q_621	Pavg	Q_avg
seconds	(psi)	Liter	PSI	Liter	PSI	Liter	PSI	Liter
2.8	10.673	0.311	9.654	0.294	9.603	0.297	9.977	0.301
2.85	9.858	0.294	0.482	0.281	0.431	0.281	3.590	0.285
2.9	0.482	0.295	1.807	0.236	1.552	0.237	1.280	0.256
2.95	2.928	0.238	1.603	0.193	1.807	0.177	2.113	0.203
3	0.686	0.165	1.399	0.134	1.858	0.135	1.314	0.145
3.05	1.45	0.103	1.297	0.105	1.297	0.104	1.348	0.104
3.1	0.686	0.089	0.431	0.075	0.686	0.089	0.601	0.084
3.15	1.247	0.074	1.145	0.059	1.297	0.074	1.230	0.069
3.2	0.278	0.06	0.278	0.045	1.043	0.06	0.533	0.055
3.25	1.094	0.045	1.247	0.044	0.941	0.059	1.094	0.049
3.3	0.89	0.045	0.839	0.045	1.043	0.044	0.924	0.045
3.35	0.992	0.045	1.145	0.044	0.584	0.044	0.907	0.044
3.4	0.992	0.03	0.89	0.03	0.482	0.044	0.788	0.035
3.45	0.941	0.03	1.145	0.029	1.043	0.03	1.043	0.030
3.5	0.89	0.029	0.992	0.03	1.094	0.03	0.992	0.030
3.55	0.992	0.029	1.145	0.03	1.094	0.03	1.077	0.030
3.6	0.992	0.03	0.941	0.03	0.89	0.03	0.941	0.030
3.65	0.941	0.015	1.043	0.015	0.89	0.03	0.958	0.020
3.7	1.196	0.03	0.992	0.03	1.043	0.015	1.077	0.025
3.75	0.992	0.015	0.992	0.015	1.297	0	1.094	0.010
3.8	1.094	0	1.043	0	0.89	0	1.009	0.000
3.85	0.992	0	1.043	0	1.145	0	1.060	0.000
3.9	0.992	0	0.992	0	1.043	0	1.009	0.000
3.95	0.941	0	1.043	0	1.094	0	1.026	0.000
4	0.89	0	1.043	0	0.89	0	0.941	0.000

E.6 Discharge timing excursion (TE) tests: TE02 cond.

t	P_314	Q_314	P_453	Q_453	P_622	Q_622	Pavg	Q_avg
seconds	(psi)	Liter	PSI	Liter	PSI	Liter	PSI	Liter
0	1.094	0	4.559	0	1.552	0	2.402	0.000
0.05	17.756	0	16.889	0	17.042	0.015	17.229	0.005
0.1	14.342	0.106	14.545	0.118	14.647	0.12	14.511	0.115
0.15	14.545	0.224	14.342	0.238	15.514	0.25	14.800	0.237
0.2	14.851	0.344	24.176	0.356	16.991	0.356	18.673	0.352
0.25	30.086	0.359	30.392	0.369	29.271	0.369	29.916	0.366
0.3	31.36	0.414	28.914	0.426	28.099	0.416	29.458	0.419
0.35	27.182	0.457	27.742	0.473	27.284	0.462	27.403	0.464
0.4	25.959	0.514	26.214	0.505	25.551	0.502	25.908	0.507
0.45	24.532	0.491	25.297	0.494	24.991	0.487	24.940	0.491
0.5	23.921	0.487	23.972	0.488	23.462	0.485	23.785	0.487
0.55	23.055	0.46	23.513	0.475	22.851	0.473	23.140	0.469
0.6	23.513	0.473	25.602	0.457	24.991	0.458	24.702	0.463
0.65	32.481	0.464	32.481	0.465	32.481	0.443	32.481	0.457
0.7	31.105	0.491	31.054	0.495	31.666	0.473	31.275	0.486
0.75	31.105	0.502	31.156	0.52	30.851	0.502	31.037	0.508
0.8	29.781	0.527	30.647	0.531	31.921	0.534	30.783	0.531
0.85	28.66	0.516	29.984	0.532	29.118	0.53	29.254	0.526
0.9	28.303	0.519	29.628	0.536	27.59	0.52	28.507	0.525
0.95	28.405	0.506	27.793	0.517	27.488	0.517	27.895	0.513
1	26.825	0.499	27.08	0.514	26.316	0.509	26.740	0.507
1.05	26.418	0.484	26.825	0.487	26.367	0.509	26.537	0.493
1.1	25.857	0.484	26.316	0.491	25.093	0.491	25.755	0.489
1.15	25.348	0.488	25.348	0.478	24.787	0.473	25.161	0.480
1.2	26.418	0.484	25.908	0.487	25.144	0.472	25.823	0.481
1.25	31.564	0.488	32.481	0.49	31.462	0.475	31.836	0.484
1.3	31.004	0.503	31.207	0.503	30.443	0.502	30.885	0.503
1.35	30.851	0.506	31.054	0.52	30.596	0.514	30.834	0.513

E.6.1 TE test data: TE02 condition cont.

t	P_314	Q_314	P_453	Q_453	P_622	Q_622	Pavg	Q_avg
seconds	(psi)	Liter	PSI	Liter	PSI	Liter	PSI	Liter
1.4	30.392	0.517	30.035	0.528	29.781	0.516	30.069	0.520
1.45	29.322	0.517	29.883	0.516	29.577	0.52	29.594	0.518
1.5	28.507	0.518	29.424	0.516	28.609	0.508	28.847	0.514
1.55	27.997	0.521	28.66	0.52	28.201	0.517	28.286	0.519
1.6	27.946	0.505	28.048	0.517	27.997	0.502	27.997	0.508
1.65	27.182	0.505	28.099	0.503	27.437	0.499	27.573	0.502
1.7	26.978	0.502	26.825	0.488	26.265	0.487	26.689	0.492
1.75	26.265	0.503	26.723	0.488	26.061	0.485	26.350	0.492
1.8	25.755	0.502	26.316	0.487	25.653	0.487	25.908	0.492
1.85	25.399	0.475	25.297	0.49	24.838	0.488	25.178	0.484
1.9	25.144	0.472	25.093	0.472	24.532	0.478	24.923	0.474
1.95	24.329	0.472	24.634	0.473	23.411	0.475	24.125	0.473
2	22.545	0.469	23.972	0.47	21.017	0.458	22.511	0.466
2.05	13.628	0.462	22.494	0.473	13.374	0.44	16.499	0.458
2.1	15.972	0.415	12.813	0.455	13.323	0.399	14.036	0.423
2.15	13.272	0.373	13.374	0.411	12.864	0.372	13.170	0.385
2.2	12.456	0.339	12.151	0.367	9.195	0.344	11.267	0.350
2.25	0.635	0.33	5.68	0.327	0.584	0.31	2.300	0.322
2.3	3.285	0.283	1.909	0.283	3.845	0.236	3.013	0.267
2.35	0.839	0.209	1.348	0.237	0.482	0.176	0.890	0.207
2.4	0.482	0.133	1.45	0.176	2.113	0.119	1.348	0.143
2.45	1.196	0.103	0.227	0.132	0.482	0.103	0.635	0.113
2.5	0.482	0.089	1.247	0.089	1.654	0.074	1.128	0.084
2.55	0.584	0.074	1.094	0.059	0.584	0.059	0.754	0.064
2.6	1.45	0.059	0.992	0.059	1.247	0.045	1.230	0.054
2.65	0.992	0.045	1.145	0.044	1.094	0.044	1.077	0.044
2.7	1.043	0.044	1.145	0.044	1.145	0.044	1.111	0.044
2.75	1.094	0.045	1.196	0.03	0.992	0.044	1.094	0.040

E.6.2 TE test data: TE02 condition cont.

t	P_314	Q_314	P_453	Q_453	P_622	Q_622	Pavg	Q_avg
seconds	(psi)	Liter	PSI	Liter	PSI	Liter	PSI	Liter
2.8	1.043	0.045	1.094	0.044	1.043	0.029	1.060	0.039
2.85	0.89	0.03	1.094	0.029	0.89	0.03	0.958	0.030
2.9	1.094	0.03	1.094	0.029	1.297	0.029	1.162	0.029
2.95	1.043	0.015	0.89	0.015	1.145	0.029	1.026	0.020
3	1.094	0.03	1.399	0.029	1.196	0.014	1.230	0.024
3.05	1.094	0.029	1.196	0.014	1.043	0.015	1.111	0.019
3.1	1.247	0.029	1.043	0.029	1.094	0.015	1.128	0.024
3.15	1.094	0.014	1.247	0.015	1.094	0.029	1.145	0.019
3.2	1.145	0.015	1.043	0.015	0.89	0.015	1.026	0.015
3.25	1.043	0.015	0.941	0.014	0.89	0.015	0.958	0.015
3.3	0.89	0.015	0.89	0.014	1.145	0.015	0.975	0.015
3.35	0.941	0.015	0.941	0.014	1.043	0.015	0.975	0.015
3.4	1.247	0.015	0.992	0	1.247	0.015	1.162	0.010
3.45	1.043	0	0.89	0	1.094	0	1.009	0.000
3.5	0.941	0	1.247	0	0.89	0	1.026	0.000
3.55	1.145	0	1.094	0	1.043	0	1.094	0.000
3.6	0.992	0	0.89	0	1.145	0	1.009	0.000
3.65	0.89	0	0.89	0	1.043	0	0.941	0.000
3.7	0.89	0	0.992	0	1.145	0	1.009	0.000
3.75	1.043	0	1.043	0	1.043	0	1.043	0.000
3.8	0.89	0	0.992	0	0.89	0	0.924	0.000
3.85	1.145	0	1.043	0	0.89	0	1.026	0.000
3.9	0.992	0	0.89	0	1.145	0	1.009	0.000
3.95	0.89	0	1.297	0	1.094	0	1.094	0.000
4	1.145	0	0.89	0	0.89	0	0.975	0.000

E.7 Discharge timing excursion (TE) tests: TE03 cond.

t	P_023	Q_023	P_154	Q_154	P_320	Q_320	Pavg	Q_avg
seconds	(psi)	Liter	PSI	Liter	PSI	Liter	PSI	Liter
0	0.89	0	0.839	0	1.043	0	0.924	0.000
0.05	17.807	0.015	17.603	0.029	17.654	0.029	17.688	0.024
0.1	16.023	0.116	14.902	0.135	14.698	0.133	15.208	0.128
0.15	14.749	0.25	15.31	0.265	14.444	0.253	14.834	0.256
0.2	13.781	0.347	13.577	0.34	13.679	0.345	13.679	0.344
0.25	12.966	0.375	12.66	0.372	12.966	0.36	12.864	0.369
0.3	12.202	0.347	11.947	0.36	12.507	0.355	12.219	0.354
0.35	12.049	0.351	11.488	0.361	11.845	0.337	11.794	0.350
0.4	10.469	0.325	11.03	0.325	10.469	0.337	10.656	0.329
0.45	10.877	0.31	10.928	0.311	10.877	0.31	10.894	0.310
0.5	10.673	0.299	10.112	0.308	10.163	0.308	10.316	0.305
0.55	10.112	0.297	10.265	0.297	10.062	0.28	10.146	0.291
0.6	10.062	0.296	9.705	0.295	10.316	0.295	10.028	0.295
0.65	24.023	0.294	24.176	0.295	24.125	0.297	24.108	0.295
0.7	23.411	0.327	23.055	0.352	22.851	0.358	23.106	0.346
0.75	22.443	0.39	22.392	0.401	23.921	0.399	22.919	0.397
0.8	21.781	0.446	22.036	0.445	21.577	0.443	21.798	0.445
0.85	21.22	0.443	20.864	0.443	20.966	0.44	21.017	0.442
0.9	20.099	0.44	19.947	0.441	20.201	0.445	20.082	0.442
0.95	19.641	0.428	20.15	0.426	19.539	0.433	19.777	0.429
1	19.182	0.431	19.08	0.414	18.877	0.431	19.046	0.425
1.05	28.965	0.428	28.965	0.411	29.067	0.414	28.999	0.418
1.1	27.742	0.443	27.182	0.455	27.59	0.455	27.505	0.451
1.15	27.233	0.473	25.246	0.484	26.978	0.473	26.486	0.477
1.2	26.978	0.494	27.437	0.505	26.571	0.498	26.995	0.499
1.25	37.577	0.505	35.691	0.49	36.456	0.503	36.575	0.499
1.3	33.857	0.517	34.519	0.517	34.825	0.517	34.400	0.517
1.35	34.01	0.545	33.704	0.543	33.347	0.551	33.687	0.546

E.7.1 TE test data: TE03 condition cont.

t	P_023	Q_023	P_154	Q_154	P_320	Q_320	Pavg	Q_avg
seconds	(psi)	Liter	PSI	Liter	PSI	Liter	PSI	Liter
1.4	32.583	0.554	32.328	0.559	32.379	0.561	32.430	0.558
1.45	31.921	0.557	31.054	0.562	31.411	0.559	31.462	0.559
1.5	31.207	0.536	30.749	0.544	30.545	0.543	30.834	0.541
1.55	30.239	0.535	29.984	0.531	30.188	0.532	30.137	0.533
1.6	29.73	0.517	29.373	0.52	29.577	0.521	29.560	0.519
1.65	29.322	0.524	28.863	0.509	29.016	0.517	29.067	0.517
1.7	28.558	0.509	28.456	0.509	28.303	0.502	28.439	0.507
1.75	27.844	0.508	28.558	0.502	28.252	0.517	28.218	0.509
1.8	27.641	0.491	27.539	0.502	26.978	0.505	27.386	0.499
1.85	27.284	0.491	27.131	0.498	26.978	0.506	27.131	0.498
1.9	26.418	0.494	26.622	0.491	26.571	0.487	26.537	0.491
1.95	26.01	0.497	25.653	0.494	25.959	0.475	25.874	0.489
2	25.653	0.49	25.501	0.491	25.246	0.472	25.467	0.484
2.05	25.348	0.476	24.532	0.473	24.838	0.478	24.906	0.476
2.1	22.596	0.472	23.004	0.458	23.004	0.476	22.868	0.469
2.15	21.883	0.449	22.29	0.461	22.138	0.458	22.104	0.456
2.2	21.373	0.448	21.475	0.458	21.322	0.441	21.390	0.449
2.25	20.915	0.434	21.068	0.443	20.66	0.441	20.881	0.439
2.3	15.666	0.431	14.291	0.43	12.864	0.429	14.274	0.430
2.35	1.756	0.401	0.227	0.404	0.278	0.384	0.754	0.396
2.4	3.743	0.328	6.851	0.343	5.119	0.31	5.238	0.327
2.45	2.368	0.254	0.38	0.252	1.603	0.236	1.450	0.247
2.5	0.533	0.192	3.845	0.162	2.011	0.163	2.130	0.172
2.55	2.877	0.147	1.909	0.132	2.113	0.133	2.300	0.137
2.6	1.297	0.119	0.482	0.118	0.839	0.103	0.873	0.113
2.65	1.297	0.09	2.164	0.104	1.552	0.103	1.671	0.099
2.7	1.501	0.089	1.45	0.088	1.603	0.073	1.518	0.083
2.75	0.38	0.074	0.482	0.074	0.839	0.074	0.567	0.074

E.7.2 TE test data: TE03 condition cont.

t	P_023	Q_023	P_154	Q_154	P_320	Q_320	Pavg	Q_avg
seconds	(psi)	Liter	PSI	Liter	PSI	Liter	PSI	Liter
2.8	1.348	0.059	1.247	0.073	1.348	0.059	1.314	0.064
2.85	1.247	0.045	0.992	0.059	1.043	0.059	1.094	0.054
2.9	1.094	0.045	1.043	0.044	0.89	0.044	1.009	0.044
2.95	0.635	0.045	1.094	0.044	0.686	0.045	0.805	0.045
3	0.992	0.03	1.247	0.029	1.247	0.044	1.162	0.034
3.05	1.043	0.03	1.145	0.03	0.482	0.03	0.890	0.030
3.1	1.043	0.03	0.839	0.03	1.348	0.03	1.077	0.030
3.15	1.247	0.03	0.89	0.03	1.043	0.015	1.060	0.025
3.2	0.431	0.03	1.094	0.03	1.145	0.03	0.890	0.030
3.25	1.247	0.014	0.89	0.015	0.992	0.015	1.043	0.015
3.3	1.043	0.029	1.145	0.015	1.043	0.03	1.077	0.025
3.35	1.145	0.015	1.145	0.014	0.839	0.015	1.043	0.015
3.4	0.992	0.015	1.043	0.014	0.89	0.03	0.975	0.020
3.45	1.094	0	1.247	0.014	0.737	0.015	1.026	0.010
3.5	0.89	0	0.89	0	1.145	0	0.975	0.000
3.55	1.043	0	1.145	0	1.043	0	1.077	0.000
3.6	0.992	0	1.094	0	1.094	0	1.060	0.000
3.65	0.992	0	1.196	0	1.145	0	1.111	0.000
3.7	0.992	0	0.992	0	1.094	0	1.026	0.000
3.75	0.992	0	1.043	0	1.145	0	1.060	0.000
3.8	1.145	0	0.89	0	0.941	0	0.992	0.000
3.85	1.094	0	1.043	0	0.89	0	1.009	0.000
3.9	1.043	0	1.094	0	1.145	0	1.094	0.000
3.95	0.89	0	1.043	0	1.043	0	0.992	0.000
4	0.89	0	0.89	0	1.094	0	0.958	0.000

Bibliography

[1] J.J. Beaman and R.G. Longoria. *Modeling of Physical Systems*. Wiley, 2018.

[2] P. C. Breedveld. Essential gyrators and equivalence rules for 3-port junction structures. *The Journal of the Franklin Institute*, 318(2):77–89, 1984.

[3] W. R. Cravey, W. M. Portnoy, and T. R. Burkes. A hybrid pulse forming technique. In *Nineteenth IEEE Symposium on Power Modulators*, pages 80–86, Jun 1990.

[4] M. Crawford, R. Subramanian, T. Watt, D. Surls, D. Motes, J. Mallick, D. Barnette, S. Satapathy, and J. Campos. The design and testing of a large-caliber railgun. *IEEE Transactions on Magnetics*, 45(1):256–260, Jan 2009.

[5] P. Dransfield. *Hydraulic control systems–design and analysis of their dynamics*. Lecture Notes in Control and Information Sciences. Springer-Verlag, 1981.

[6] T. G. Engel and W. C. Nunnally. Capacitor-based multiple-module sequentially-fired pulse forming network for nonlinear loads. In *Confer-*

ence Record of the Twenty-Sixth International Power Modulator Symposium, 2004 and 2004 High-Voltage Workshop., pages 145–148, May 2004.

[7] T. G. Engel and W. C. Nunnally. Design and operation of a sequentially-fired pulse forming network for non-linear loads. *IEEE Transactions on Plasma Science*, 33(6):2060–2065, Dec 2005.

[8] J.V. Lebacqz G.N. Glasoe. *Pulse generators*. Dover Publishing, New York, NY, 1948.

[9] A. H. Griffin, O. S. F. Zucker, and D. M. Giorgi. Sequentially switched pfn for inductive and resistive loads. In *Eighth IEEE International Conference on Pulsed Power*, pages 296–298, June 1991.

[10] E. A. Guillemin. A historical account of the development of a design procedure for pulse forming networks. techreport Report 692, MIT Radiation Laboratory, Cambridge, Mass., October 1942.

[11] P. C. Breedveld J. J. Beaman. Physical modeling with eulerian frames and bond graphs. *Journal of Dynamic Systems, Measurement, and Control*, 110(2):182–188, June 1988.

[12] Raul G. Longoria Javier A. Kypuros. Model synthesis for design of switched systems using a variable structure system formulation. *Journal of Dynamic Systems, Measurement, and Control*, 125:618–629, January 2004.

[13] D.C. Karnopp, D.L. Margolis, and R.C. Rosenberg. *System Dynamics: Modeling and Simulation of Mechatronic Systems.* A Wiley-Intersience publication. Wiley, 2000.

[14] S. Katz. Mechanical potential drops at a fluid branch. *Journal of Basic Engineering*, 89(4):732–736, December 1967.

[15] F. Liu, X. Zhao, and S. He. The design of a dsp-based pfn trigger timing control system and the experimental study. In *2012 16th International Symposium on Electromagnetic Launch Technology*, pages 1–6, May 2012.

[16] R. Marshall. The taerf scientific railgun theoretical performance. *IEEE Transactions on Magnetics*, 18(1):11–15, Jan 1982.

[17] R. A. Marshall and W. F. Weldon. Analysis and performance of rail gun accelerators powered by distributed energy systems. Publication No. PN-63 Center for Electromechanics, University of Texas at Austin, June 1980. 14th Pulse Power Modulation Symposium, Orlando, Florida, June 3-5.

[18] I. R. McNab. Pulsed power for electric guns. *IEEE Transactions on Magnetics*, 33(1):453–460, Jan 1997.

[19] W. C. Nunnally, S. M. Huenefeldt, and T. G. Engel. Results from a 750 kj computer controlled sequentially-fired pulse forming network. In *Conference Record of the 2006 Twenty-Seventh International Power Modulator Symposium*, pages 419–422, May 2006.

[20] Henry Paynter. The gestation and birth of bond graphs. University of Texas at Austin, Mechanical Engineering, Public webpage, 2000. Located on the web at: https://www.me.utexas.edu/ longoria/paynter/hmp/Bondgraphs.html.

[21] R. M. Roark, M. E. Parten, L. B. Masten, and T. R. Burkes. Pulse-forming networks with time-varying or nonlinear resistive loads. *IEEE Transactions on Electron Devices*, 26(10):1541–1544, Oct 1979.

[22] C. R. Rose. Type-e pulse-forming-network theory and synthesis. In *2015 IEEE Pulsed Power Conference (PPC)*, pages 1–6, May 2015.

[23] B. Willson and A. E. Traver. The use of control volume analysis and non-potential junction concepts to model liquid piston engine dynamics. In *1987 American Control Conference*, pages 1436–1443, June 1987.

[24] Bryan Dennis Willson. *Historical, Analytical, and Experimental Investigatoin of Internal Combustion, Liquid Piston Pumping Engines.* PhD thesis, University of Texas at Austin, December 1988.